AFIT/GE/ENP/91D-01

DTIC
S DEC 2 0 1991
C D

AD-A243 754

||||||||||||||||||||||||||||||||

STEADY-STATE PRODUCTION

AND QUENCHING OF $Br(^2P_{1/2})$

THESIS

Ralph F. Tate

Captain, USAF

AFIT/GE/ENP/91D-01

91-19033

||||||||||||||||||||||||||||||||

91 12 24 067

REPORT DOCUMENTATION PAGE

Public reporting burden for this collection of information is estimated to average 1 hour per response, including the time for reviewing instructions, searching existing data sources, gathering and maintaining the data needed, and completing and reviewing the collection of information. Send comments regarding this burden estimate or any other aspect of this collection of information, including suggestions for reducing this burden, to Washington Headquarters Services, Directorate for Information Operations and Reports, 1215 Jefferson Davis Highway, Suite 1204, Arlington, VA 22202-4302, and to the Office of Management and Budget, Paperwork Reduction Project (0704-0188), Washington, DC 20503

1. AGENCY USE ONLY (Leave blank)	2. REPORT DATE November 1991	3. REPORT TYPE AND DATES COVERED Master's Thesis

4. TITLE AND SUBTITLE
STEADY-STATE PRODUCTION AND QUENCHING OF Br($^2P_{1/2}$)

5. FUNDING NUMBERS

6. AUTHOR(S)
Captain Ralph F. Tate

7. PERFORMING ORGANIZATION NAME(S) AND ADDRESS(ES)
Air Force Institute of Technology, WPAFB OH
45433-6583

8. PERFORMING ORGANIZATION REPORT NUMBER
AFIT/GE/ENP/91D-01

9. SPONSORING/MONITORING AGENCY NAME(S) AND ADDRESS(ES)
Dr Gordon Hager
PL/LIO
Kirtland AFB NM 87117-6008

10. SPONSORING/MONITORING AGENCY REPORT NUMBER

11. SUPPLEMENTARY NOTES

12a. DISTRIBUTION/AVAILABILITY STATEMENT
Approved for public release; distribution unlimited

12b. DISTRIBUTION CODE

13. ABSTRACT (Maximum 200 words)

The spin-orbit relaxation of Br($^2P_{1/2}$) atoms has been investigated in a steady-state infrared fluorescence experiment. A CW argon ion laser operating at 488 nm was used to photodissociate gas-phase Br_2 into equal quantities of Br($^2P_{3/2}$) and Br($^2P_{1/2}$) atoms. The resulting 2.7 μm emission was observed as a function of added quenching gas. A steady-state analysis was used to determine Br($^2P_{1/2}$) quenching rates for SF_6, N_2, O_2, He, Ne, Ar, Kr, and Xe, relative to quenching by the parent molecule. Limitations in the apparatus prevented determination of the quenching rate coefficient for Br_2. Recommendations are made for improvements in the apparatus and analysis for future research.

14. SUBJECT TERMS
Bromine, Spin-orbit relaxation, Halogens, Quenching, energy transfer

15. NUMBER OF PAGES
128

16. PRICE CODE

17. SECURITY CLASSIFICATION OF REPORT	18. SECURITY CLASSIFICATION OF THIS PAGE	19. SECURITY CLASSIFICATION OF ABSTRACT	20. LIMITATION OF ABSTRACT
Unclassified	Unclassified	Unclassified	UL

NSN 7540-01-280-5500

AFIT/GE/ENP/91D-01

STEADY-STATE PRODUCTION

AND QUENCHING OF Br($^2P_{1/2}$)

THESIS

Presented to the Faculty of the School of Engineering

of the Air Force Institue of Technology

Air University

In Partial Fulfillment of the

Requirements for the Degree of

Master of Science in Electrical Engineering

Ralph F. Tate, B.S.

Captain, USAF

October 1991

Approved for public release; distribution unlimited

Preface

This research begins a project at AFIT to better understand and contribute to the knowledge of spin-orbit relaxation mechanisms involved in interactions between gas-phase $Br(^2P_{1/2})$ atoms and molecular or atomic collision partners. An apparatus was designed and built to investigate the quenching of $Br(^2P_{1/2})$ atoms by selected collisional partners through a steady-state analysis. I found this work gratifying, in seeing a design become a working apparatus, and challenging, in that much theory had to be learned and understood.

I wish to thank Captain Glen P. Perram, my advisor for giving me the opportunity to conduct research in his laboratory. The support, encouragement, and expertise he provided throughout this effort is greatly appreciated. I also wish to thank Dr. Gordon Hager, at the Phillips Laboratory for encouraging my interest in lasers and allowing me to work in his laboratory prior to coming to AFIT. Finally, I wish to thank my wife, Shelly for her love, understanding, and support during the past 18 turbulent months.

<div align="right">Ralph F. Tate</div>

Table of Contents

List of Figures

List of Tables

Abstract

The spin-orbit relaxation of $Br(^2P_{1/2})$ atoms has been investigated in a steady-state infrared fluorescence experiment. A CW argon-ion laser operating at 488 nm was used to photodissociate gas-phase molecular bromine into equal quantities of $Br(^2P_{1/2})$ and $Br(^2P_{3/2})$ atoms. The resulting 2.7 μm emission was observed as a function of added quenching gas. A steady-state analysis was used to determine $Br(^2P_{1/2})$ quenching rates for SF_6, N_2, O_2, He, Ne, Ar, Kr, and Xe, relative to quenching by the parent molecule. Limitations in the apparatus prevented determination of the rate coefficient for Br_2. Recommendations are made for improvements in the analysis and apparatus for further research.

STEADY-STATE PRODUCTION AND QUENCHING OF $Br(^2P_{1/2})$

I. Introduction

Overview

The Air Force (Phillips Laboratory/LIDC) is interested in developing a new class of infrared lasers operating in the 3 to 5 μm region for electro-optic countermeasures. One promising concept for such a laser system is to use the energy transfer from gas-phase electronically excited halogen atoms to vibrational modes of a suitable molecular laser species. For example, energy transfer from electronically excited bromine atoms ($Br(^2P_{1/2})$) to CO_2 has resulted in stimulated CO_2 emission being observed at 4.3, 10.6, and 14.1 μm (19:1051).

Much research has been devoted to analyzing the spin-orbit relaxation of one halogen, iodine, due in part to the success of chemical oxygen-iodine lasers (COIL) and photolytic iodine lasers. Less information is available on the spin-orbit relaxation of $Br(^2P_{1/2})$, with most relaxation rate measurements being made with time-resolved pulsed photolysis or vacuum ultraviolet spectroscopic techniques.

This thesis concentrates on the experimental design and techniques necessary to measure spin-orbit relaxation of

$Br(^2P_{1/2})$ by selected molecular species through a steady-state analysis. Details of the design and experimental procedure are presented in the applicable sections of this thesis.

Background

The $Br(^2P_{1/2})$ electronically excited state of bromine is 0.456 eV (3685 cm^{-1}) above the ground $Br(^2P_{3/2})$ state and is the result of spin-orbit coupling. With a strongly forbidden electric dipole transition to the $Br(^2P_{3/2})$ state, $Br(^2P_{1/2})$ has a metastable lifetime of 1.12 seconds (16:160). This radiative lifetime permits observation of $Br(^2P_{1/2})$ concentration by fluorescence detection techniques (12:382). The spin-orbit relaxation of $Br(^2P_{1/2})$ by several quenching species has been researched and will be reviewed in a later section.

Various experimental techniques have been employed to produce $Br(^2P_{1/2})$ atoms in sufficient number density to observe kinetic behavior. These techniques include flash photolysis, flow discharges, shock tubes, and more recently, laser photolysis of bromine and bromides (4:509;12:405;15:314). It is the laser photolysis of bromine that is of interest here.

Molecular bromine has a strong continuous absorption spectrum centered about the blue-green region of the visible spectrum. Absorption of light between 518 and 450 nm

2

dissociates the molecule into one ground $Br(^2P_{3/2})$ atom and one excited state $Br(^2P_{1/2})$ atom (2:227). A simple kinetic model for the production and quenching of $Br(^2P_{1/2})$ atoms is given in the following equations:

$$Br_2 + h\nu \longrightarrow Br + Br^* \tag{1.1}$$

$$Br^* + Q \xrightarrow{k_0} Br + Q \tag{1.2}$$

$$Br^* + Q \xrightarrow{k_1} Br + Q^\dagger \tag{1.3}$$

$$Br^* + Br_2 \xrightarrow{k_2} Br + Br_2 \tag{1.4}$$

$$Q^\dagger + M \xrightarrow{k_M} Q + M \tag{1.5}$$
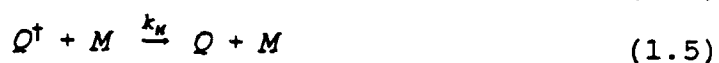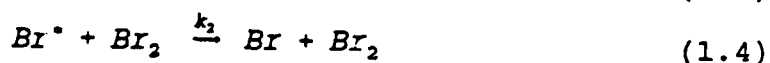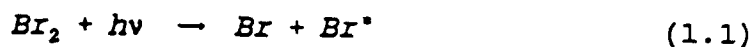
where

$Br^* = Br(^2P_{1/2})$

$Br = Br(^2P_{3/2})$

Q = quenching molecule

$Q^\dagger$ = vibrationally excited quenching molecule

$M = Br_2,\ Q$

$k_0,\ k_1,\ k_2,$ and k_M = quenching rate coefficients

and

$h\nu$ = incident photon energy ($\lambda < 518$ nm)

In the above kinetic equations it is the rate coefficients that provide insight into the quenching mechanisms, both physical and chemical. In particular, by measuring k_1 and k_0 it is possible, in principle, to determine the relative amounts of electronic energy going

3

into vibrational and translational/rotational modes respectively.

Problem Statement

Significant differences exist among reported values of Br^* quenching rate coefficients for the same quenching species. In certain instances, only one value for a quenching rate coefficient has been reported for quenching species of current interest. Accurate quenching data is required to provide insight into the energy transfer kinetics involved in spin-orbit relaxation of Br^* atoms. The purpose of this thesis is to design and conduct experiments to accurately measure the quenching of Br^* by diatomic and polyatomic quenching gases that are of current interest and to possibly resolve some of the differences that exist between reported values.

Summary of Current Knowledge

Leone and Wodarczyk were the first to investigate electronic-to-vibrational (E→V) energy transfer by means of pulsed laser excitation. In their experiment, the output of a pulsed Nd^{3+}:YAG ($\lambda=473$ nm) laser was used to photodissociate Br_2, producing Br^* and Br atoms in a 1:1 ratio. The time-resolved infrared (IR) emission from Br^* and collision partners HCl and HBr was observed through a wavelength selective filter wheel and sensitive IR detector combination (15:314).

4

Operating under the constraint $[Q] \gg [Br]$, $[Br^*]$, $[Q^\dagger]$, where Q is either HCl or HBr and applying Eqns (1.1) through (1.5), a first-order behavior was observed such that

$$\frac{d[Br^*]}{dt} = [Br^*]_0 e^{-k_q t} \tag{1.6}$$

and

$$\frac{d[Q^\dagger]}{dt} = \frac{k_1 [Br^*]_0 [Q]}{(k_q - K_M)} \{e^{-K_M t} - e^{-k_q t}\} \tag{1.7}$$

where

$$k_q = (k_0 + k_1)[Q] + k_2 [Br_2] \tag{1.8}$$

and

$$K_M = \sum_M k_M [M] \tag{1.9}$$

In this approximation, the rate of decay of Br^* fluorescence equals the rise in $Q^\dagger$ fluorescence (25:67). The quenching rate coefficients were determined by plotting the measured rate of fluorescence decay, divided by the total system pressure, against the mole fraction (X) of Q. The total rate coefficient $(k_0 + k_1)$ is evaluated at $X_Q = 1$, and k_2 is evaluated at $X_Q = 0$ (15:314). The E→V transfer rate coefficient (k_1) was determined from Br^* and $Q^\dagger$ fluorescence intensities evaluated at the t=0 intercept of

the decaying exponentials given by Eqs (1.6) and (1.7). The quenching rate coefficients reported by Leone and Wodarczyk for HCl, HBr, and Br_2 are listed, along with all other known rate coefficients for $Br(^2P_{1/2})$ quenching, in Table 1 at the end of this section. They summarized their results:

> It is important to note that 50% or more of the overall quenching of Br* by HCl and HBr is E→V transfer. . . .Further experiments in progress together with theoretical calculations may allow greater insight into the fundamental nature of E→V transfer mechanisms (15:315).

Later, Wodarczyk and Sackett used the same techniques and apparatus as described above to measure the quenching of $Br(^2P_{1/2})$ by HF. One improvement was made to enhance the accuracy of the analysis: they monitored the intensity of the laser light entering and exiting the reaction cell. The log of the ratio of the incident and transmitted intensities of the laser light was found to be linearly proportional to the Br_2 pressure and was calibrated before each experiment. By measuring both the total pressure and the Br_2 pressure, a continuous direct measure of the mole fraction of Br_2 was available (25:66).

In determining the quenching rate coefficients, Wodarczyk and Sackett plotted the measured fluorescence decay rate divided by the total pressure against the mole fraction of Br_2, with values for k_0, k_1, and k_2 determined as previously described. They found the quenching of Br* by HF

6

to be very fast (nearly gas kinetic) and attributed this behavior to efficient E→V energy transfer, "likely due to the availability of several strongly allowed near-resonant product channels" (25:68).

Hariri and others continued to investigate the quenching of Br* by larger molecules. Their experimental technique differed in that a coaxial flashlamp-pumped dye laser was used to photodissociate Br_2. As described earlier, the Br* and molecular spontaneous emissions were observed as the ratio of Br_2-to-quenching gas was varied, with the rate coefficients being determined from extrapolated data plots. The quenching gases that were investigated for E→V energy transfer included: HCN (7:1872-1875), CO_2, COS, and CS_2 (8:4454-4462).

HCN was found to be a very efficient quencher of Br*, with 88% of the quenching collisions resulting in excitation of the v_3 mode of HCN (7:1874). Quenching of Br* by CO_2 was found to be an order of magnitude more efficient than COS or CS_2 (8:4460). This near resonant E→V transfer mechanism in CO_2 has been exploited in the development of Br* pumped CO_2 lasers (18:305).

Hofmann and Leone used a similar flashlamp-pumped dye laser arrangement to investigate the collisional deactivation of $Br(^2P_{1/2})$ atoms with halogen and interhalogen molecules. In their experiments the Br* emission intensity was observed with a 2.7 μm bandpass filter and InSb detector

7

combination. Gases were mixed at known initial pressures

allowing calculable partial pressures of products to be

determined according to known equilibrium constants

(11:316). The measurement procedure for a mixture of Br_2

and I_2 was explained as follows:

> The observed exponential decay of the Br^* emission
> intensity, characterized by the time constant τ_{obs},
> is related to the gas pressures and rate
> coefficients in the following manner:
>
> $$1/\tau_{obs} = k_{Br_2}P_{Br_2} + k_{I_2}P_{I_2} + k_{IBr}P_{IBr}$$
>
> . . .Twelve measurements were carried out with
> initial pressure ratios of Br_2/I_2 in the range
> from 10:1 to 1:4 with total halogen pressures from
> 0.02-2 torr and 50 torr of argon. . . .These data
> were computer-analyzed by a three-parameter least-
> squares fit resulting in values for the rate
> coefficients (11:316).

Hofmann and Leone performed the same procedure as

described above to obtain rate coefficients for quenching of

Br^* by Br_2, IBr, ICl, BrCl, and Cl_2. Their efforts revealed

differences in rate coefficients over two orders of

magnitude. Molecules containing iodine were found to be

more efficient quenchers than BrCl and Cl_2. In discussing

their results, Hofmann and Leone offered the following

explanation for the large differences in the observed rates:

> The relatively small vibrational quanta associated
> with the halogen and interhalogen molecules
> investigated here, with ω_e values ranging from 214
> cm^{-1} (I_2) to 564 cm^{-1} (Cl_2) do not support the idea
> of an effective E→V transfer mechanism. Instead a
> deactivation mechanism involving a potentially

8

reactive pathway of intermediate trihalogen complexes seems to be much more likely (11:317).

Grimley and Houston investigated the E→V energy transfer from Br* to H_2, HD, and D_2 in an effort to compare experimental results to available theoretical results. The experimental observation of the vibrational excitation in hydrogen is made difficult by the lack of a permanent dipole moment. Their method involved indirectly monitoring the E→V transfer from Br* to hydrogen by observing the CO fluorescence following subsequent V→V transfer from hydrogen to CO (6:5184). The fluorescence from Br* and CO was observed by an InSb detector with appropriate interference filters. A 4.44 μm filter was used to isolate the CO emission, and a 2.7 μm filter was used to isolate the Br* emission (6:5184).

Their investigation concluded that a high fraction of the Br* electronic energy was transferred to vibrational modes in H_2 and HD, and a lesser fraction of electronic energy was transferred to D_2 vibration. The experimental results were in qualitative agreement with theoretical conclusions with the exception of quenching of Br* by D_2, where direct E→V transfer was not observed (6:5184-5488).

The quenching of Br* by nitric oxide (NO) was recently studied by Wight in an effort to resolve discrepancies in earlier reported values (see Table 1). To avoid the problem of Br_2 reacting with NO at room temperature, Wight used a

9

ArF excimer laser to photodissociate CF_3Br, thus producing
Br^*. The vibrationally excited NO molecules were detected
through IR fluorescence at 5.4 μm with an HgCdTe detector
(24:2684). The total quenching rate coefficient was
determined by measuring the rise time of NO fluorescence as
a function of NO and CF_3Br pressures.

Wight concluded that approximately 84% of the E$\rightarrow$V
transfer collisions excite NO to the $\upsilon = 2$ level, and 14% to
the $\upsilon = 1$ level (24:2686).

The quenching rate of Br* with O_2, H_2O, D_2O, and HDO as
collision partners has recently been measured by Taatjes and
others by using a laser double resonance method. A pulsed
dye laser operating at 500 nm was used to produce spin-orbit
excited bromine atoms through photolysis of Br_2. The
population difference (Br* - Br) was monitored by an F-
center probe laser tuned to the $Br(^2P_{1/2})\leftarrow Br(^2P_{3/2})$ transition.
The probe beam was propagated through the reaction cell and
imaged on a fast IR detector where the absorption (or gain)
encountered by the probed laser beam was detected (21:12).

As the ratio of Br_2-to-quenching gas was varied, the
time-resolved detector signal was digitized, averaged, and
stored in a microcomputer for analysis. The rate
coefficients were determined using a method similar to that
previously described by Hofmann and Leone (11:316).

Of particular interest to this thesis, the researchers
reported that the quenching of Br* by O_2 was extremely slow,

10

disagreeing with previously reported results by four orders of magnitude (21:2). To test for possible systematic errors, the quenching rate of Br* with CO_2 was measured by the same method and was found to be in excellent agreement with previous values. (8:4454-4462; 21:1-15). An attempt will be made in this thesis effort to resolve the discrepancy between O_2 quenching rate coefficients.

The researchers summarized their results as follows:

> The observed rates for H_2O, HDO, and D_2O can be qualitatively explained by E→V models based on long-range dipole-quadrapole interactions. Quenching of Br* by oxygen is found to be very inefficient, in dramatic disagreement with previous determinations (21:11).

All known quenching rate coefficients for the spin-orbit relaxation of Br* atoms are shown below in Table 1.1. For completeness, results of experiments prior to laser-excited quenching studies are included. Table 1 clearly shows that discrepancies exist between some of the rate coefficients for certain quenching species. The objective of this thesis effort is to design, develop, and implement an experimental approach sensitive enough to resolve some of these discrepancies and to provide quenching rate data for quenching species not previously investigated.

TABLE 1.1

Known Rate Coefficients for
Spin-orbit Relaxation of $Br(^2P_{1/2})$

QUENCHING SPECIES	QUENCHING RATE COEFFICIENT (10^{-12} cm^3/molecule-s)	REFERENCE
Ar	$< 2.0 \times 10^{-4}$	(4:514)
Br_2	19.0 1.2 ± 0.3 0.48 ± 0.05 0.47 ± 0.04	(4:514) (7:1875) (15:317) (11:317)
BrCl	0.029 ± 0.014	(11:317)
Cl_2	0.022 ± 0.014	(11:317)
CO	0.0073 0.00107 ± 0.00005	(4:514) (6:5184)
CO_2	15 ± 1	(8:4458) (18:306) (21:15)
COS	1.4 ± 0.1	(8:4458)
CS_2	1.1 ± 0.1	(8:4458)
CF_4	0.21	(4:514)
CF_3Br	0.05	(4:514)
CH_4	4.2	(4:514)
D_2	5.7 0.68	(4:514) (6:5184)
D_2O	9.6 2.2 ± 0.4	(4:514) (21:15)
H_2	4.7 2.7	(4:514) (6:5184)
HD	6.4	(6:5184)
HBr	1.1 1.4 0.84 ± 0.11	(4:514) (12:407) (15:317)
HCl	8.6 5.2 ± 0.4	(12:407) (15:317)
HF	34 ± 6	(25:68)

QUENCHING SPECIES	QUENCHING RATE COEFFICIENT (10^{-12} cm^3/molecule-s)	REFERENCE
HCN	20 ± 2	(7:1875)
H_2O	32 62 51 ± 3	(4:514) (12:407) (21:15)
HDO	19 ± 4	(21:15)
I_2	1.86 ± 0.37	(11:317)
IBr	3 1.0 ± 0.14	(4:514) (11:317)
ICl	0.9 ± 0.4	(11:317)
N_2	0.0025	(4:514)
NO	47 2.0 5.3	(4:514) (12:407) (24:2683)
N_2O	2.6 ± 0.8	(18:306)
O_2	34 0.0015	(4:514) (21:15)

Scope

This thesis will concentrate on the design and procedures of an experiment to accurately measure the spin-orbit relaxation of $Br(^2P_{1/2})$ in the presence of a quenching gas. A steady-state analysis will be used, whereby gas-phase electronically excited bromine atoms will result from the photodissociation of Br_2 by a continuous wave (CW) argon-ion laser. A quenching gas will be added to the mixture, and its effect on the number density of $Br(^2P_{1/2})$ atoms will be evaluated.

13

Approach

An experimental apparatus will be designed to permit the safe handling and mixing of high-purity Br_2 and other gases for the purpose of determining the rate of spin-orbit relaxation of Br^* atoms. Figure 1.1 is a diagram of the proposed experimental apparatus.

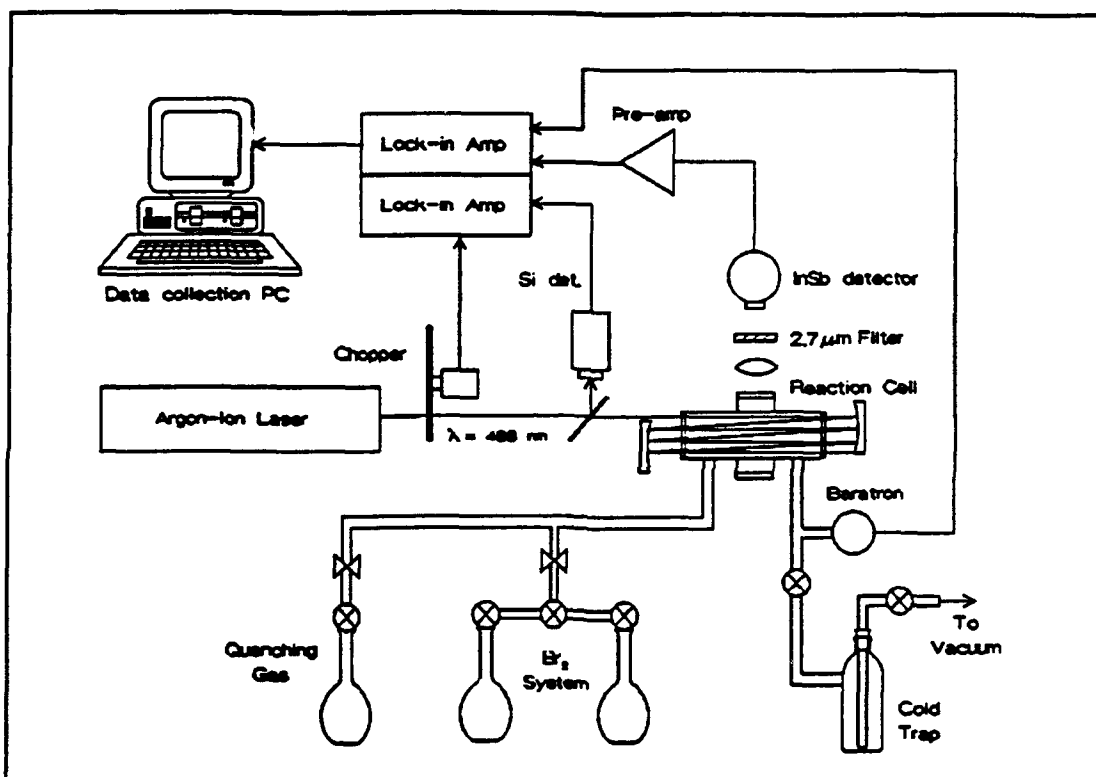Figure 1.1. Proposed Experimental Apparatus

Initially, the steady-state production of Br^* atoms as a function of Br_2 pressure will be investigated. Radiation from a CW argon-ion laser will be passed through a reaction cell containing bromine gas. The resultant Br^* population will be monitored by observing the 2.7 μm fluorescence as a function of bromine gas pressure. A sensitive InSb

14

detector, fitted with a 2.7 μm bandpass filter, will be used to detect the Br$^*\to$Br emission. Lock-in detection techniques will be employed to improve the signal-to-noise ratio of the fluorescence.

The voltage output of the lock-in amplifier, which is an indication of Br* concentration, and the voltage signal from the manometer, which is an indication of Br$_2$ concentration, will be recorded into a personal computer for subsequent processing. From the two voltage signals, an optimum Br$_2$ pressure for the production of Br* will be determined.

The following first-order differential equation describes the time-dependent behavior of the Br* concentration:

$$\frac{d[Br^*]}{dt} = k_p[Br_2] - \frac{[Br^*]}{\tau_R} - k_{Br_2}[Br_2][Br^*] \qquad (1.10)$$
$$- k_Q[Q][Br^*]$$

where

$$[Br_2] = Br_2 \text{ concentration}$$
$$[Br^*] = Br^* \text{ concentration}$$
$$[Q] = \text{quenching species concentration}$$
$$k_p = \text{pump rate coefficient}$$
$$k_{Br_2}, \ k_Q = \text{quenching rate coefficients}$$
$$\tau_R = \text{radiative lifetime}$$

In the steady state, Eq (1.10) can be set to zero, and with the $1/\tau_R$ term neglected, can be solved for [Br*] such that

$$[Br^*] = \frac{k_p[Br_2]}{k_{Br_2}[Br_2] + k_Q[Q]} \qquad (1.11)$$

Taking the ratio of Eq (1.11) with [Q] = 0 and Eq (1.11) with [Q] at a known concentration results in

$$\frac{[Br^*]_{[Q]=0}}{[Br^*]} = 1 + \frac{k_Q[Q]}{k_{Br_2}[Br_2]} \qquad (1.12)$$

By recording the Br* fluorescence intensity as a function of quenching gas pressure, and using Eq (1.12), the unknown quenching rate relative to quenching by Br_2 can be determined.

With the apparatus operating properly, the quenching of Br* by CO_2 will be investigated. The measured quenching rate will be compared to published values as a means of validating and refining the method used.

The measurement of Br* quenching by O_2 will be attempted in an effort to resolve disagreement between published values. If time permits, quenching by N_2, SF_6, CF_4, I_2, Cl_2, and the rare gases will also be investigated.

Summary

This completes the introductory material concerning the experiment. Chapter II will present the fundamental theory to support the experimental effort. Chapter III describes the experimental apparatus in detail. Chapter IV lists the procedures followed in performing the experiment. Chapter V reveals the experimental results. Chapter VI states conclusions and offers recommendations for future work.

II. Theory

Introduction

This chapter presents the fundamental theory relevant to the experiment. The first section is a basic description of the bromine atom. This is followed by a discussion on the photochemistry of molecular bromine. Lastly, an analysis of the quenching kinetics involved in the experiment is presented.

Description of Bromine Atom

Bromine (Br) is a member of the halogen family of elements, which also includes fluorine, chlorine, and iodine. In its elemental state Br forms a diatomic molecule (Br_2). Two stable isotopes of bromine exist in near-equal abundance: ^{79}Br and ^{81}Br. To simplify the following analysis, only one isotope will be considered.

With an atomic number of 35, and an atomic weight of 79.904, bromine has 35 protons, 43 neutrons, and 35 electrons. It is the configuration of the electrons that is of interest here. In a simple model for complex atoms, the electrons are said to populate a series of shells and subshells of increasing energy levels, while simultaneously satisfying the Pauli exclusion principle. A standard notation has been adopted to describe how the shells and subshells are populated. For Br in the ground electronic configuration this notation is $1s^2 2s^2 2p^6 3s^2 3p^6 3d^{10} 4s^2 4p^5$

18

(23:B-4). Noting that a number of shells and subshells are completely filled in the Br atom, the description can be condensed by neglecting the notation for the lower-lying completed shells. This abbreviated notation for Br can be written as $4p^5$. In this notation, the leading number 4, denotes the principal quantum number n which can take on values n = 1,2,3,4,5, etc. These numbers correspond to the letter notation for shells K,L,M,N,O, etc., indicating an N-shell ground configuration for Br. The letter p in the notation denotes the angular momentum quantum number l of an individual electron where l = 0,1,2,3 corresponds to s,p,d,f respectively. Accordingly, for the 4p subshell, l = 1. The superscript 5 in the $4p^5$ notation denotes the number of electrons in the 4p subshell, which is one electron less than a filled subshell. This fact is important in determining the energy levels of the atom.

According to quantum theory, the energy of an electron in a many-electron atom depends not only on its principal quantum number, but also on its angular momentum quantum number. Collectively, the total angular momentum of the atom is given as the vector sum of the individual electron orbital angular momenta and the individual electron spin momenta. This total angular momentum is determined by the electrons in the unfilled shells, given that individual angular momenta in filled shells sum to zero. The total angular momentum is expressed as

$$J = \sum_{i=1}^{N} (l_i + s_i) \qquad (2.1)$$

Where

   J = total angular momentum vector

   l_i = electron orbital angular momentum vector

   s_i = electron spin angular momentum vector

(3:56). For Br an **LS** coupling scheme is used to obtain J where

$$L = \sum_i l_i \qquad (2.2)$$

$$S = \sum_i s_i \qquad (2.3)$$

and

$$J = L + S \qquad (2.4)$$

Corresponding to J are two quantum numbers J and M_J. Allowed values for J are given by

$$L+S \geq J \geq |L-S| \qquad (2.5)$$

Where

20

L = total angular momentum quantum number

and

S = total angular momentum quantum number.

For the five electrons in the $4p^5$ subshell, the orbital angular momenta sum to give a state with L = 1, and S = 1/2 (12:13). From Eq (2.5) two values for J are obtained:

J = 3/2, and J = 1/2.

Allowed values for M_J, the magnetic quantum number are given by

$$+J \geq M \geq -J \qquad (2.6)$$

The **LS** or (Russel-Saunders) coupling scheme provides a convenient means of labeling the quantum state of an atom using

$$N^{2S+1}L_J \qquad (2.7)$$

where N denotes the orbit number (22:368). By convention, letters are used for L such that L = 0,1,2,3 corresponds to S,P,D,F respectively. Using this notation, with N=4, L=P, S=1/2, and J=3/2 or 1/2, two quantum levels are described for bromine: $4^2P_{1/2}$ and $4^2P_{3/2}$ (read as "four doublet P one-half" and "four doublet P three-halves"). These two levels have different energies, with $4^2P_{3/2}$ being lower. For convenience in future use, the

preceding 4 in the notation will be dropped and the levels $^2P_{1/2}$ and $^2P_{3/2}$ together will be called the fine structure.

Atomic nuclei with an odd number of protons and/or an odd number of neutrons can possess an intrinsic angular momentum or nuclear spin (3:506). This nuclear spin is designated with a vector **I**. The **LS** coupling scheme can be extended to include the nuclear spin angular momentum vector **I** as part of the total angular momentum of the atom. This vector sum **F** is given by

$$\mathbf{F} = \mathbf{J} + \mathbf{I} \qquad (2.8)$$

Corresponding to **F** are two quantum numbers, F and M_F. Values for F are given by

$$J+I \geq F \geq |J-I| \qquad (2.9)$$

At this point it should be noted that the magnetic quantum numbers M_J and M_F result in states which are degenerate, or have the same energy for a given quantum level. Therefore, they do not contribute to this description of the bromine atom, (with zero external magnetic field), and will be neglected.

Using I = 3/2 for the bromine nucleus (8:461), and the previously derived values for J in Eq (2.9), results in F = 3,2,1,0 for the $^2P_{1/2}$ level and F = 2,1 for the $^2P_{3/2}$ level. The different values for F in each level result in states

22

with different energies. The 6 resulting energy levels comprise the hyperfine structure.

A basic energy level diagram of the bromine atom is shown in Figure 2.1. The diagram indicates the fine structure as well as the hyperfine structure and gives the calculated energy difference between the $^2P_{1/2}$ and $^2P_{3/2}$ levels in wave numbers (1:234). From this value of v_0, a transition wavelength of 2.7 μm is determined. Also shown in Figure 2.1 are the allowed transitions ($\Delta F = 0, \pm 1$) between the hyperfine states. The energy differences among the hyperfine states within each level are small and take on different values according to the isotope involved. For this reason, they are not shown in Figure 2.1. However, these small energy differences and isotope shifts give rise to an overlapping hyperfine spectrum for atomic bromine which can be partially resolved at low pressures (13:212). In this experiment, relatively high pressure operation is expected and these small energy differences are not crucial to the analysis.
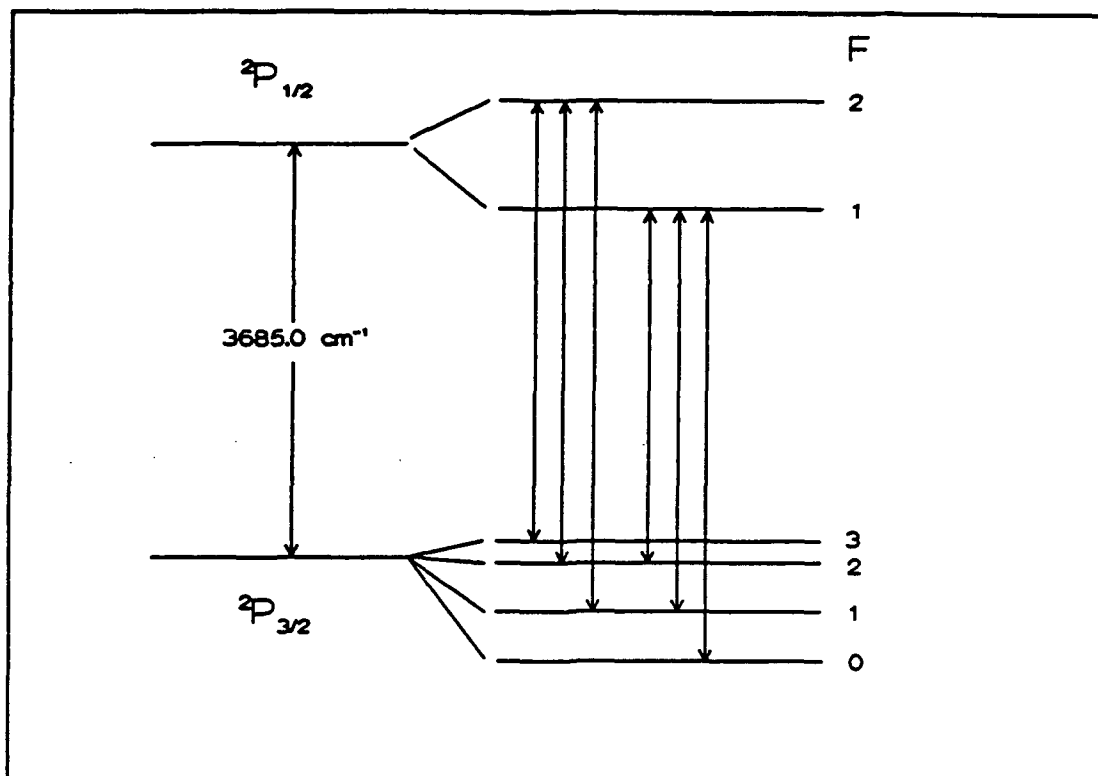
Figure 2.1. Bromine Atom Energy Level Diagram

The spontaneous emission probability (Einstein A coefficient) for a $^2P_{1/2} \rightarrow {}^2P_{3/2}$ transition has been measured and is given as A = 0.898 sec^{-1} (1:234). This gives a radiative lifetime for the Br atom of τ = 1.11 sec. This radiative lifetime is exploited, through fluorescence detection techniques, in determining the change in Br($^2P_{1/2}$) atom concentration as a function of quenching gas pressure; the very purpose of this experiment.

This section has provided a simple description of the Br atom and has diagrammed the electronic energy levels resulting from spin-orbit coupling. The next section will discuss one mechanism by which Br($^2P_{1/2}$) atoms are produced.

Photochemistry of Molecular Bromine

Basically, photochemistry deals with physical and chemical changes brought on by the interaction of light with a molecule. A change is induced only by light that is absorbed by the molecule, and it involves raising the molecule to an excited electronic state and/or dissociating the molecule into products (16:3). In this section, a brief description of the Br_2 molecule will be presented followed by a discussion of the photochemical properties of the diatomic bromine.

It was shown in the preceding section that Br atoms can exist only in certain discrete states. These states are the result of coupling the electron spin angular momentum with the electron orbital angular momentum. For the diatomic Br_2 molecule, two other mechanisms contribute to the quantum description: the vibration and rotation of the molecule. However, it can be shown that in comparison with the dissociation energy of the molecule, the rotational and vibrational energies do not contribute significantly in initiating photochemical reactions (16:11). Given that a photochemical reaction results from the absorption of visible and ultraviolet light, the electronic transitions of the molecule are of primary importance.

Electrons in a diatomic molecule such as Br_2 move about a cylindrically symmetric field with respect to the internuclear axis. This results in the electron orbital

angular momentum being defined along the internuclear axis. The component of the electron angular momentum along this axis is designated M_L and takes on values of

$$M_L = L, \; L-1, \; L-2, \; \ldots, \; -L \tag{2.10}$$

in units of $h/2\pi$, where L is the quantum number of the electrons orbital angular momentum (16:11). The corresponding quantum number for the component of the orbital angular momentum is defined as $\Lambda = |M_L|$ and can take on values $\Lambda = 0,1,2,\ldots L$ which correspond to $\Lambda = \Sigma, \Pi, \Delta, \Phi, \ldots$

Similar to the atomic description, the spins of the individual electrons in the molecule form a vector sum to give S which has a component M_S along the internuclear axis in units of $h/2\pi$. For molecules, M_S is written as Σ and takes on values

$$\Sigma = S, \; S-1, \; S-2, \ldots, \; -S \tag{2.11}$$

The labeling of the quantum states in molecules is similar to that used in atoms and is given as

$$^{2\Sigma+1}\Lambda_{\Lambda+\Sigma} \tag{2.12}$$

where the $2\Sigma+1$ superscript is the multiplicity and the $\Lambda+\Sigma$ subscript gives the multiplet component. For Br_2, $L = 1$ and $\Lambda = \Sigma, \Pi$. As a result, the ground state for Br_2 is $^1\Sigma$ (read

as singlet sigma), and the excited states are $^3\Pi$ (read as triplet pi) (16:185). By convention, the molecular ground state is called the X state and the excited states of increasing energy are called A,B,C,..., for states with the same multiplicities, or a,b,c,..., for states with different multiplicities. This letter designator usually precedes the spectrographic notation defined above.

When two atoms are brought together to form a diatomic molecule, various forces interact to either attract or repel the other atom. This interaction potential can be expressed as a function of the separation of the nuclei (22:551). Figure 2.2 shows a potential energy diagram for Br_2, where the vertical axis is energy in electron-volts (eV) and the horizontal axis is the internuclear distance between the nuclei in angstroms (Å). The states are identified in spectroscopic notation, with solid curves indicating potential energies for bound molecular states and a dashed curve representing a repulsive state. The vibrational and rotational energy levels that exist within each electronic state are not shown on this diagram for the sake of clarity. It is made obvious by Figure 2.2 that if sufficient energy is absorbed by the bromine molecule, dissociation can occur resulting in either $Br(^2P_{3/2}) + Br(^2P_{3/2})$ or $Br(^2P_{1/2}) + Br(^2P_{3/2})$ as the products.
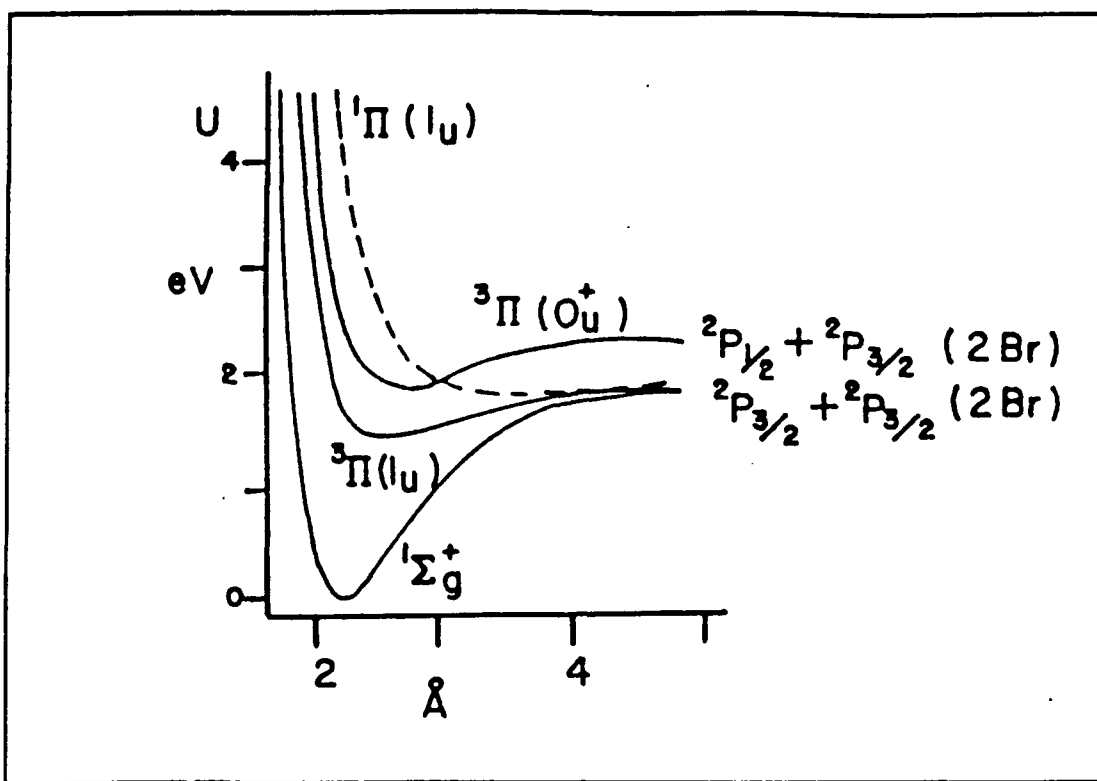
Figure 2.2. Br_2 Potential Energy Diagram (16:186)

The absorption of light by a molecule is expected to obey the Beer-Lambert law (16:59) such that

$$I = I_0 e^{-\sigma Nl} \qquad (2.13)$$

where

> I = transmitted light intensity (watts cm^{-2})
>
> I_0 = incident light intensity (watts cm^{-2})
>
> N = concentration (molec cm^{-3})
>
> l = absorption path length (cm)

and

> σ = absorption cross section (cm^2)

Figure 2.3 is a graph of absorption coefficients of Br_2
for wavelengths in the region of 2000 to 6000 Å. The
absorption coefficients ϵ are in units of liters mol^{-1} cm^{-1},
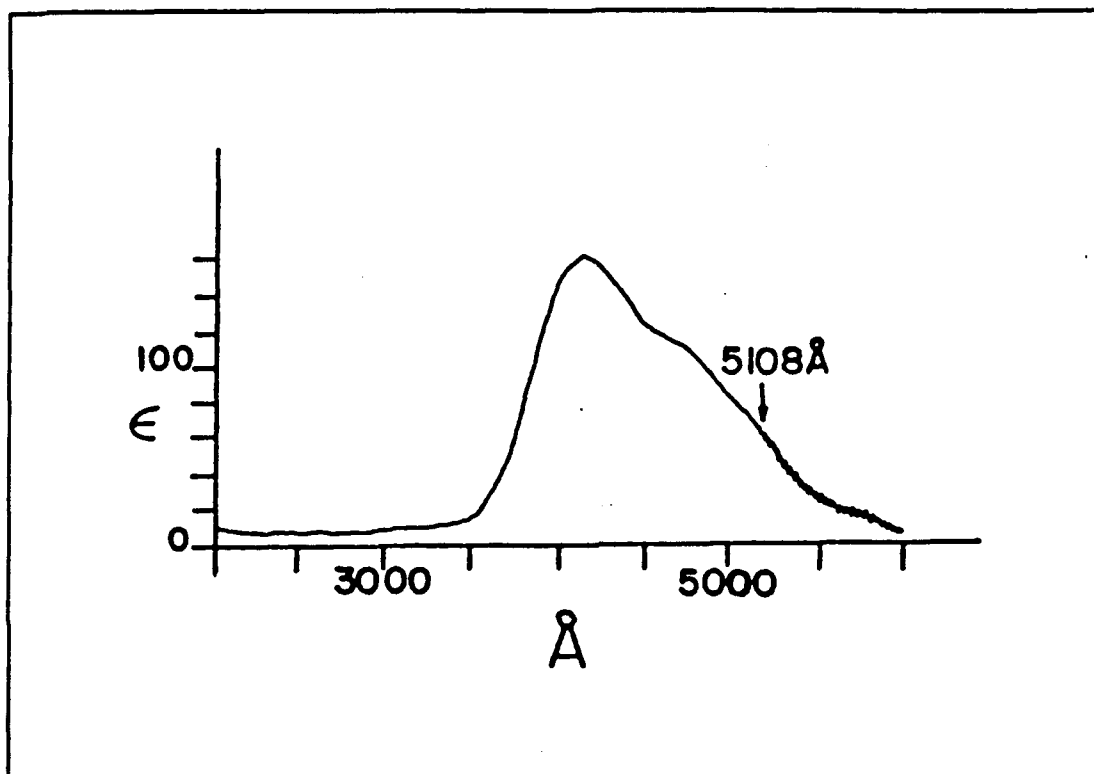base 10 at room temperature (16:186).

Figure 2.3. Absorption Coefficients for Br_2 (16:186)

The absorption spectrum illustrated in Figure 2.3
clearly shows a discrete structure (banded region) from
about 6000 to 5110 Å, followed by a continuum from 5110 to
3000 Å. From 3000 to 1560 Å another continuum is observed
(16:185). The discrete structure is the result of incident
visible radiation accessing resonant transitions between
ground vibrational levels and vibrational levels in the
$B^3\Pi(0_u^+)$ state ($v' \leftarrow v'' = 0$, where v' designates vibrational

levels in the upper state and υ'' indicates those in the $X^1\Sigma_g^+$ state) (16:59). The υ' levels converge to a continuum of higher wave numbers, with the convergence limit indicated on Figure 2.3 at 5108 Å.

For wavelengths between 5108 and about 3500 Å, the molecule dissociates from the $B^3\Pi(0_u^+)$ state into one $Br(^2P_{1/2})$ atom and one $Br(^2P_{3/2})$ atom (16:59). Wavelengths shorter than 3500 Å have resulted in two $Br(^2P_{3/2})$ atoms being born from the repulsive $^1\Pi$ state (16:187). For completeness, it should be noted that another (weak) banded region has been detected between 8180 and 6450 Å and corresponds to a transition to the $A^3\Pi(1_u)$ state (16:185).

In this experiment, an argon-ion laser operating at a wavelength of 488 nm (4880 Å) is used to photodissociate Br_2 into $Br(^2P_{1/2})$ + $Br(^2P_{3/2})$ atoms as described above. The energy required for dissociation into $Br(^2P_{1/2})$ + $Br(^2P_{3/2})$ atoms is found from the convergence limit wavelength and is equal to 2.427 eV. The energy of the 488 nm radiation is 2.541 eV. This results in an additional 0.114 eV of energy, most likely increasing the translational energy of the recoiling photofragments.

This completes the description of the relevant photochemistry for molecular bromine. A process has been detailed such that the absorption of 488 nm laser radiation by Br_2 results in equal amounts of $Br(^2P_{1/2})$ and $Br(^2P_{3/2})$ atoms. The next section will discuss mechanisms whereby the

$Br(^2P_{1/2})$ atoms make a transition to the ground $Br(^2P_{3/2})$ state.

Analysis of Quenching Kinetics

There are essentially two ways in which a $Br(^2P_{1/2})$ atom can make a transition to the $Br(^2P_{3/2})$ state: a radiative transition, or a non-radiative transition. A radiative transition occurs when the atom spontaneously emits radiation in the process of relaxing to the ground state. This radiation will have a wavelength corresponding to the energy difference between the two states. For the $Br(^2P_{1/2})$ → $Br(^2P_{3/2})$ transition, a simple equation can be written.

$$Br^{\bullet} \xrightarrow{k_0} Br + h\nu \qquad (2.14)$$

where

        Br* = $Br(^2P_{1/2})$ atom

        Br   = $Br(^2P_{3/2})$ atom

        $h\nu$ = energy of photon emitted (2.7 μm)

and

        k_0 = radiative rate

A non-radiative transition is usually the result of a collision between the Br* atom and another body of mass. The collisional partner could be a molecule, an atom, or the walls of the vessel containing the gas. In the simple analysis presented here, collisions with gas molecules or

atoms are assumed to dominate the relaxation or quenching of
the Br* atoms to the ground state. A simple kinetic scheme
describes this mechanism.

$$Br^* + Q \xrightarrow{k_Q} Br + Q^\dagger \qquad (2.15)$$

where

        Q = molecular or atomic collision partner

        $Q^\dagger$ = excited collision partner

and

        k_Q = quenching rate

Equation (2.15) is not a complete description of the
collisional process. The energy given up by the Br* atom in
the collision is in effect "carried off" by the collisional
partner in the form of translational, rotational,
vibrational, or vibronic energy. Also, numerous collisions
may be required to completely relax the electronically
excited atom.

For the case of molecular collision partners with one
vibrational mode, the transferred electronic energy can
populate more than one vibrational level in the acceptor
molecule, within the constraints of energy conservation
(7:383). This implies that the rate constant k_Q is actually
a summation of individual rate constants for each
vibrational level being populated, expressed as

$$k_Q = \sum_{i=0}^{i=v_{max}} k_i \qquad (2.16)$$

where

v_{max} = highest vibrational level populated

and

k_i = rate constant for Br* + Q($v=0$) → Br + Q($v=i$)

Within the confines of this experiment however, the value for k_Q can only be obtained and at best, relative to the quenching due to the parent Br_2 molecule.

Combining the photodissociation process for the production of Br* atoms with the relaxation processes described above, results in a first-order time-dependent rate equation for Br* atom concentration

$$\frac{d[Br^{\bullet}]}{dt} = k_p[Br_2] - k_0[Br^{\bullet}] - k_{Br_2}[Br_2][Br^{\bullet}] \qquad (2.17)$$
$$- k_Q[Q][Br^{\bullet}]$$

where

$[Br_2]$ = Br_2 concentration (molec cm^{-3})

$[Br^{\bullet}]$ = Br* concentration (atoms cm^{-3})

$[Q]$ = quenching species concentration (molec cm^{-3})

k_p = pump rate coefficient (atoms molec^{-1} sec^{-1})

k_{Br_2}, k_Q = quenching rate coefficients (molec^{-1} cm^3 sec^{-1})

k_0 = radiative rate (sec^{-1})

Operating under steady-state conditions (CW argon-ion laser pump), Eq (2.17) can be set equal to zero.

$$k_p[Br_2] - k_0[Br^*] - k_{Br_2}[Br_2][Br^*] - k_Q[Q][Br^*] = 0 \qquad (2.18)$$

Solving Eq (2.18) for [Br*] results in

$$[Br^*] = \frac{k_p[Br_2]}{k_0 + k_{Br_2}[Br_2] + k_Q[Q]} \qquad (2.19)$$

In the experiment, the intensity I of the Br* → Br 2.7 μm emission is detected, and is proportional to [Br*].

$$I = K\frac{k_p[Br_2]}{k_0 + k_{Br_2}[Br_2] + k_Q[Q]} \qquad (2.20)$$

where K is a proportionality constant dependent upon detector field-of-view, filter transmission, clear aperture, etc..

When considering the case where no quenching gas is present ([Q] = 0), Eq (2.20) can be simplified to give the detected signal intensity as a function of Br_2 concentration.

$$I = K\frac{k_p[Br_2]}{k_0 + k_{Br_2}[Br_2]} \qquad (2.21)$$

Equation (2.21) is shown graphically in Figure 2.4 with the relative intensity on the vertical axis and the Br_2 pressure (concentration) along the horizontal axis. Note that as the intensity signal approaches the asymptotic value, it approximates
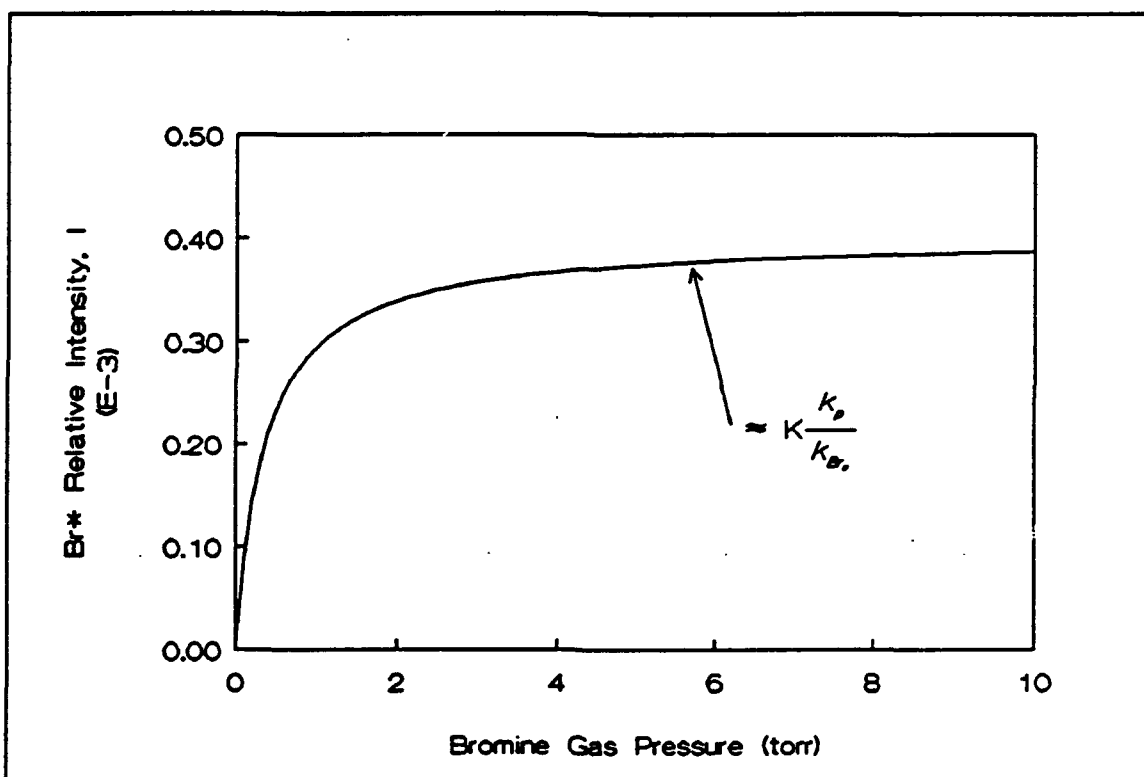
$$I \approx K \frac{k_p}{k_{Br_2}} \qquad (2.22)$$

Figure 2.4. Br* Intensity vs Bromine Pressure

Taking the inverse of both sides of Eq (2.21) results in

$$\frac{1}{I} = \frac{k_0 + k_{Br_2}[Br_2]}{K k_p [Br_2]} \qquad (2.23)$$

35

This can be further simplified to

$$\frac{1}{I} = \frac{k_0}{Kk_p} \frac{1}{[Br_2]} + \frac{k_{Br_2}}{Kk_p} \qquad (2.24)$$

Equation (2.24) takes the form of a simple linear equation:

$$y = mx + b \qquad (2.25)$$

where

$$y = \frac{1}{I}$$

$$x = \frac{1}{[Br_2]}$$

$$m = \frac{k_0}{Kk_p}$$

$$b = \frac{k_{Br_2}}{Kk_p}$$

Plotting the inverse of the intensity signal versus the inverse of the bromine pressure allows a linear fit to be made to the data, with slope m and intercept b giving the ratios indicated above. By taking the ratio of b to m, the quenching rate coefficient for Br_2 can be determined relative to the radiative rate k_0 where

$$\frac{b}{m} = \frac{k_{Br_2}}{k_0} \qquad (2.26)$$

36

Consider now the case where a quenching gas is present and the bromine pressure is set to give an intensity approaching the asymptotic value given by Eq (2.22). Then Eq (2.21) can be simplified to give

$$I = K \frac{k_p [Br_2]}{k_{Br_2} [Br_2] + k_Q [Q]} \qquad (2.27)$$

Taking the ratio of Eq (2.27), with $[Q] = 0$, and Eq (2.27), with $[Q]$ at a known concentration, gives

$$\frac{I_{[Q]=0}}{I_{[Q]\neq 0}} = \frac{k_{Br_2} [Br_2] + k_Q [Q]}{k_{Br_2} [Br_2]} \qquad (2.28)$$

Simplifying Eq (2.28) further results in

$$\frac{1}{I_{norm}} = 1 + \frac{k_Q [Q]}{k_{Br_2} [Br_2]} \qquad (2.29)$$

where

$$\frac{1}{I_{norm}} = \frac{I_{[Q]=0}}{I_{[Q]\neq 0}}$$

Equation (2.29) is a linear function of $[Q]$ in the same form as Eq (2.25) where

$$y = \frac{1}{I_{norm}}$$

$$x = [Q]$$

$$m = \frac{k_Q}{k_{Br_2}[Br_2]}$$

$$b = 1$$

By plotting the inverse of the normalized Br* emission signal against the quenching gas pressure, a linear fit can be made to the data with the slope m giving the ratio indicated above. Multiplying the slope m by the constant bromine gas pressure gives the rate coefficient for the quenching species relative to the quenching due to Br_2.

This completes the description of the Br* quenching kinetics. Data from the experiment will be reduced and analyzed according to the equations presented in this section.

III. Experimental Apparatus

Introduction

This chapter describes the experimental apparatus in detail. Figure 3.1 schematically depicts the various components brought together to perform the experiment. The apparatus can be divided into three systems: the gas-handling system, the argon-ion laser, and the detection and data collection system. Each system and its components will be described in the following paragraphs.
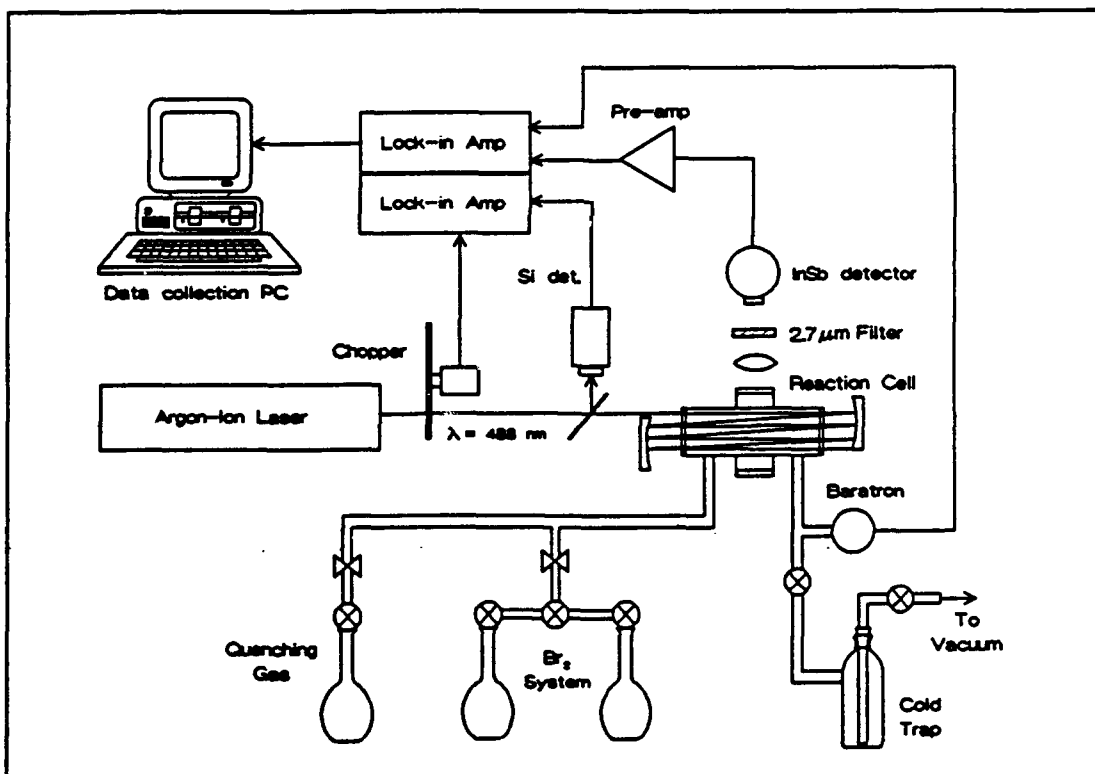

Figure 3.1. Experimental Apparatus

Gas-Handling System

The gas-handling system is illustrated in Figure 3.2 and is comprised of four subsystems: the bromine source, the mixing manifold, the reaction cell, and the vacuum assembly. All subsystems are plumbed together with 1/2 in. outside diameter (OD) in-line glass stopcock valves and 1/2 in. OD stainless steel flex-tube. Plumbing components are joined with Cajon Ultra-Torr fittings. Each subsystem is described in detail in the following paragraphs.
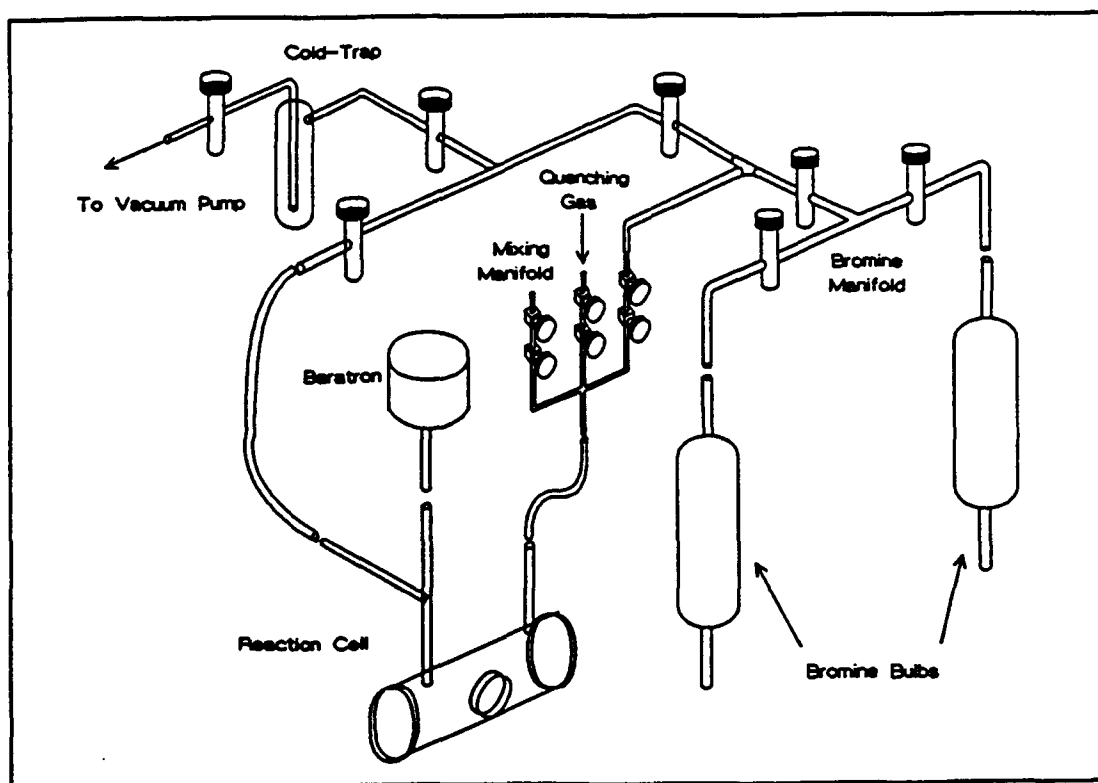

Figure 3.2. Gas-Handling System

Bromine Source. The bromine source consists of two glass bulbs, 2.75 in. OD and approximately 15 in. long, connected with Ultra-Torr fittings to a valve assembly as shown in Figure 3.2. Two bulbs are required for vacuum distillation of the bromine. The distillation procedure will be described in a later chapter. The valve assembly allows transfer of the bromine vapor to the mixing manifold, the vacuum assembly, or between the two bulbs.

Mixing Manifold. The mixing manifold is designed for controlled mixing of up to three different gases within the reaction cell. The manifold is constructed of 1/4 in. OD stainless steel tubing connected with SwageLok fittings. There are three inlet lines and one outlet line. Each inlet line is fitted with a Nupro 1/4 in. stainless steel ball valve followed by a Nupro 1/4 in. stainless steel needle valve. The ball valves provide positive cutoff of gas flow and the needle valves allow precise control of gas flow. In this experiment only two of the inlets were required: one for bromine, and one for a selected quenching gas. The outlet line is attached to the inlet tube of the reaction cell via a 1/4 in. OD stainless steel flex-tube and Ultra-Torr fittings.

Reaction Cell. The reaction cell is constructed of 2 in. OD glass tubing, approximately 4 in. long. Pyrex windows, 1/4 in. thick and 2 in. dia. are cemented to the open ends of the cell. Two, 1 in. diameter openings are

made along opposite sides of the cell such that flat, circular windows can be attached. A 1 in. dia., 0.2 in. thick calcium fluoride (CaF$_2$) window (Oriel Model 43371) is mounted to one of the openings with Torr-Seal compound to permit observation of the 2.7μm Br* emission. CaF$_2$ provides approximately 90% transmission over a spectral range of 150 nm to 9 μm. A 1 in. dia., 1/8 in. thick Pyrex window is attached to the opposite opening with Torr-Seal compound.

Two, 1/2 in. OD glass tubes extend from the top of the reaction cell to allow for gas flow through the cell. The short, inlet tube is attached to the mixing manifold as previously described. The longer, outlet tube includes a sidearm for coupling to the vacuum assembly. The other end of the outlet tube is attached to a capacitance manometer (MKS APS 302W Series Baratron) for monitoring reaction cell pressure.

Vacuum Assembly. The vacuum assembly consists of a liquid nitrogen (LN2) cooled cold trap followed by a vacuum pump (Varian Model SD 200 pump station). The cold trap is included to prevent bromine vapor from reaching the pump oil and causing damage to the vacuum pump. It also increases the overall vacuum of the system. A valve is placed at the inlet of the cold trap and another valve is placed between the cold trap and vacuum pump to facilitate removal of the cold trap without shutting down the pump.

The pump station includes a diffusion pump followed by a roughing pump. Initial vacuum checks indicated there was no need for the diffusion pump and it was bypassed. The outlet of the vacuum pump is connected to the exhaust duct in the laboratory and is vented outside of the building.

Argon-Ion Laser

A Spectra Physics Model 164 argon-ion laser provides the radiation necessary to photodissociate molecular bromine and create a detectable amount of Br*. The laser is rated at 1.3 watts continuous wave (CW) at a wavelength of 488 nm. It incorporates a prism and highly reflective flat mirror in a stable optical assembly to facilitate the required single-frequency operation at 488 nm wavelength. A laser power meter and feedback control system in the laser power supply reduces power fluctuations in the laser output and permits long operating times with stable output power.

The 1.2 mm dia. laser beam is passed through an optical chopper (Stanford Research Model SR540) where it is amplitude modulated at 371 Hz for subsequent synchronous detection. A small amount of the beam is split off via a glass microscope slide and is directed into an optical detector for monitoring power fluctuations. The remaining beam propagates through the reaction cell, along the axis of the cell. Metallic mirrors are placed on either side of the reaction cell as shown in Figure 3.1, and are adjusted to

direct the laser beam several times back and forth through the cell.

Detection and Data Collection System

Two optical detectors and lock-in amplifiers, a capacitance manometer and a Zenith 248 personal computer (PC) comprise the detection and data collection system. Basically, three signals are measured and recorded: the intensity of Br* emission, the relative argon-ion laser intensity, and the total gas pressure in the reaction cell. The following paragraphs will describe each component in detail.

Br* Signal Detection. Figure 3.3 depicts the components making up the Br* detection system. As previously described a CaF_2 window is mounted to one side of the reaction cell, transverse to the laser beam, to permit observation of the 2.7 μm Br* emission. This radiation is collected through a combination of two CaF_2 lenses: a 1 in. dia., 50 mm focal length (f) lens, followed by a 2 in. dia. f=100 mm lens. The small lens is placed approximately 50 mm from the axis of the laser beam. The larger lens is placed 50 mm away from the small one, along the same axis. This lens combination was found, through experimentation, to maximize the collection of the weak 2.7 μm radiation.
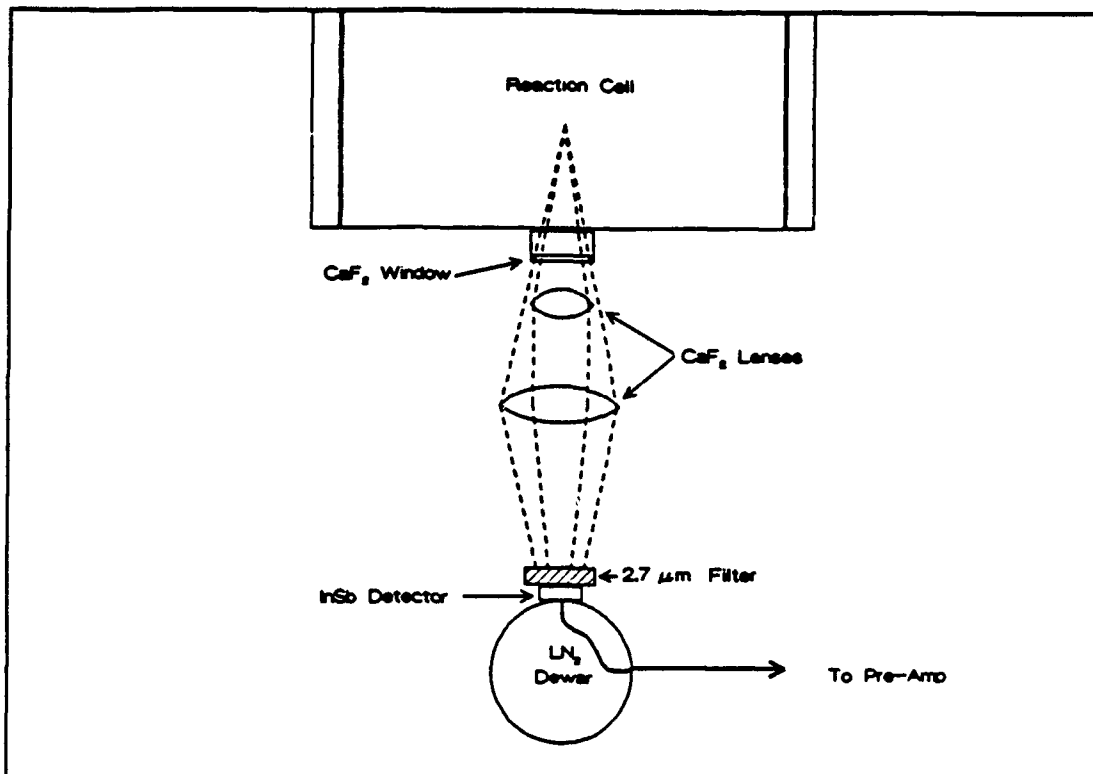
Figure 3.3. Br* Detection System

An EG&G Judson Model J10D indium antimonide (InSb)
detector is placed approximately 100 mm behind the large
CaF_2 lens to detect the Br* signal. The detector is
photovoltaic and generates a current proportional to the
intensity of the photons absorbed. It has a detection range
of 1 to 5 μm. A sapphire window is included in front of the
detector and provides about 60% transmission of 2.7 μm
radiation. The InSb detector is mounted in a vacuum dewar
and is operated at LN2 temperature (77° K). The dewar
package is mounted to an X-Y-Z translation stage to allow
adjustment of detector position for signal optimization. A
2.7 μm bandbass filter with a full-width half maximum (FWHM)

45

bandwidth of 92.6 nm is placed directly against the sapphire window of the InSb detector package. The filter is required to eliminate unwanted background radiation outside of the region of interest and to improve signal-to-noise ratio.

The optical components, detector assembly, and reaction cell are enclosed in a black painted cardboard box to reduce the amount of stray light incident on the detector. A black opaque cloth is draped over the top of the box as well to completely seal the enclosure from room lights.

The weak current signal from the InSb detector is applied to the input of an EG&G Judson Model PA-9 two-stage preamplifier. The first stage provides a transimpedance gain of 1×10^5 V/A. The second stage provides additional gain of 10 V/V. The resultant voltage signal is applied to the input of a Stanford Research Model SR510 lock-in amplifier.

The SR510 performs a phase detection of the voltage signal representing the Br* emission intensity, against the reference frequency of the optical chopper. This provides substantial improvement in the signal-to-noise ratio by reducing signals not modulated by the reference frequency. The SR510 also provides up to 4 analog-to-digital (A/D) inputs for signals from other sources. In addition, all functions of the lock-in can be computer-controlled via an RS-232 interface. These features are fully exploited and are described in the section on data collection.

Detection of Laser Radiation. Approximately 15% of the
argon-ion laser beam is split-off and directed into an EG&G
Model SGD-100A photodiode to provide a relative indication
of laser output and a means of monitoring power fluctuations
in the output. Additionally, a 488 nm bandpass filter with
a bandwidth of 1 nm FWHM is placed in front of the detector
to facilitate tuning of the laser to the 488 nm line. The
output of the detector is applied to the input of an EG&G
Princeton Applied Research (PAR) Model 5301 lock-in
amplifier for phase detection against the reference
frequency of the optical chopper. The 0 to 10 V output
signal from the lock-in is connected to one of the A/D
inputs of the SR510 for subsequent recording.

Cell Pressure Measurement. As previously described, a
capacitance manometer (baratron) is attached to the outlet
tube of the reaction cell for the purpose of monitoring
total gas pressure within the cell. Two baratrons are made
available: a 0 to 10 torr unit (MKS 122AA-00010AB), and a 0
to 100 torr unit (MKS 122AA-00100AB). The pressure range
required is dependent upon the type of experiment being
performed and will be revealed in a later section. In
either case, the 0 to 10 V output of the selected baratron
is a linear representation of the measured pressure and is
applied to a second A/D input on the SR510 lock-in amplifier
for subsequent recording.

Data Collection. Data collection is performed on a Zenith 248 PC running a software package designed for, and included with the SR510 lock-in amplifier. The software essentially functions as a data recorder, displaying and recording up to 3 different signals from the SR510 into data arrays. The data arrays can be further processed and stored to disk as files.

In this particular configuration, the signals recorded are: the voltage output of the SR510, representing the Br* emission intensity, the voltage output of the baratron, representing the cell pressure, and the voltage output of the PAR lock-in amplifier, representing the argon-ion laser intensity. Under software control, all 3 signals are digitized by the SR510's internal A/D converter and are transmitted to the computer's memory via the RS-232 serial interface. A sample rate of 5 Hz is selected, allowing up to 880 seconds of recorded data for each channel. Further data reduction is required and is described in a later chapter.

This completes the description of the experimental apparatus. A detailed discussion of experimental procedures will follow in the next chapter.

IV. Experimental Procedures

Introduction

This chapter describes the procedures followed in obtaining data from the experiments. First, some preliminary procedures are described; tasks that are performed only once in preparation for the experiments. Routine procedures are then described, listing tasks performed on a daily basis to ready the apparatus for experiment. Following that, procedures are discussed for the steady-state production of Br* atoms, and quenching by Br_2. A description of procedures used in recording relative quenching of Br* by other gases is presented next. Lastly, the procedures followed in reducing the data for analysis are described.

Preliminary Procedures

System Leak Check. Prior to flowing any gases in the apparatus, a leak check is performed on the gas-handling system. First, all components in the system are brought to vacuum and the baratron is zero-referenced to the thermocouple gauge on the vacuum pump. The inlet valve on the vacuum assembly is then closed, and the pressure is monitored via the 10 torr baratron. An acceptable leak rate of less than 0.01 torr per minute was observed. After the

initial vacuum check, bromine is loaded into the bulbs and vacuum distillation is performed as described below.

Bromine Operations. Initially, about 20 ml of liquid bromine is poured into one of the bromine bulbs. This operation is performed under a well-ventilated fume hood, and rubber gloves are worn for added protection. The bulb is placed in LN2, and the bromine is frozen. The bulb is then capped and transported, within an LN2-filled dewar, to the apparatus, where it is connected to the bromine manifold. Since the bulb was exposed to atmospheric gases, the bromine must be vacuum distilled.

Vacuum distillation is performed through repeated freeze-thaw cycles, and requires two bromine bulbs as previously described. First, the bulb containing the liquid bromine is frozen in a bath of LN2. Then appropriate valves are opened to permit the evacuation of the bulb via the vacuum assembly. When the pressure reaches near 0 torr, the LN2 is removed and the bulb is allowed warm.

At the first indication of bromine vapor pressure, the valve to the vacuum assembly is closed and the valve between the two bromine bulbs is opened. The empty bulb is then placed in an LN2 bath and the bulb containing the bromine is allowed to return to room temperature. The bromine is drawn into the cooled bulb, leaving unwanted residue in the warmer bulb. Once the transfer is complete, the filled bulb is closed off and the other bulb is evacuated via the vacuum

assembly. This routine is repeated several times to further purify the bromine. The amount of bromine initially loaded was more than enough for all experiments performed and no additional bromine or distillation was required.

Routine Procedures

Laser Operations. The argon-ion laser is turned on and allowed to warm-up for approximately 30 minutes before any measurements are made. After the warm-up, the laser is adjusted for operation on the 488 nm line. This is accomplished by maximizing the signal detected through the 488 nm bandpass filter/SGD-100A detector combination while adjusting the position of the tuning prism/mirror assembly in the laser. Since moving the prism causes a translation in the beam as well, the detectors position is readjusted to maintain maximum signal.

For most experiments, the laser power is adjusted to approximately 800 mW and is maintained to within 0.5% of this value by the feedback control system of the laser. When the laser is not being used for extended periods, the output power is reduced to approximately 30 mW (minimum value) to help prolong the tube life.

Equipment Warm-up. While the laser is stabilizing, all other equipment is powered up and allowed to stabilize for approximately 30 minutes. During this time the dewars for the cold trap and the InSb detector are filled with LN2.

Br* Production and Quenching by Bromine

Initially, the valve between the vacuum assembly and the reaction cell is closed, and a small amount of bromine vapor (5 torr) is allowed to flow into the reaction cell via the mixing manifold. The laser power is adjusted to a nominal value of 800 mW, and the InSb detector is positioned for maximum signal indication on the SR510 panel meter (15-20 μV). To increase sensitivity and reduce signal fluctuations due to noise, the SR510s bandpass filter is enabled, and the time constant is set to 3 seconds on the low pass filter. With the Br* signal maximized, the cell is evacuated once again and the computer is set to record data.

To begin data collection, the SR565 data acquisition program is invoked and is commanded to record the cell pressure into the first array, the Br* intensity signal into the second array, and the laser intensity signal into the third array. The sample rate is set to 5 Hz and the recording is started. The Br* signal and the pressure signal are displayed on the computer screen for a visual indication while recording.

With the recorder running, the cell is closed off and the needle valve on the bromine side of the mixing manifold is slowly opened. The bromine flow rate is adjusted to approximately 0.1 torr per second and is allowed to flow until the total cell pressure equals or exceeds 10 torr, the maximum range of the baratron. At this point the recorder

is stopped and the data arrays are saved as a file to the hard disk for further processing. The vacuum valve is opened and the cell is again evacuated. This procedure is repeated several times to ensure good correlation between data sets.

Br* Quenching Experiments

The gas selected for the quenching experiment is connected to the second inlet of the mixing manifold via 1/4 in. OD teflon tubing (line) and a gas regulator valve. The regulator is set for minimal pressure in the line. The valve at the regulator end is closed, the ball valve and needle valve at the manifold end are opened, and the line is evacuated to near zero torr. The vacuum valve is then closed, along with the ball valve and needle valve, and the regulator valve is opened to permit the quenching gas to fill the teflon line. This fill/purge routine is repeated twice to remove contaminants in the quenching gas plumbing.

The flow rate is now set for the quenching gas. The vacuum valve is closed, the ball valve on the mixing manifold is opened, and the needle valve is adjusted to allow approximately 0.1 torr per second of gas flow into the cell. The position of the micrometer on the needle valve is noted, and the ball valve and needle valve are closed.

With the flow rate setting determined, the mixing manifold and reaction cell are again evacuated. First, the

ball valve on the mixing manifold is closed. The needle
valve on the manifold, and the vacuum valve between the cell
and cold trap are then opened to bring the system to vacuum.
This evacuates the system up to the outlet of the ball valve
on the manifold and prevents "leakage" of the quenching gas
through the needle valve. Once evacuated, the needle valve
on the manifold is set to the position recorded earlier for
the desired flow rate.

As described earlier, the Br* signal is again
maximized. The vacuum valve is closed off and about 5 torr
of bromine vapor is allowed to flow into the reaction cell.
The laser power is increased to the nominal setting of 800
mW and the InSb detector is positioned to maximize the Br*
signal indicated on the SR510. With this accomplished, the
cell is once again evacuated and then refilled with 5 torr
of bromine.

The data acquisition software is now invoked and set
to record the cell pressure, the Br* signal, and the laser
intensity signal at the 5 Hz rate. The program is started
and about 30 seconds of data is recorded to provide an
initial value of Br* signal at a constant Br_2 pressure of 5
torr. The ball valve on the mixing manifold is now opened
to allow the quenching gas to flow through the needle valve
into the reaction cell. The recording is continued until
the Br* signal is reduced significantly by the quenching,

and/or the total cell pressure reaches the limit of the baratron (usually 100 torr).

When the limit is reached, the ball valve and needle valve controlling the quenching gas are shut and the recording is continued for another 30 seconds. The recording is then stopped, and the data for the entire run is displayed on the screen. The signal representing the laser power output is checked to see if any significant power fluctuations occurred during the recording. If so, the data is discarded and another run is recorded. The Br* signal data is plotted against the pressure signal data as a quick check of the quenching observed. The data is then stored to disk for further processing.

The procedures outlined here are repeated at least twice for each quenching gas. This gives a minimum of three sets of data for each quenching measurement made.

Data Reduction

The data recorded for all experiments are stored in binary files by the data acquisition software. In order to perform the analysis outlined in Chapter II, further processing of the quenching data is required.

Initial processing of the data is accomplished by the data acquisition software. The binary file for a data run is read into the program and the voltage signal representing the cell pressure is scaled according to the pressure range

of the baratron used. For the 10 torr baratron no scaling
is required. For the 100 torr baratron, the voltage value
is multiplied by 10 to give the actual pressure recorded.
At this point, the processing is dependent upon the type of
data recorded.

For the Br* production and bromine quenching data, no
further processing is required and the data is rewritten to
the file it was retrieved from. For the other quenching
data, the signal representing Br* emission intensity is
displayed and the average initial value is determined. This
is the Br* emission intensity for a constant Br_2 pressure of
5 torr and no quenching gas present, as described in Eq
(2.27) with $[Q] = 0$. This value is then divided into the
Br* signal array to normalize the data values. The
resultant normalized array is equivalent to the inverse of
Eq (2.28). Unfortunately the array cannot be inverted by
the data acquisition software to satisfy Eq (2.28). The
inversion must be accomplished in later processing.

The pressure data array is now displayed and the
initial Br_2 pressure is subtracted from the total pressure
values to give a zero baseline. This leaves only the
pressure of the quenching gas in the array. The data arrays
are now rewritten to the file they were retrieved from.

The binary format of data files is difficult to work
with. For this reason the files are converted to an ASCII
(American Standard Code for Information Interchange) format.

A simple conversion routine was written in the C programming language to convert the files. A listing of the program is included in Appendix A.

Further processing of the data is required in order to complete the analysis. For the Br* production and bromine quenching data, the Br* signal array and the cell pressure array must be inverted to satisfy Eq (2.23) in the analysis. For the other quenching data, the Br* signal array must be inverted. A simple MathCAD program was written to perform the required inversion and rewrite the files for subsequent plotting and fitting. A listing of the program is included in Appendix A.

A graphics presentation program call Slidewrite is used to create plots of the quenching data. It is also used to perform a least-squares fit to the data. The quenching data is also passed through a program written in BASIC to determine the uncertainties in the slope and intercept values for each plot. This BASIC program is listed in Appendix A.

This completes the description of the procedures followed in the quenching experiments and the required data reduction. The next chapter will present the results of the experiments.

V. Results

Introduction

This chapter details the observations made during the experiments and the analysis made on the data collected. First, the results of two initial observations are presented: the determination of the absorption cross section for Br_2, and the determination of the percent of dissociation. Next, the results of the Br* production and bromine quenching experiments are given with an emphasis on other mechanisms contributing to the process. Finally, the results of the quenching of Br* by molecular and atomic collision partners are revealed. The data from all measurements are plotted and made available in Appendix B.

Absorption Cross Section

A simple experiment was run to determine the absorption cross section of Br_2 at a wavelength of 488 nm. The mirrors on either side of the reaction cell were blocked so the laser beam could make a single pass through the cell. A second SGD-100A detector was placed in the apparatus to monitor the laser radiation transmitted through the cell. This signal was attenuated to match the output of the original SGD-100A detector with no gas present in the cell.

The ratio of the two detector signals was recorded as a function of increasing bromine vapor pressure. This

measurement was repeated two more times. Figure 5.1 shows
one of the plots of I/I_0 versus Br_2 pressure.
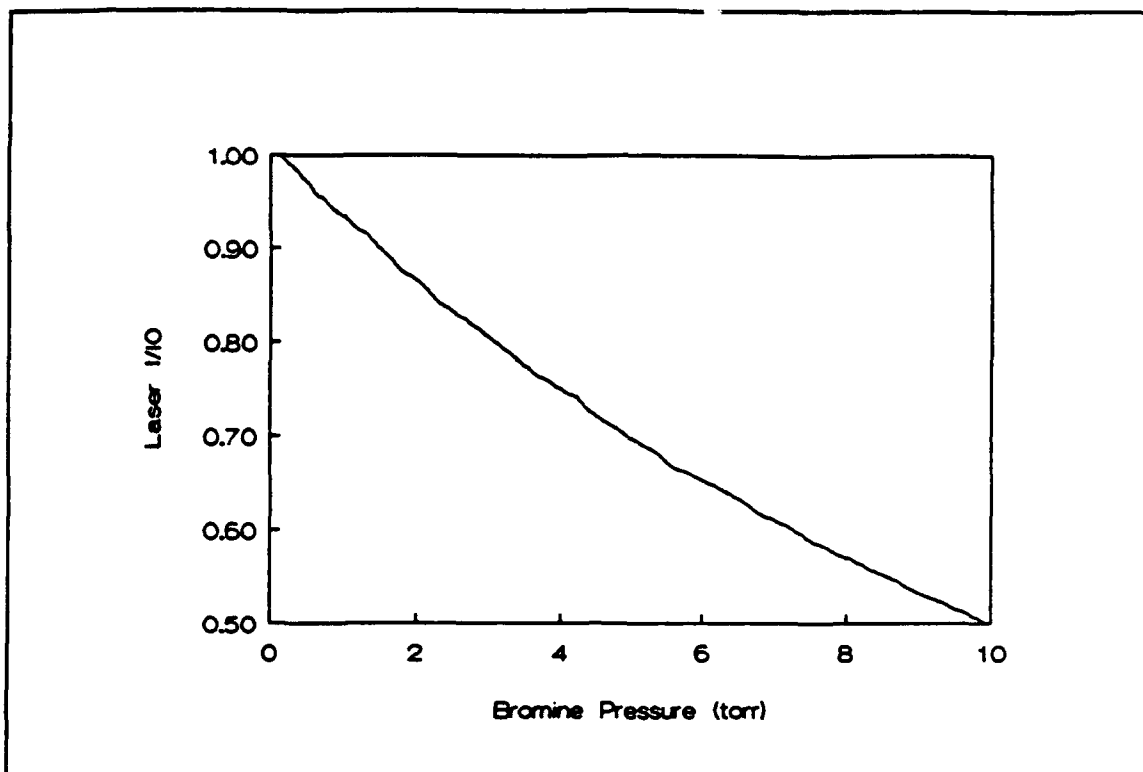
Figure 5.1. I/I_0 versus Bromine Pressure

The data was reduced by solving Eq (2.13) for σ, the
absorption cross section in cm^2. This was accomplished with
a linear fit to a plot of the log of I/I_0 versus Br_2
pressure as shown in Figure 5.2. The value of σ is
determined from the slope of the line. A temperature of
$300^\circ K$ was assumed, and pathlength $l = 10$ cm was used.

$$\sigma \ (cm^2) \ = \ \ln\frac{I}{I_0}\frac{1}{l(3.22 \times 10^{16})P_{Br_2}} \tag{5.1}$$
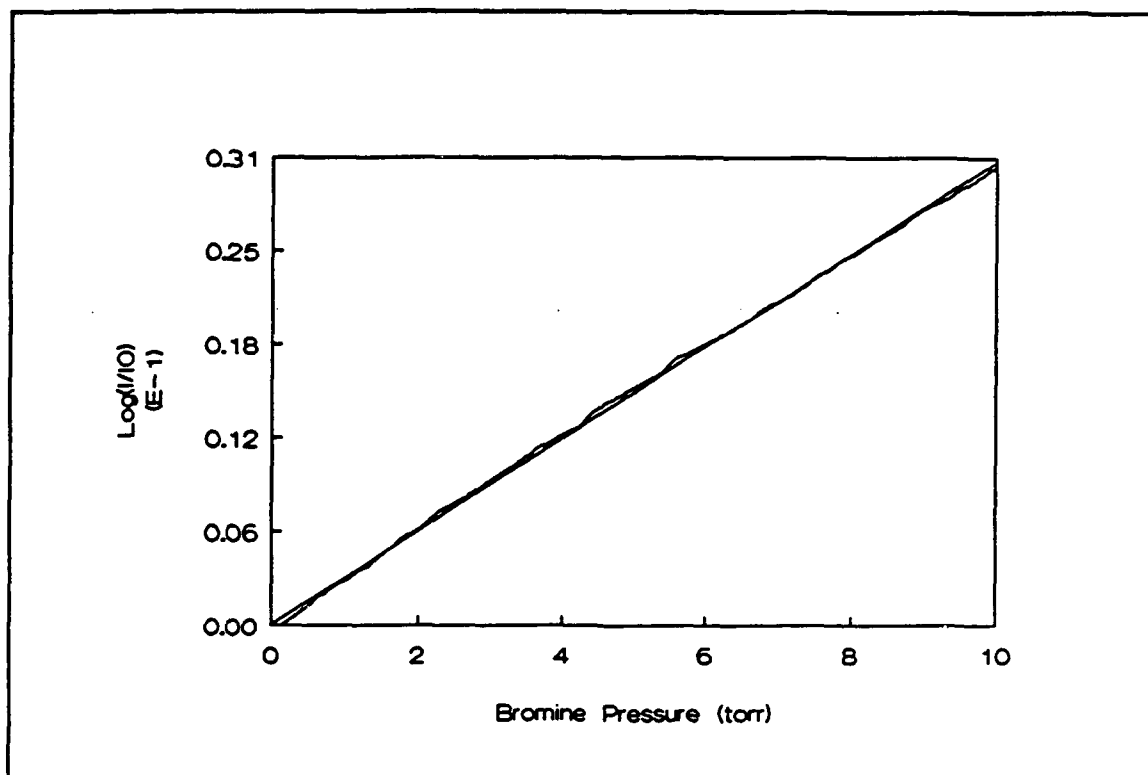
Figure 5.2. Log(I/I_0) versus Br_2 Pressure

Table 5.1 lists the values of σ obtained for each set of data, and the mean value within one standard deviation. The mean value is compared to a previous value obtained by Seery and Britton for a wavelength of 490 nm (20:2264).

TABLE 5.1

Absorption Cross Section of Br_2
at a Wavelength of 488 nm

Measured Values (10^{-19} cm^2)	Mean Value (10^{-19} cm^2)	Previous Value (10^{-19} cm^2)
0.91		
0.94	0.93 ± 0.01	1.55 ± 0.01
0.92		

The percent of Br_2 dissociated was determined by recording the change in bromine vapor pressure within the cell as the laser was turned on and off. An initial pressure of 5 torr of bromine was used. An average increase of 1.9% above the initial pressure was recorded when the laser was unblocked. This increase is attributed to Br* atom production, with 1.9% of the bromine being dissociated.

Br* Production and Quenching by Molecular Bromine

Initially, the Br* emission signal was difficult to locate. After several hours of making changes in optical alignment, detector position, bromine pressure, and lock-in parameters, the signal was finally located and maximized. It was found that the detector had to be mounted in a stable X-Y-Z translation stage to permit precise alignment. The lenses were placed in the configuration described in Chapter III, and the SR510 lock-in bandpass filter had to be engaged to permit stable operation in the μV signal range. Multiple passes of laser light through the cell were not necessary and the mirrors were blocked for all measurements. Signal levels from 15 to 20 μV were obtained from 5 torr of bromine vapor and 800 mW of laser output power.

Figure 5.3 is an example of the data taken during this series of experiments. Three different runs were recorded with t..e bromine pressure in the cell being slowly ramped from 0 to 10 torr. An unexpected trend is indicated in all the plots. As the pressure is increased beyond about 6

torr, the Br* emission signal begins to drop off. This is
not predicted in the analysis give by Eqs (2.21) and (2.22).
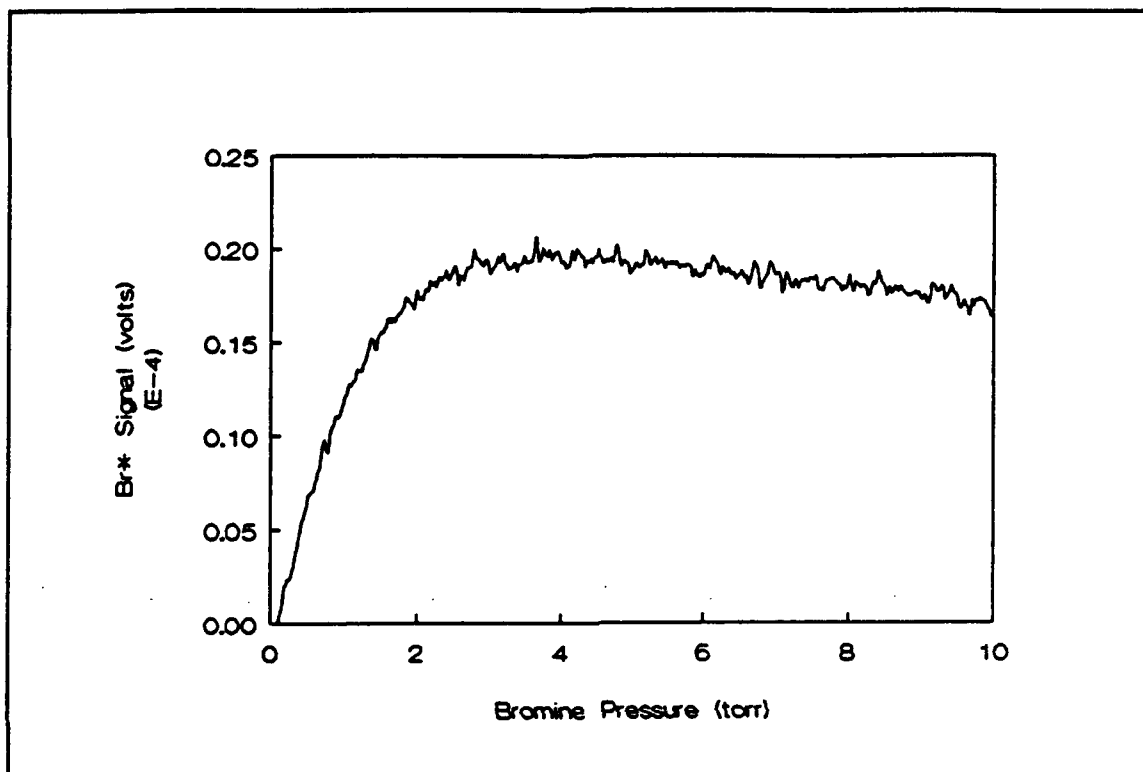
Figure 5.3.   Br* versus Br$_2$ Pressure

A simple explanation can be made for this behavior.
The pump rate coefficient, k_p in Eqs (2.17) through (2.22)
is assumed to be constant. In other words, the number of
Br* atoms produced is linearly proportional to the intensity
of the laser. The intensity of the laser however, is not
constant at the point of observation, 5 cm into the cell.
The beam propagates along a 5 cm path of bromine vapor,
being absorbed as predicted by the Beer-Lambert law given in
Eq (2.13). This implies that k_p is a function of bromine
vapor pressure and can be written as

$$k_p = Ce^{-kPl} \qquad (5.2)$$

where

C = constant of proportionality

k = absorption coefficient (torr^{-1} cm^{-1})

P = Br$_2$ vapor pressure (torr)

l = absorption pathlength (cm)

Using l = 5 cm, and the value of 0.003 for k, converted from the experimentally determined value for σ, results in Eq (2.21) being rewritten as:

$$I = K\frac{CPe^{-(0.015)P}}{k_0 + k_{Br_2}P} \qquad (5.3)$$

where

P = Bromine pressure (torr)

k_{Br_2} = quenching rate coefficient (torr^{-1} sec^{-1})

Taking the inverse of Eq (5.3) and rearranging gives:

$$\frac{1}{I}e^{-(0.015)P} = \frac{k_0}{K}\frac{1}{P} + \frac{k_{Br_2}}{K} \qquad (5.4)$$

where

K = KC (combined proportionality constant)

63

The right side of Eq (5.4) is the same as Eq (2.24), an equation of a line. The left side Eq (5.4) is the inverse intensity multiplied by a decreasing exponential function of pressure.

A plot of the inverse intensity versus inverse pressure for one of the data sets is represented in Figure 5.4. The data values for the inverse intensity were multiplied by the exponential function of pressure to reduce the curvature evident at large values of P (small values of 1/P). A linear regression analysis is made on the data, and the slopes and intercepts, along with their respective uncertainties, are calculated. These values are presented in Table 5.2 for all three data sets.
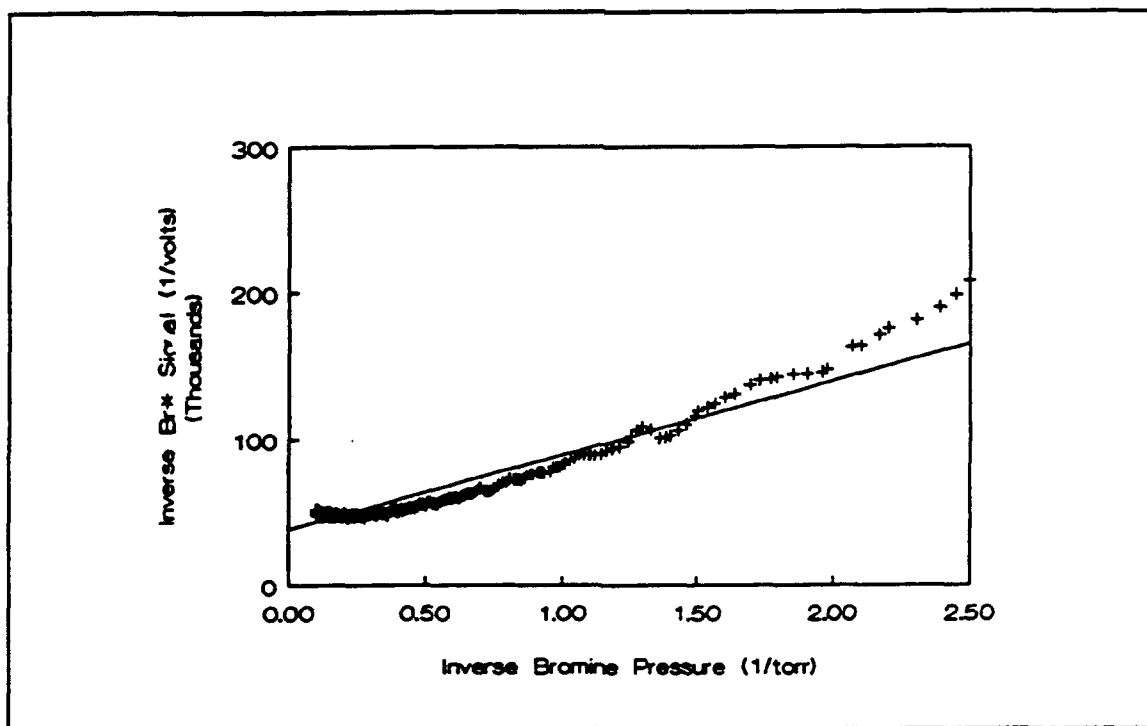
Figure 5.4. 1/I versus 1/P

TABLE 5.2

Least-squares Fit to Br* Data

Test No.	Slope $(x10^3)$	Slope Uncertainty $(x10^3)$	Intercept $(x10^3)$	Intercept Uncertainty $(x10^3)$
1	83.84	1.01	34.76	0.51
2	68.13	7.84	38.67	0.38
3	50.62	6.00	38.78	0.30

A mean value of $6.75x10^4$ for the slope, and $3.74x10^4$ for the intercept are determined from the above data. Using the relation given by Eq (2.26)

$$\frac{b}{m} = \frac{k_{Br_2}}{k_0} \tag{2.26}$$

where m is the slope and b is the intercept, gives

$$\frac{k_{Br_2}}{k_0} = 0.55 \pm 0.14 \ (torr^{-1}) \tag{5.5}$$

Using the value of 0.89 sec^{-1} (1:234) for the radiative rate k_0, results in $k_{Br_2} = 0.49$ $(torr^{-1} \ sec^{-1})$ or

$k_{Br_2} = 1.52x10^{-17}$ $(cm^3 \ molec^{-1} \ sec^{-1})$. This rate is about 4 orders of magnitude smaller than the most recent measured rate of $0.48x10^{-12}$ $(cm^3 \ molec^{-1} \ sec^{-1})$ (11:317). This large difference in rate coefficients cannot be accounted for in

65

the simple analysis presented and implies that another
mechanism, such as wall deactivation, is removing Br* atoms.

An attempt was made to fit the equation

$$y = e^{a/x}(bx + c) \tag{5.6}$$

to the data represented in Figure 5.4, where

$$y = \frac{1}{I}; \quad x = \frac{1}{[Br_2]}; \quad a = \sigma l; \quad b = \frac{k_0}{K}; \quad c = \frac{k_{Br_2}}{K}$$

The fit to the measured data was improved, but the value
obtained for a was an order of magnitude larger than the
expected value determined earlier and the values obtained
for b and c did not agree with those shown in Table 5.2. A
more elaborate model is required to account for effects of
wall deactivation and diffusion in the data.

What can be deduced from the Br* production data is an
optimum pressure for the production of Br* atoms. For all
remaining quenching experiments, the Br_2 pressure will be
maintained at 5 torr. This permits a simpler analysis of
the relative quenching by other gases as described in Eq
(2.29).

Quenching of Br* by Other Gases

The quenching of Br* by SF_6, CO_2, O_2, N_2, and the rare
gases He, Ne, Ar, Kr, and Xe was investigated with quenching

rate coefficients determined relative to quenching by the parent molecule. The results for SF_6, O_2, and N_2 are presented first, followed by an analysis of the unexpected CO_2 results. Lastly, the rare gas quenching results will be discussed.

Figure 5.5 shows a typical plot of the quenching data obtained for one of the diatomic gases (Oxygen). This data was reduced further, as described in Chapter IV, to give the linear relationship shown in Figure 5.6. A linear regression analysis is made on the data and the slope and intercept, along with their respective uncertainties, are determined. The slope values are multiplied by the Br_2 pressure of 5 torr to give the relative quenching rate coefficients.
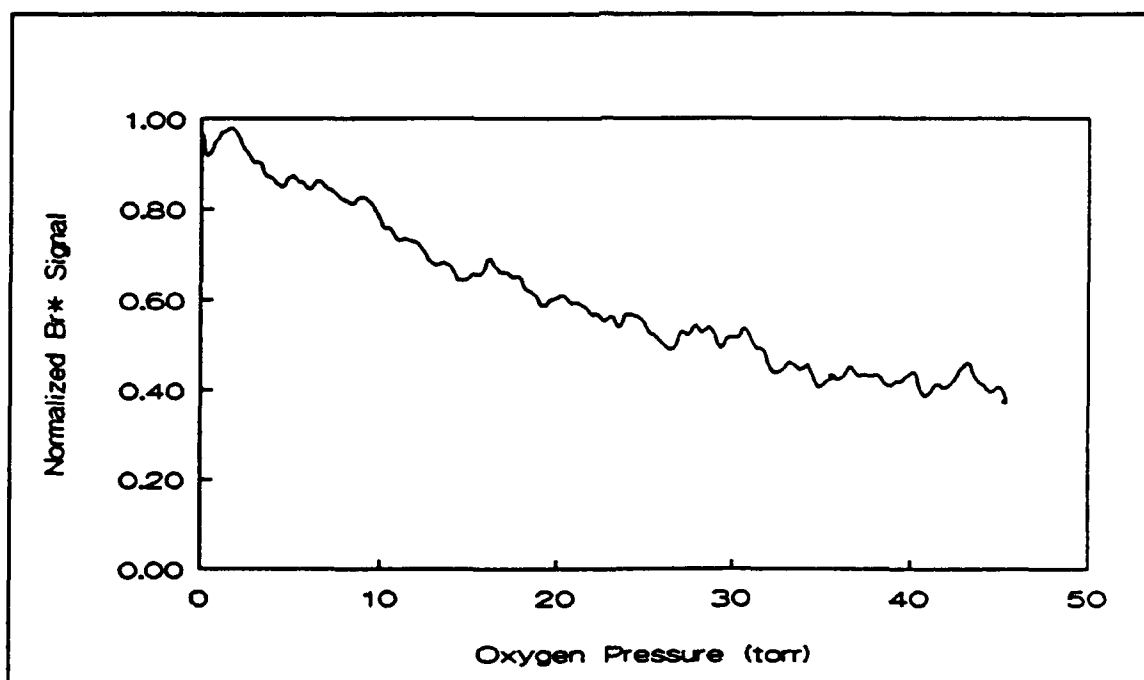
Figure 5.5. O_2 Quenching of Br*
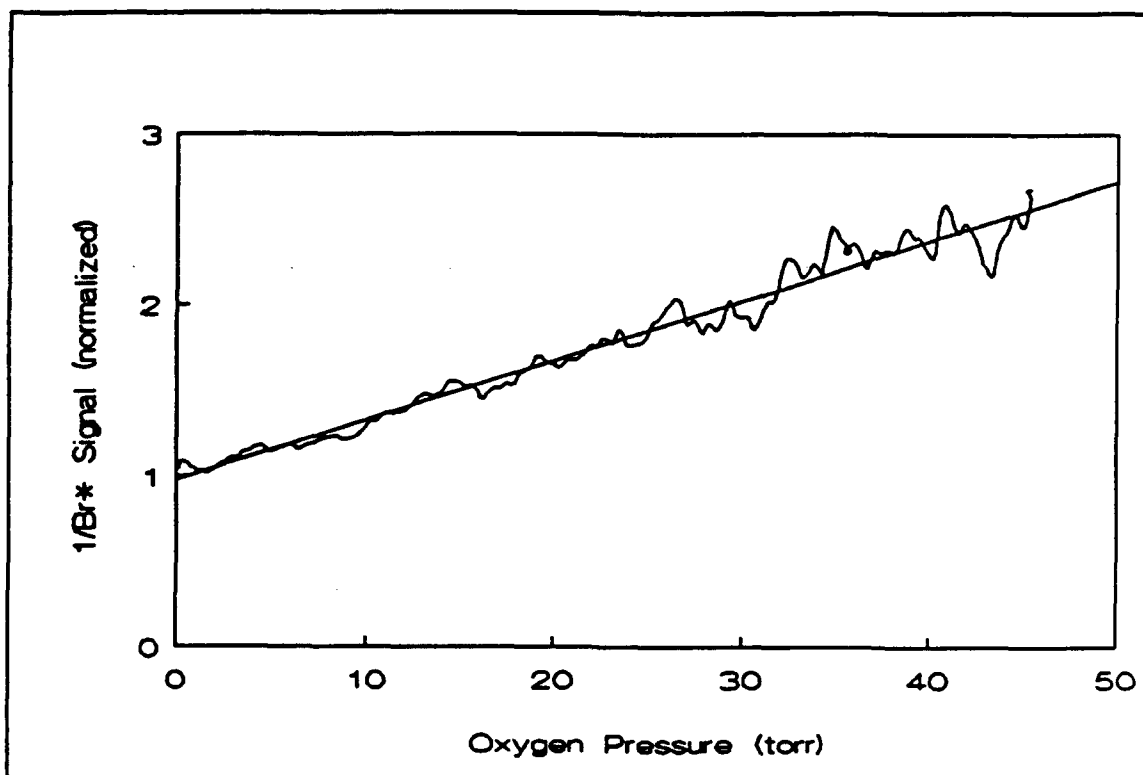
Figure 5.6.   1/Br* Normalized vs O_2 Pressure

Sulfur Hexafluoride, Nitrogen, and Oxygen.   Table 5.3
lists the relative quenching rate coefficients determined
for SF_6, N_2, and O_2 from the slope of the linear regression
analysis of the inverse Br* signal data.   The relative rates ·
are obtained from the weighted average of the slopes for
each series of tests and are given within 1 standard
deviation.   Results of the linear regression analysis are
given in Appendix B.   The known purities of the gas samples
are also shown in Table 5.3.

TABLE 5.3

Relative Quenching Rates for SF_6, N_2, and O_2

Gas Sample	Purity (%)	Relative Rate
SF_6	99.900	9.22 ± 1.11
N_2	99.999	1.95 ± 0.15
O_2	99.994	0.18 ± 0.05

It is made evident that quenching by SF_6 is over 5 times greater than quenching by N_2, and quenching by O_2 is nearly an order of magnitude less than quenching by N_2. The relatively fast quenching by SF_6 suggest a possible E→V transfer to one or more vibrational modes of the large molecule. A quick comparison of rate coefficients taken from Table 1.1 reveals that the recently measured rate for O_2 (17:15) is about 4 orders of magnitude slower than the previous measurement for O_2 (4:514), and about 1/2 the rate previously measured for N_2 (4:514). The relative rates reported here lend support to the slower absolute rate for O_2 and suggests that the N_2 rate is faster than what was previously determined.

Carbon Dioxide. The spin-orbit relaxation of Br* by CO_2 is perhaps the most studied and best known E→V transfer mechanism (8:4454;18:305;21:15). The total quenching rate coefficient has been determined by several different experimental methods and is consistently reported as 15 ± 1

$x10^{-12}$ (cm^3 $molec^{-1}$ sec^{-1}) (8:4458;18:306;21:15). It was intended in this thesis to use the CO_2 quenching rate as a "baseline" for all other relative rate measurements. By measuring the CO_2 quenching relative to Br_2 quenching and using the literature value for the CO_2 rate, a rate coefficient could be determined for Br_2. This would allow all subsequent quenching rate measurements to be reported relative to the CO_2 rate. A limitation in the apparatus did not permit this.

Figure 5.7 is a plot of the normalized detected emission signal as a function of CO_2 pressure. As indicated, the detected signal increases nearly an order of magnitude as the CO_2 pressure is increased to about 0.5 torr. Further increases in CO_2 pressure results in the steady decrease of the emission signal.

Prior investigations have determined that the a near-resonant E→V transfer occurs bet en the Br* atom and the (10^01) and possibly the (02^01) tional modes of CO_2 (19:1051). Transitions from the (10^01) and (02^01) states terminating on the (00^00) level are allowed and result in strong molecular fluorescence centered at 2.69 and 2.77 μm respectively (10:274). A fraction of this fluorescence is obviously passing through the 2.7 μm bandpass filter and is overwhelming the initial Br* emission signal as indicated in the above plot. As the CO_2 pressure is increased, a self-quenching of the fluorescence is observed resulting from

collisional deactivation by $CO_2(00^00)$ via V→V transfer
(5:2285).
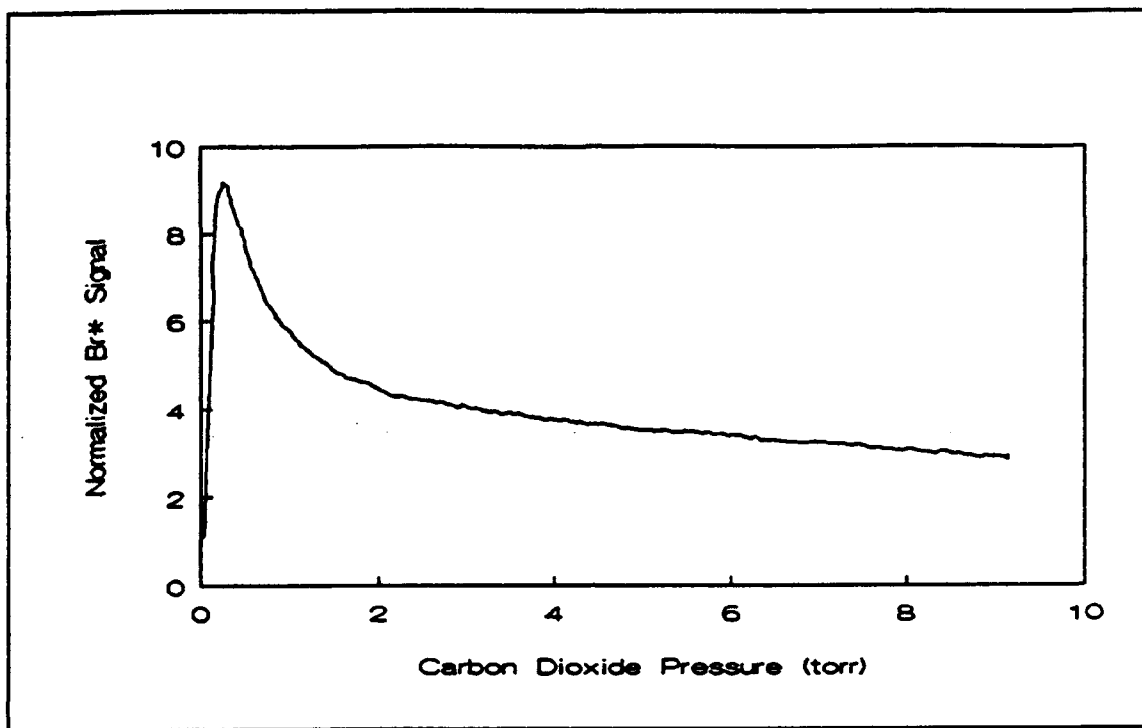
Figure 5.7. Detected Signal vs CO_2 Pressure

A simple kinetic scheme was proposed in an effort to describe and possibly fit a curve to the CO_2 data (17:1). The following set of equations were proposed:

$$Br_2 + h\nu \xrightarrow{k_p} Br + Br^*$$

$$Br^* \xrightarrow{k_0} Br + h\nu$$

$$Br^* + Br_2 \xrightarrow{k_1} Br_2 + Br$$

$$Br^* + CO_2 \xrightarrow{k_2} Br + CO_2^\dagger \qquad (5.7)$$

$$CO_2^\dagger \xrightarrow{k_3} CO_2 + h\nu$$

$$CO_2^\dagger + Br_2 \xrightarrow{k_4} CO_2 + Br_2$$
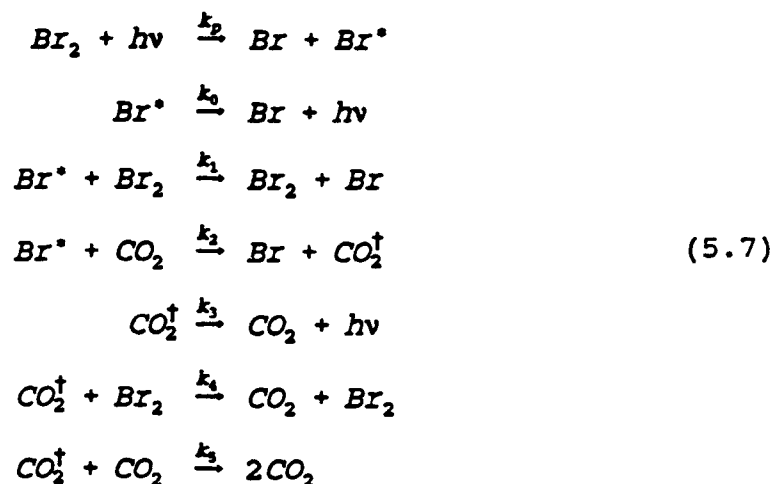
$$CO_2^\dagger + CO_2 \xrightarrow{k_5} 2CO_2$$

From the above kinetic equations, two time-dependent equations can be written for $[Br*]$ and $[CO_2{}^\dagger]$.

$$\frac{d[Br^*]}{dt} = k_p[Br_2] - k_0[Br^*] - k_1[Br_2][Br^*] - k_2[CO_2][Br^*] \qquad (5.8)$$

and

$$\frac{d[CO_2^\dagger]}{dt} = k_2[Br^*][CO_2] - k_3[CO_2^\dagger] - k_4[Br_2][CO_2^\dagger] - k_5[CO_2][CO_2^\dagger] \qquad (5.9)$$

Setting Eqs (5.8) and (5.9) to zero (steady state) and solving for $[Br*]$ and $[CO_2{}^\dagger]$ gives

$$[Br^*] = \frac{k_p[Br_2]}{k_0 + k_1[Br_2] + k_2[CO_2]} \qquad (5.10)$$

and

$$[CO_2^\dagger] = \frac{k_2[Br^*][CO_2]}{k_3 + k_4[Br_2] + k_5[CO_2]} \qquad (5.11)$$

72

The intensity of the signal observed is assumed to be proportional to the sum of the individual intensities such that

$$I = C_1 [Br^\bullet] + C_2 [CO_2^\dagger] \qquad (5.12)$$

Substituting Eqs (5.10) and (5.11) into Eq (5.12) and dividing the result by I_0 (Eq (5.12) with $[CO_2] = 0$) gives a 3-parameter nonlinear equation such that

$$\frac{I}{I_0} = \frac{A}{A + [CO_2]} + \frac{B[CO_2]}{(A + [CO_2])(C + [CO_2])} \qquad (5.13)$$

where

$$A = \frac{(k_0 + k_1)}{k_2} [Br_2]$$

$$B = A \frac{C_2}{C_1} \frac{k_2}{k_5}$$

$$C = \frac{(k_3 + k_4)}{k_5} [Br_2]$$

$$\frac{I}{I_0} = \text{normalized detected emission}$$

Several attempts were made to fit Eq (5.13) to the CO_2 data with little success. It was concluded that a more complex model was required to explain the convoluted emission signal and was beyond the scope of this thesis.

Rare Gases. Quenching of Br* by Helium, Neon, Argon, Krypton, and Xenon was investigated, in what is believed to

73

be the first attempt to observe quenching of Br* by the rare gases. The relative quenching rates for the rare gases are presented in Table 5.4 along with the purity of the gas samples used. The relative rates were determined from the weighted average of the slopes and are shown within one standard deviation of error. Values for the slopes and intercepts determined from the linear regression routine can be found in Appendix B.

TABLE 5.4

Relative Br* Quenching Rates
for The Rare Gases

Gas	Purity (%)	Relative Quenching Rate
He	99.999	0.420 ± 0.037
Ne	99.996	0.123 ± 0.002
Ar	99.999	0.208 ± 0.043
Kr	99.997	0.170 ± 0.025
Xe	99.997	0.355 ± 0.01

This completes the results of the experiments. Conclusions are drawn in the next chapter and recommendations are made to enhance future work and to resolve problems encountered during this effort.

VI. Conclusions and Recommendations

Introduction

This section addresses the conclusions reached after performing the experiments and offers recommendations for future work in this area.

Conclusions

A CW argon-ion laser was used to photodissociate gas-phase molecular bromine, producing a detectable amount of spin-orbit excited bromine atoms. The intensity of the 2.7 μm Br* emission was observed as a function of added quenching gas. The rate of quenching by the added gas was determined, relative to quenching by the parent molecule, through a steady-state analysis of the kinetic reactions.

Qualitative conclusions can be formed from the results of the analysis. The quenching due to O_2 was found to be slow, about an order of magnitude less than that attributed to Br_2. This result supports the findings of Taatjes and others (21:15). Quenching by the rare gases was also found to be less than that attributed to Br_2. This was anticipated given the small probability of transition on collision (4:511; 4:514). It would be difficult to go beyond this simple analysis without knowing the absolute rate coefficient for the parent molecule, or at least determining the relative rate due to CO_2.

Although no quantitative information can be obtained from this series of initial experiments, this work has clearly demonstrated the utility of a steady-state quenching analysis. Relative quenching rates can be obtained very quickly and easily in comparison to time-resolved, pulsed-photolysis techniques. Improvements in the apparatus and analysis could lead to more accurate relative rates and possibly determinations of absolute quenching rate coefficients. It is recommended that further work be done in this lucrative area.

Recommendations

Determination of CO_2 Quenching Rate. The inability to observe the relative quenching by CO_2 was detrimental in quantifying any of the other relative quenching rate measurements. Three possible solutions are available. A 2.7 μm bandpass filter with a narrower bandpass would prevent the CO_2 fluorescence from reaching the detector. An absorption cell filled with CO_2 placed between the observation window on the reaction cell and the detector might also prevent the molecular fluorescence from being detected. And lastly, a grating monochromator could be placed in front of the detector and to adjusted to pass only the Br* fluorescence.

Wall Deactivation of Br*. The wall deactivation of Br* atoms could be investigated by placing teflon on the inner

surface of the reaction cell and repeating the Br* emission vs bromine pressure experiments. A comparison of those results with the present results should indicate the effect of wall deactivation relative to quenching by the parent molecule.

Three-Body Recombination. It has been suggested that this third order mechanism could be significant and should be investigated (17:1). One additional equation is required to describe the reaction:

$$Br^* + Br + M \xrightarrow{k} Br_2^\dagger + M \qquad (6.1)$$

where

Br = ground state Br atom

M = collision partner

and

$Br_2^\dagger$ = excited Br_2 molecule

Including Eq (6.1) with Eqs (2.14) and (2.15) and rewriting Eq (2.17) gives

$$\frac{d[Br^*]}{dt} = k_p[Br_2] - k_0[Br^*] - k_1[Br_2][Br^*] \\ - k_2[M][Br^*] - k_3[Br][M][Br^*] \qquad (6.2)$$

Following the same steps presented in Chapter II, Eq (6.2) results in:

$$\frac{1}{I_{norm}} = 1 + \frac{(k_2 + k_3 [Br])}{k_1 [Br_2]} [M] \qquad (6.3)$$

which is similar to Eq (2.29). By varying the bromine atom concentration over a series of test runs, either by changing the laser power or Br_2 concentration, the relative three-body recombination rate could be determined.

Determination of Br_2 Quenching Rate. Using time-resolved pulsed-photolysis techniques discussed in Chapter I, the absolute rate of Br* quenching by Br_2 could be determined for the apparatus. An available excimer-pumped dye laser could be used to photodissociate Br_2, resulting in Br* atoms. The subsequent Br* fluorescence is observed as a function of time and is expected to follow

$$I = I_0 e^{-t/\tau_{obs}} \qquad (6.4)$$

where

$$\frac{1}{\tau_{obs}} = \frac{1}{\tau_{rad}} + k_{Br_2} [Br_2] \qquad (6.5)$$

Plotting $1/\tau_{obs}$ vs Br_2 pressure gives the Br_2 quenching rate as the slope of the line. The intercept of the line gives the radiative rate plus any non-radiative Br*→Br rate such as wall deactivation.

<u>Temperature Dependence of Quenching Rates</u>. The

temperature dependence of the relative quenching rates could

be determined by accurately controlling the temperature of

the gases within the reaction cell. Data would be collected

for a given quenching gas at several different temperatures.

The analysis would look for a functional dependence on

temperature.

Appendix A: Data Reduction Programs

This appendix contains listings of the computer programs used in the data formatting and reduction required to analyze the results of the experiments. The first program is a routine written in C to convert the binary data files into an ASCII format. The next two programs are MathCAD routines used to perform the necessary inversion of the data values. The last program listed is a linear regression routine written in BASIC to fit a line to the experimental data.

```
/*********************CONVERT.C *******************/
/*                                                */
/* Author: Capt R.F. Tate              21 Aug, 1991*/
/*                                                */
/*Purpose:  This program reads files created by the */
/*SR565 software and converts the binary data into  */
/*an ASCII format.  The output file is always 1000  */
/*or less data points, to fit into most plotting    */
/*routines.                                         */
/*                                                  */
/**************************************************/

#include <stdio.h>
#include <conio.h>

FILE *out_file;
FILE *in_file;

char array_data[10];
char in_file_name[20];
char out_file_name[20];

int points, arrays, increment;
float data;
long time_data;
float* data_pointer = &data;
long* time_pointer = &time_data;

main()
    {
    clrscr();
    get_file_name();
    open_files();
    get_points();
    read_data();
    fcloseall();
    }

get_file_name()
    {
    clrscr();
    puts("Enter name of file to be converted.");
    gets(in_file_name);
    puts("");
    puts("Enter name of output file.");
    gets(out_file_name);
    }


open_files()
    {
    if((in_file = fopen(in_file_name, "rb")) == NULL)
        {
        puts("Error opening input file.");
        exit(0);
        }
```

```c
    if((out_file = fopen(out_file_name, "w")) == NULL)
        {
        puts("Error opening output file.");
        exit(0);
        }
    }


get_points()
    {
    int *array_val = (int*)array_data;
    fread(array_data,2,2,in_file);
    points = *array_val - 1;
    arrays = *(array_val +1);
    printf("Number of points in each array: %d\n\n",points);
    printf("Number of arrays:  %d\n\n",arrays);
    if (points <= 1000)
        increment = 1;
    else if (points > 1000 && points <= 2000)
        increment = 2;
    else if (points > 2000 && points <= 3000)
        increment = 3;
    else if (points > 3000)
        increment = 4;
    }

read_data()
    {
    int i,j,k;

/*  point to the top of the data area in the input file  */

    puts("Writing output file...");

    fseek(in_file,184L,SEEK_SET);

    for(i=0,k=0;i<points;k++)
        {
        fseek(in_file,(long)(184+4*i),SEEK_SET);
        fprintf(out_file,"%4d ",k);
        for(j=0;j<arrays;++j)
            {
            fseek(in_file,(long)(points*4*j),SEEK_CUR);
            fread(data_pointer,4,1,in_file);
            fseek(in_file,(long)(184+4*i),SEEK_SET);
            fprintf(out_file,"%e ",data);
            }
        fprintf(out_file,"\n");
        i+=4;        /* print every fourth element */
        }
    }
```

BROMINE.MCD

This MCAD routine performs the required inversion
of the normalized Br* signal and bromine pressure
data. It also multiplies the Br* signal data by the
decreasing exponential function of pressure

Read data file into matrix:

$$M1 := READPRN(infile)$$

Put matrix columns into vectors:

$$y1 := M1^{<0>} \qquad x1 := M1^{<1>}$$

Write Br* and pressure data out without laser
intensity data for plotting routine.

$$WRITEPRN(xyout) := augment(x1,y1)$$

Take inverse of Br* and pressure vectors:

$$y1 := \overrightarrow{\left[\frac{1}{y1}\right]} \qquad x1 := \overrightarrow{\left[\frac{1}{x1}\right]}$$

Multiply through by decreasing exponential term

$$y1 := \overrightarrow{\left[y1 \cdot e^{-0.015 \cdot \frac{1}{x1}}\right]}$$

Write inverted data out to a file:

$$WRITEPRN(invxy) := augment(x1,y1)$$

83

QUENCH.MCD

This MCAD routine processes the Br* quenching data
by taking the inverse of the normalized Br* signal
data and stripping away the laser intensity data.
An output file is written, containing the pressure
data and the inverted normalized Br* signal data.

Read data files into matrix:

$$m1 := READPRN(in1)$$

Convert matrix to vectors:

$$y1 := m1^{<1>} \qquad x1 := m1^{<0>}$$

Take inverse of normalized Br* signal data...

$$y1 := \overrightarrow{\left[\frac{1}{y1}\right]}$$

Write inverse Br* data and pressure data out
to a file for fitting and plotting.

$$WRITEPRN(outfile) := augment(x1,y1)$$

84

```
10 REM **** WEIGHTED LINEAR REGRESSION ROUTINE ****
20 REM **** GPPERRAM 24 NOV 1986 ******************
30 REM **** REVISED 26 SEP91 by RFTATE ************
40 CLS
50 PRINT "WEIGHTED LINEAR REGRESSION ROUTINE"
60 DIM X(800),Y(800)
70 PRINT "WHAT IS THE NAME OF THE FILE?"
80 INPUT F$
90 REM **** ROUTINE TO READ DATA FILE ****
100 OPEN "i",#1,F$
110 INPUT #1,N
120 FOR I=1 TO N:INPUT#1,X(I),Y(I):NEXTI
130 CLOSE#1
140 REM **** SET WEIGHTING TO ONE ****
150 W=1!
160 S1=0!:S2=0!:S3=0!:S4=0!:S5=0!:S6=0!:
170 FOR I=1 TO N
180 S1=X(I)/W^2+S1
190 S2=(X(I)/W)^2+S2
200 S3=Y(I)/W^2+S3
210 S4=(Y(I)/W)^2+S4
220 S5=X(I)*Y(I)/W^2+S5
230 S6=1/W^2+S6
240 NEXTI
250 DELTA=S6*S2-S1^2
260 INTERC=(S2*S3-S1*S5)/DELTA
270 SLOPE=(S6*S5-S1*S3)/DELTA
280 VAR=0
290 FOR I=1 TO N
300 VAR=VAR+(Y(I)-INTERC-SLOPE*X(I))^2/W^2
310 NEXTI
320 VAR=VAR/(N-2)
330 ERRINT=SQR(S2*VAR/DELTA)
340 ERRSLP=SQR(S6*VAR/DELTA)
350 VAR=VAR*S6/N
360 CORR=SLOPE*SQR(DELTA)/SQR(S6*S4-S3^2)
370 REM **** PRINT STATISTICS TO PRINTER ****
380 LPRINT:LPRINT:LPRINT
390 LPRINT:LPRINT " Weighted Linear Regression Routine"
400 LPRINT:LPRINT " File:",F$
410 LPRINT:LPRINT " intercept = ",INTERC
420 LPRINT " uncert = ",ERRINT
430 LPRINT:LPRINT " slope =",SLOPE
440 LPRINT " uncert = ",ERRSLP
450 LPRINT:LPRINT " variance = ",VAR
460 LPRINT " correlation = ",CORR
470 END
```

Appendix B: Experimental Data Plots

This appendix contains all data collected from the quenching experiments. Data are presented in three formats: plots of normalized Br* signal intensity vs quenching gas pressure, plots of inverse normalized Br* signal intensity vs quenching gas pressure, and the results of the linear regression analysis of the data sets.

SF6DATA1
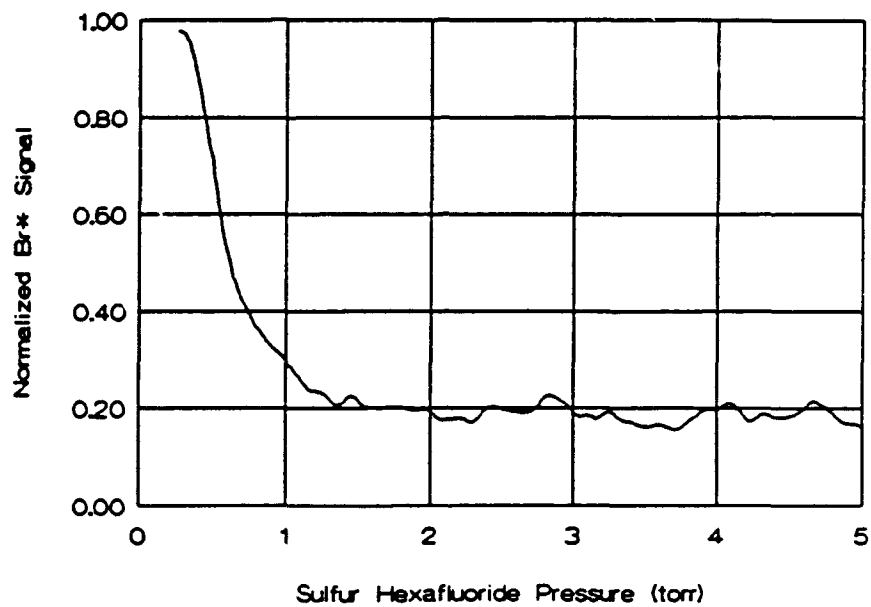
SF6FIT1
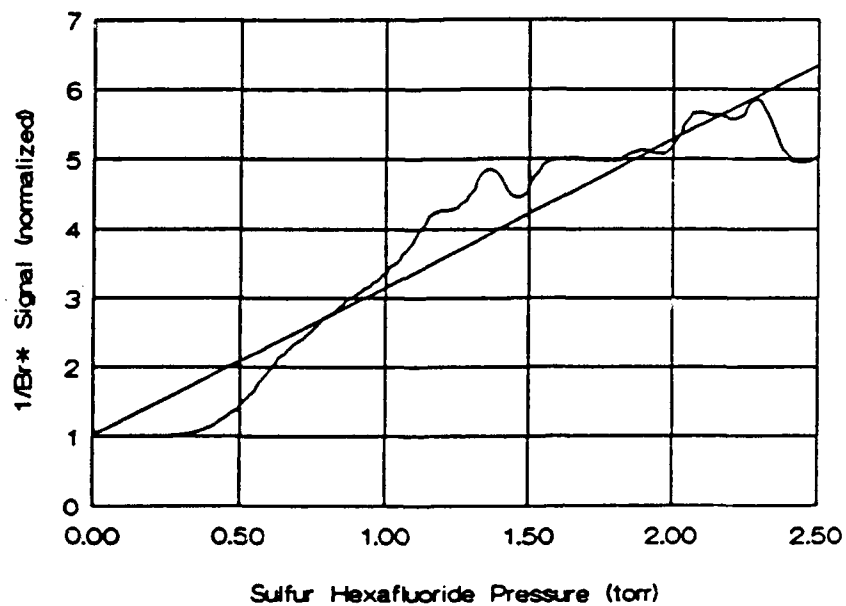
SF6DATA2
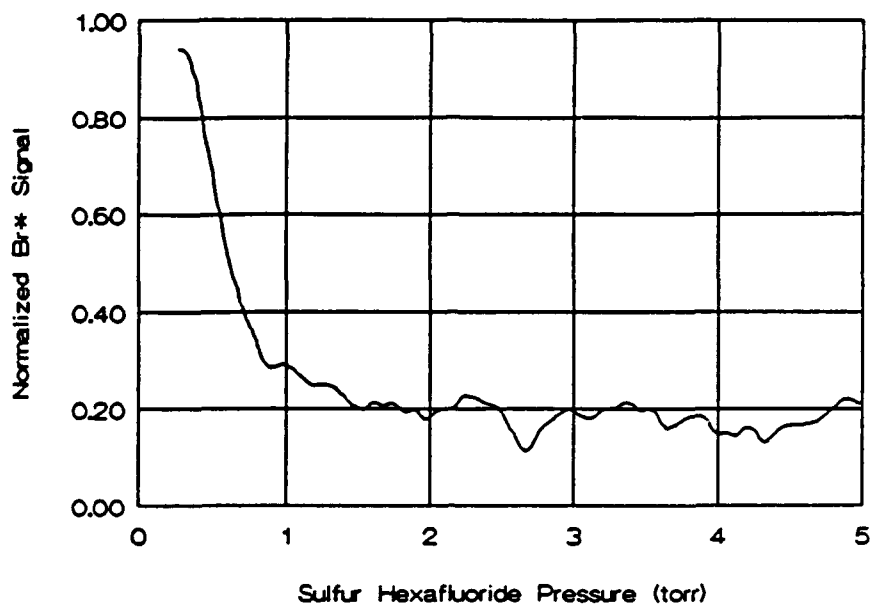
SF6FIT2
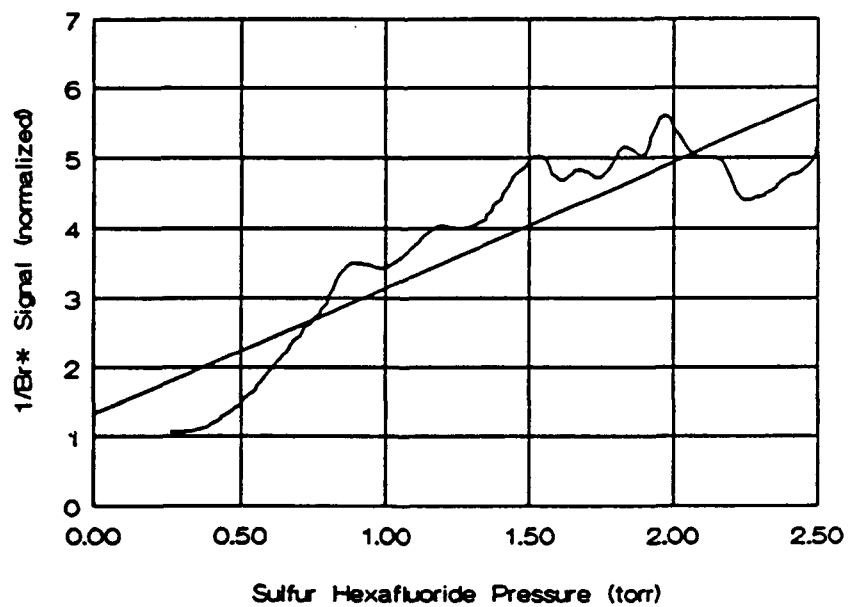
Weighted Linear Regression Routine

File: sf61.prn

intercept =   1.020941
uncert =   .1035663

slope =   2.132204
uncert =   6.772189E-02

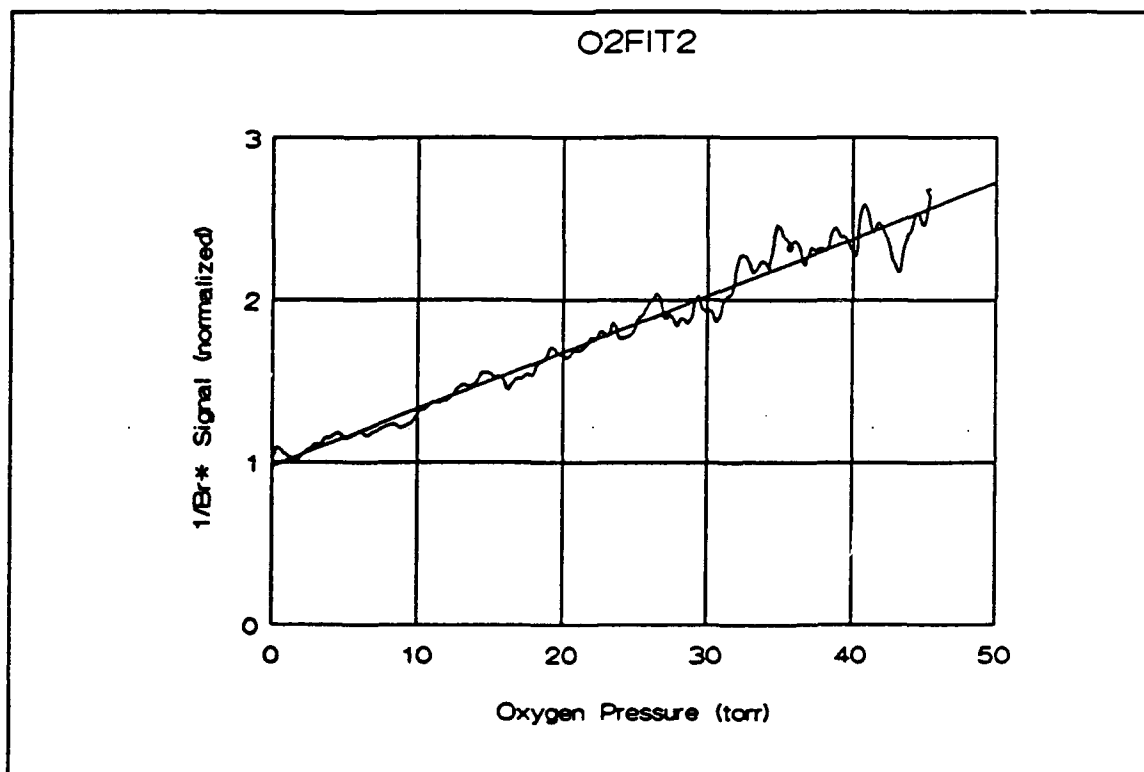variance =   .2825119
correlation = .9340192

Weighted Linear Regression Routine

File: sf62.prn

intercept =   1.322701
uncert =   .1094598

slope =   1.815042
uncert =   7.181484E-02

variance =   .3680415
correlation = .8898117

Weighted Linear Regression Routine

File: sf63.prn

intercept =   1.764661
uncert =   .137692

slope =   1.592669
uncert =   9.016653E-02

variance =   .6665137
correlation = .7860184

N2DATA 1

Normalized Br* Signal vs Nitrogen Pressure (torr)

N2FIT 1

1/Br* Signal (normalized) vs Nitrogen Pressure (torr)
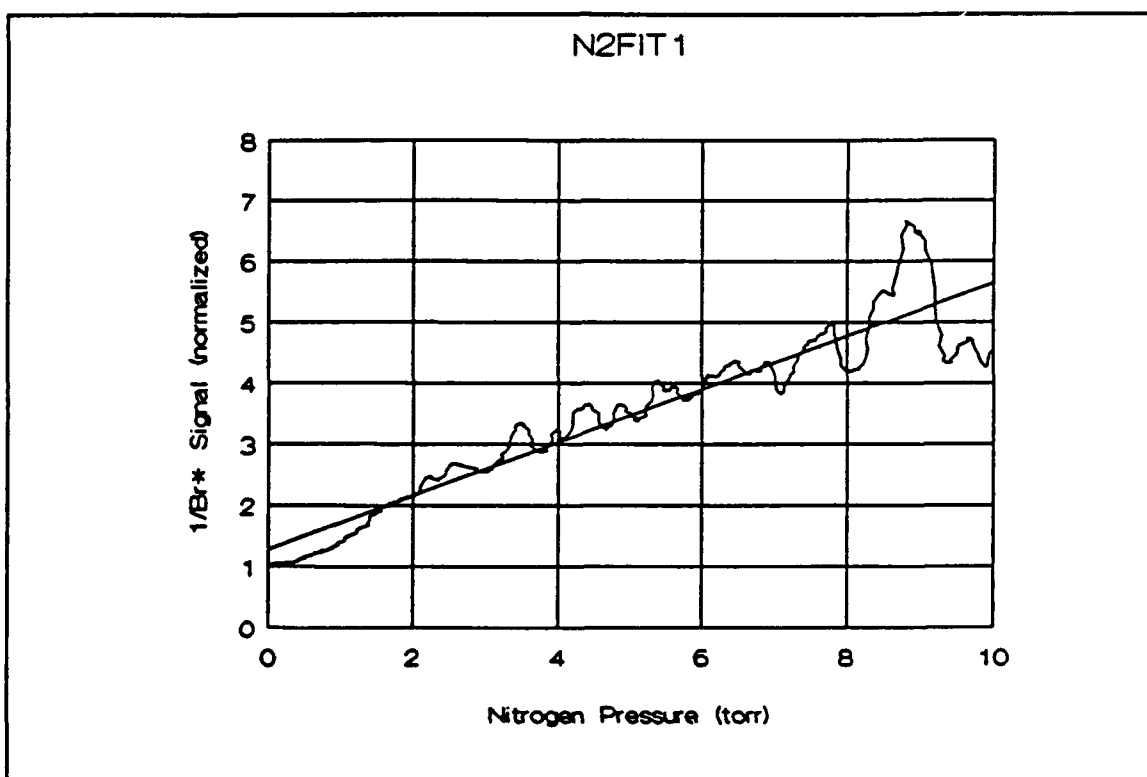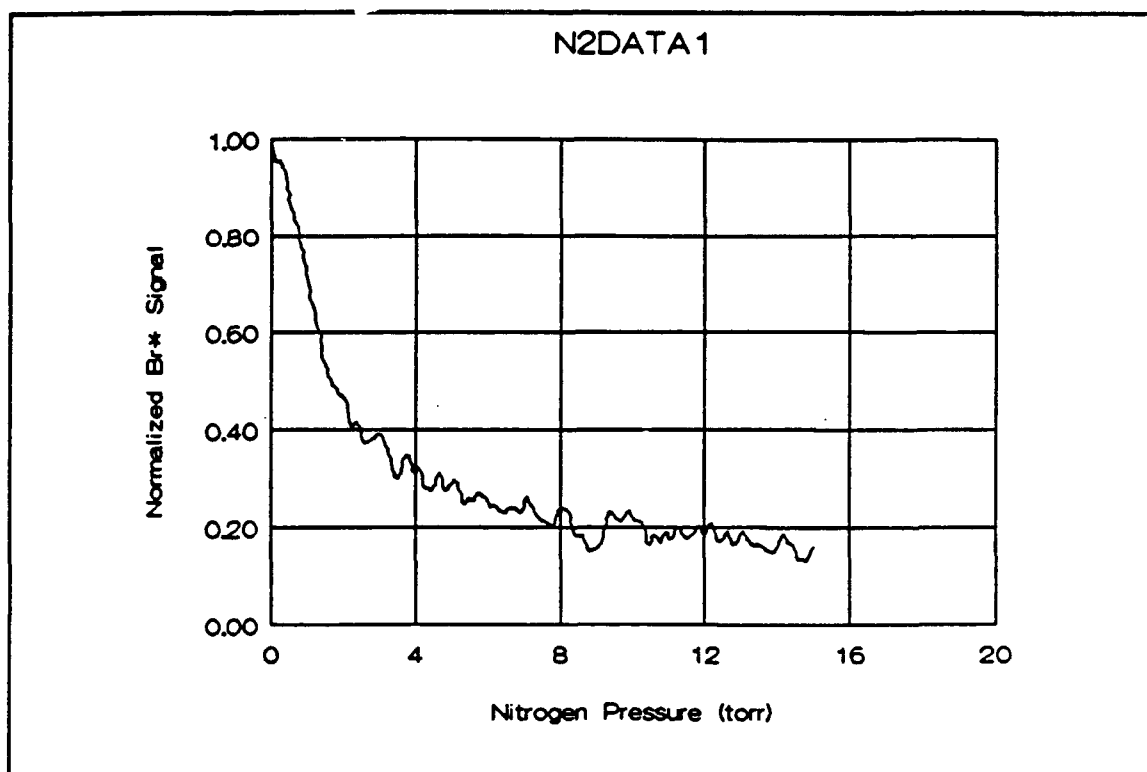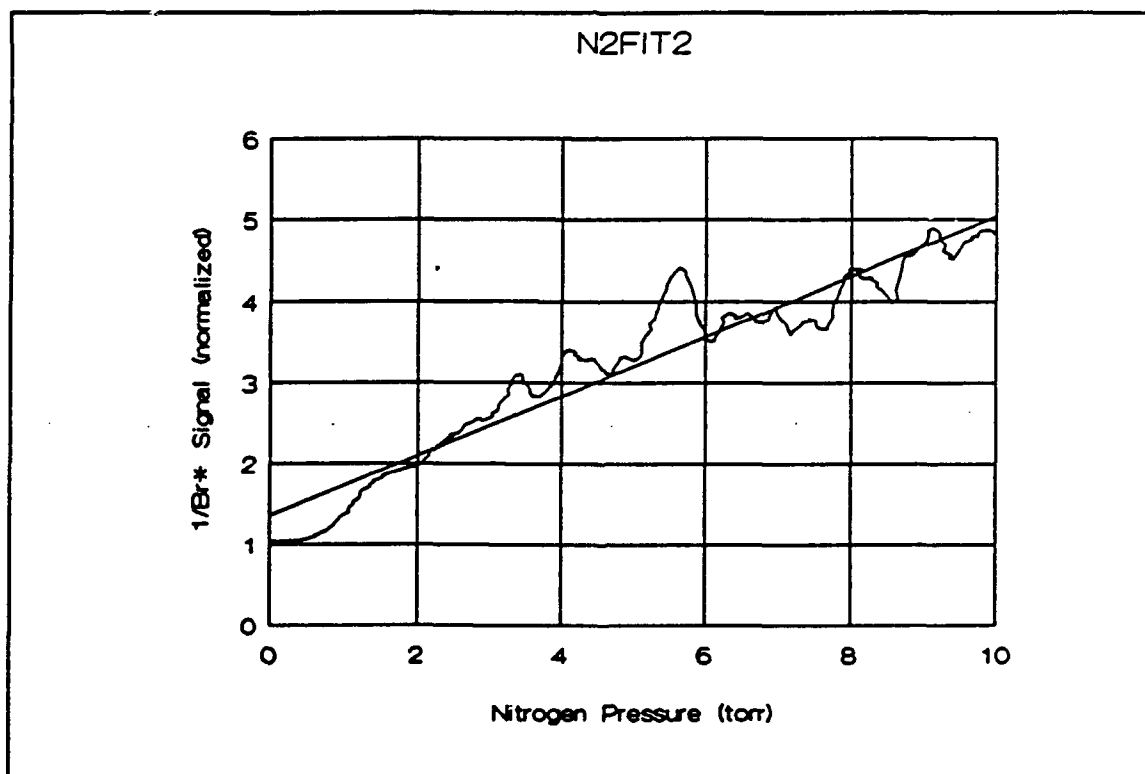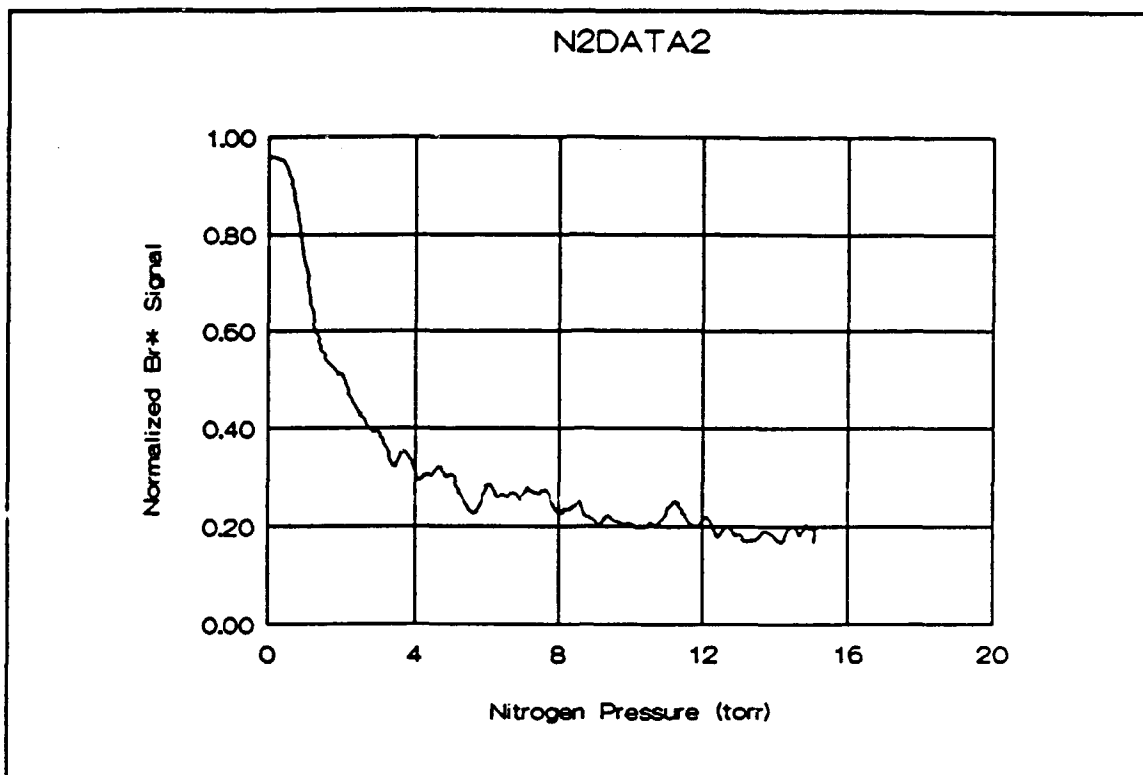
N2DATA2

N2FIT2

N2DATA3
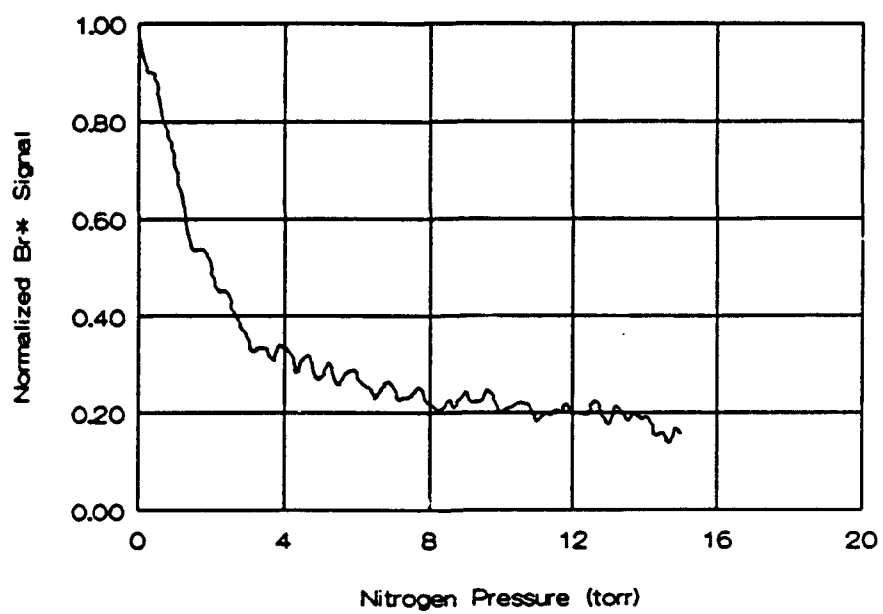
N2FIT3
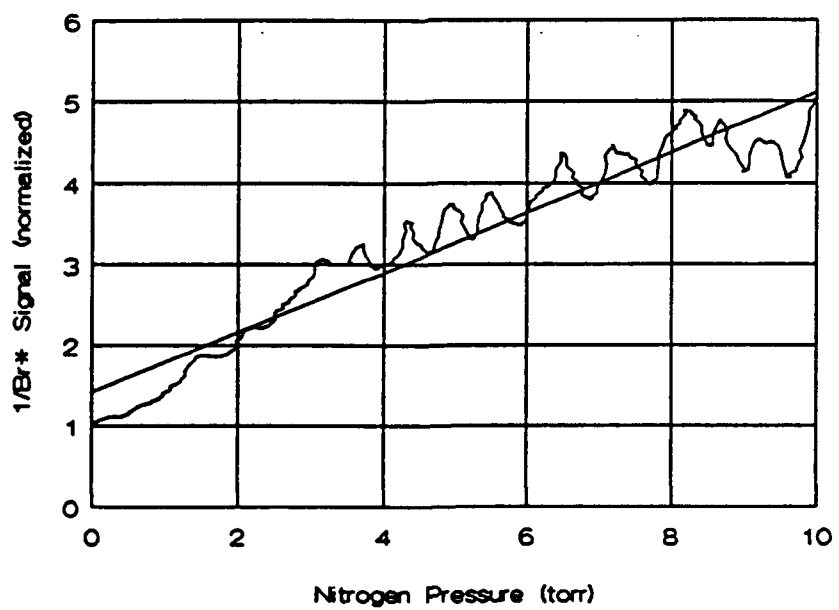
Weighted Linear Regression Routine

File: nitro1.prn

intercept =   1.287363
uncert =   4.884776E-02

slope =   .4354184
uncert =   8.426691E-03

variance =   .2074941
correlation =   .9394917
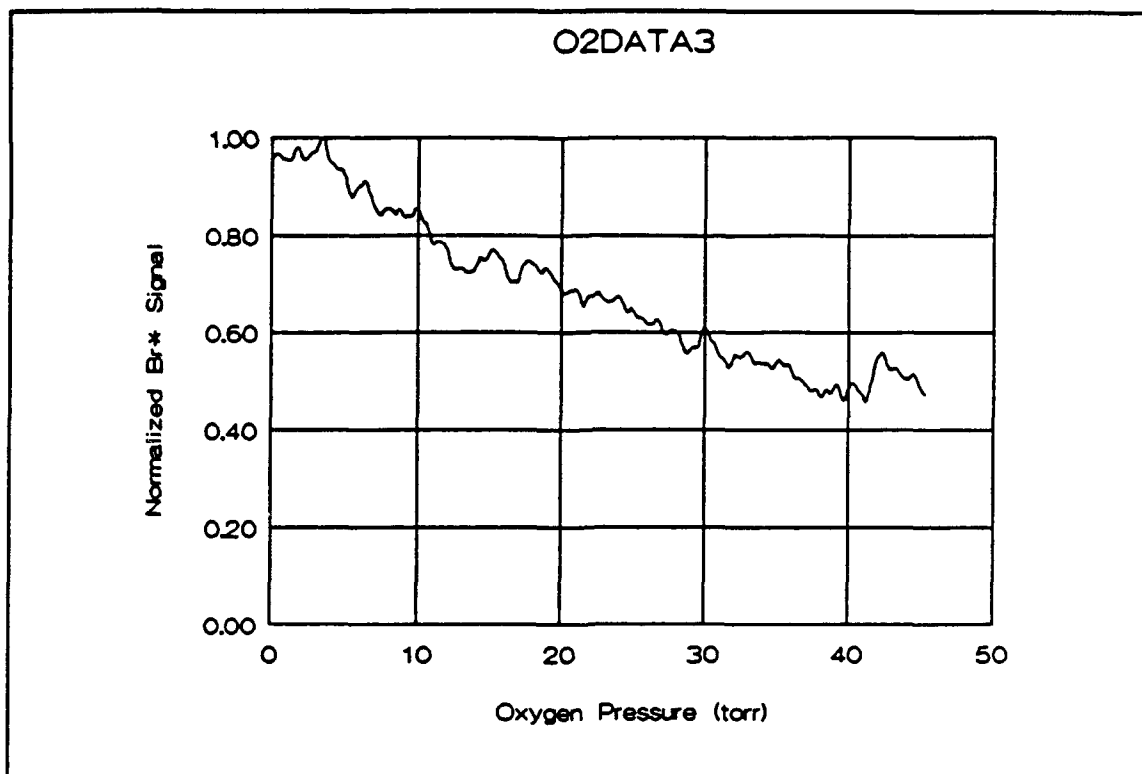

Weighted Linear Regression Routine

File: nitro2.prn

intercept =   1.357175
uncert =   3.724657E-02

slope =   .3685259
uncert =   6.392722E-03

variance = ´   9.954764E-02
correlation =   .9588963

Weighted Linear Regression Routine

File: nitro3.prn

intercept =   1.420926
uncert =   3.519599E-02

slope =   .369119
uncert =   6.066084E-03

variance =   .102652
correlation =   .9572621

O2DATA1

O2FIT1

94

O2DATA2

O2FIT2

95

O2DATA3

Normalized Br* Signal vs. Oxygen Pressure (torr)

O2FIT3

1/Br* Signal (normalized) vs. Oxygen Pressure (torr)

96
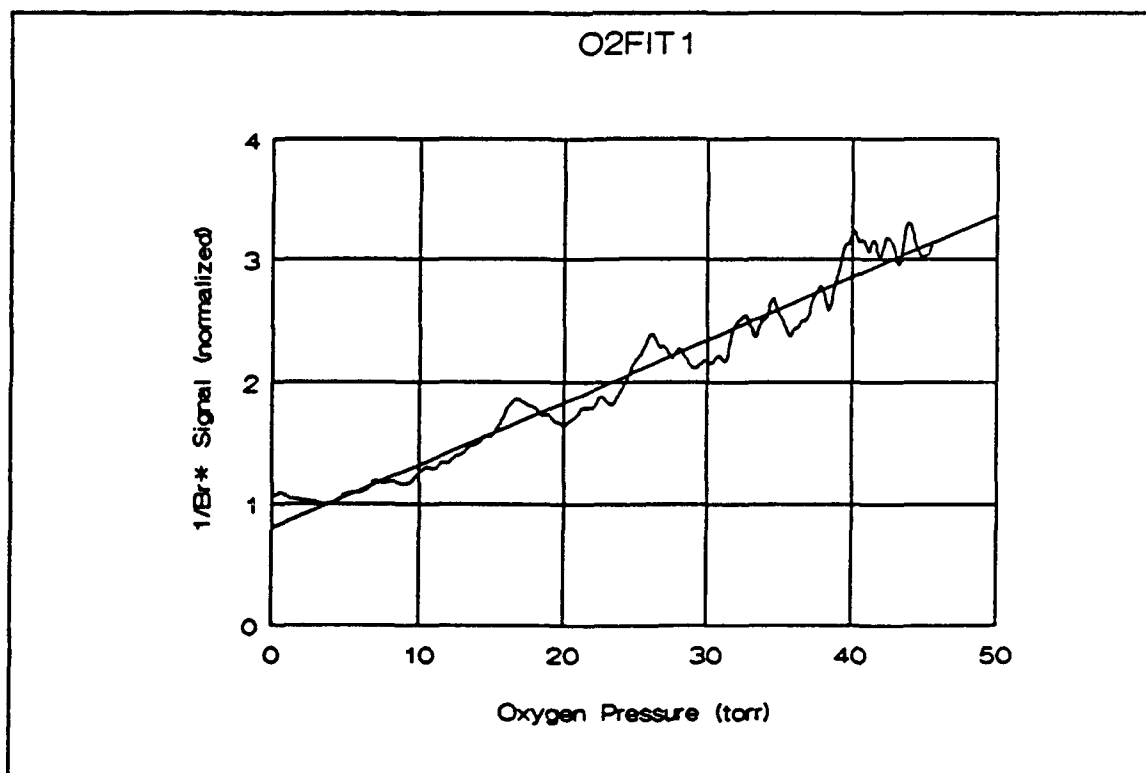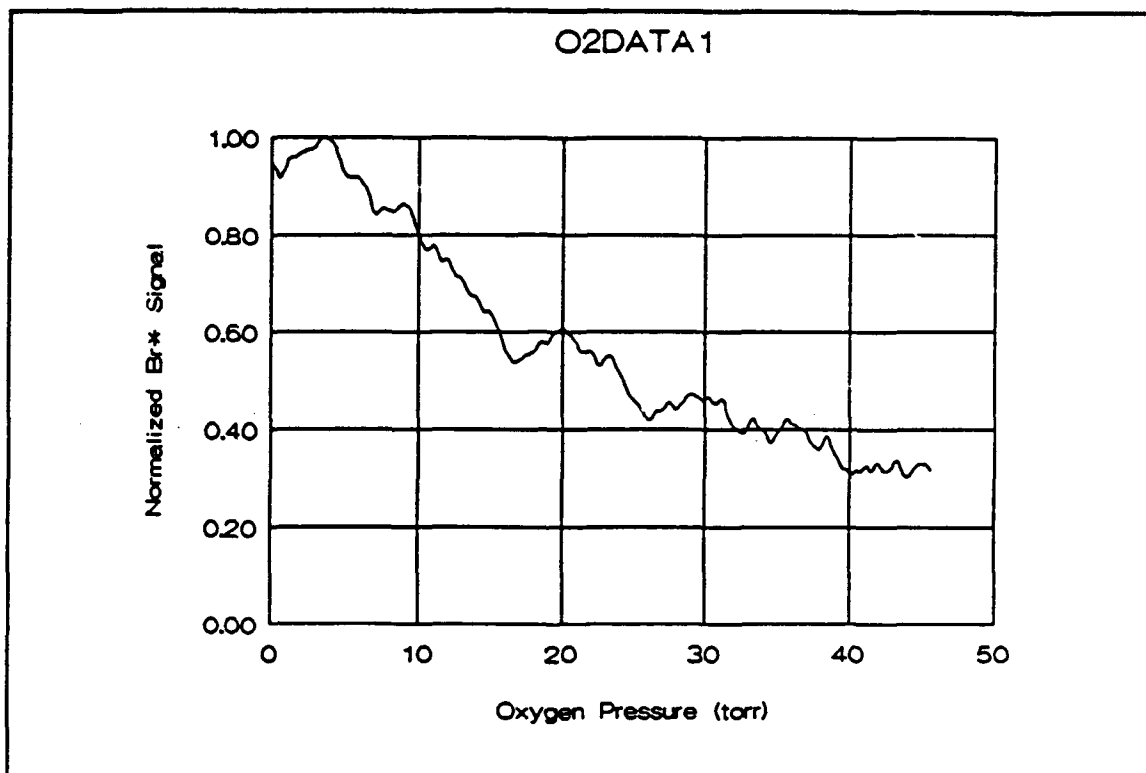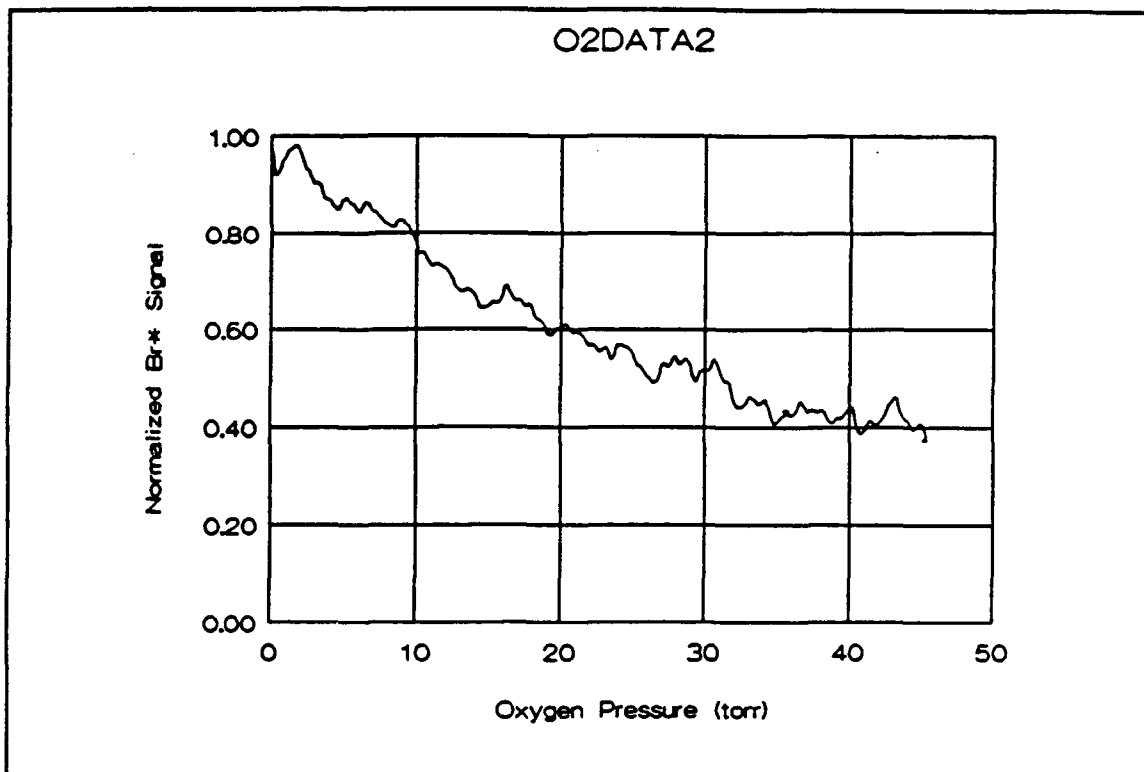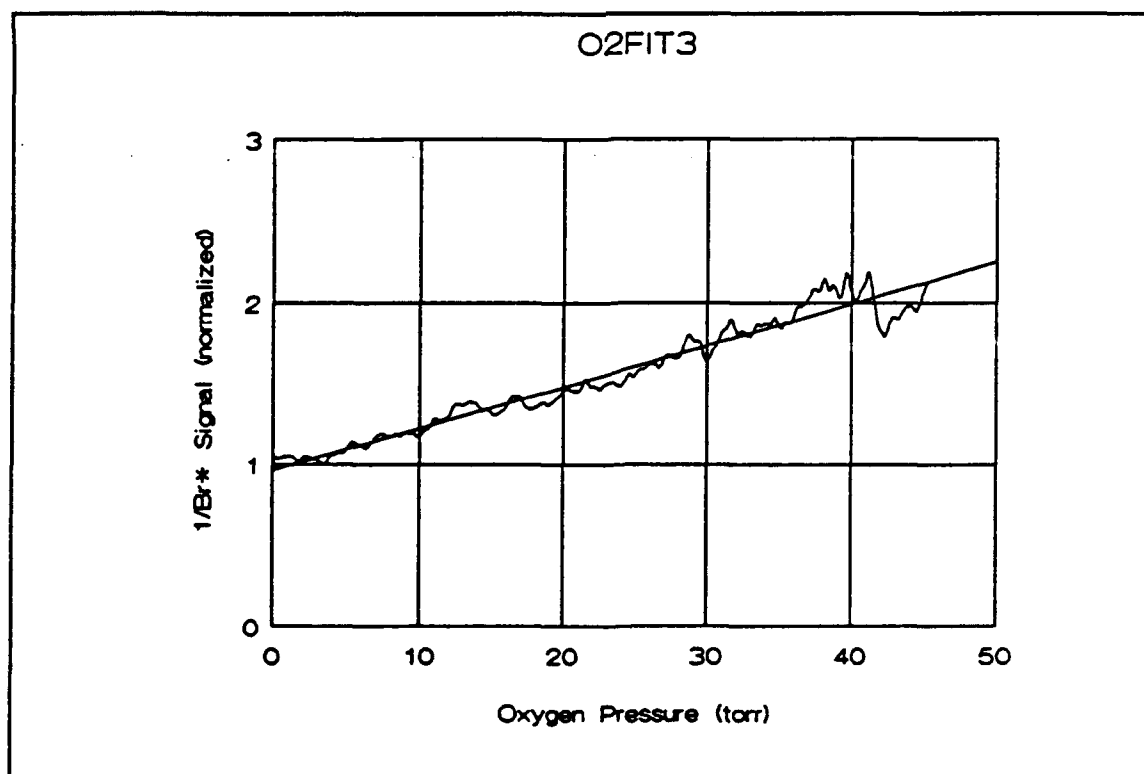
```
Weighted Linear Regression Routine

File:            OXYGEN1.PRN

intercept =      .803628
uncert =         1.178296E-02

slope =          5.127286E-02
uncert =         4.356365E-04

variance =       1.786826E-02
correlation =    .9814695




Weighted Linear Regression Routine

File:            OXYGEN2.PRN

intercept =      .9751826
uncert =         8.423528E-03

slope =          3.493443E-02
uncert =         3.191677E-04

variance =       6.350476E-03
correlation =    .9856246




Weighted Linear Regression Routine

File:            OXYGEN3.PRN

intercept =      .9652843
uncert =         5.551033E-03

slope =          2.559217E-02
uncert =         2.142883E-04

variance =       5.268567E-03
correlation =    .9770433
```
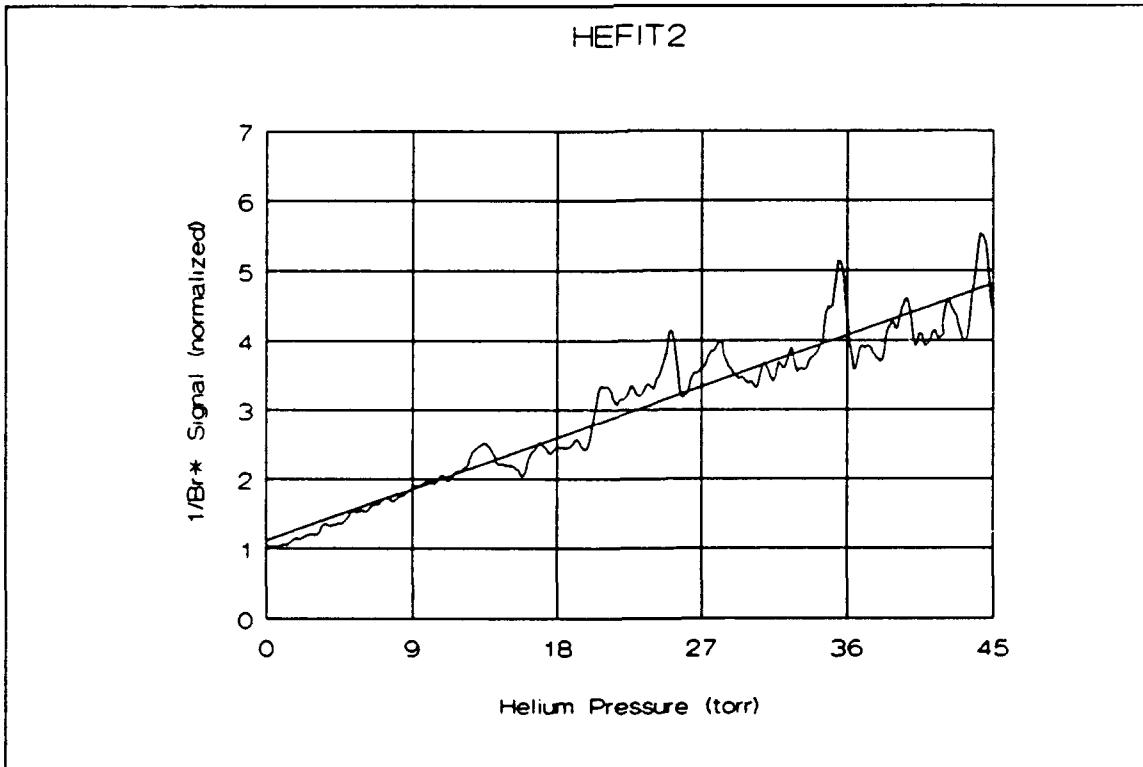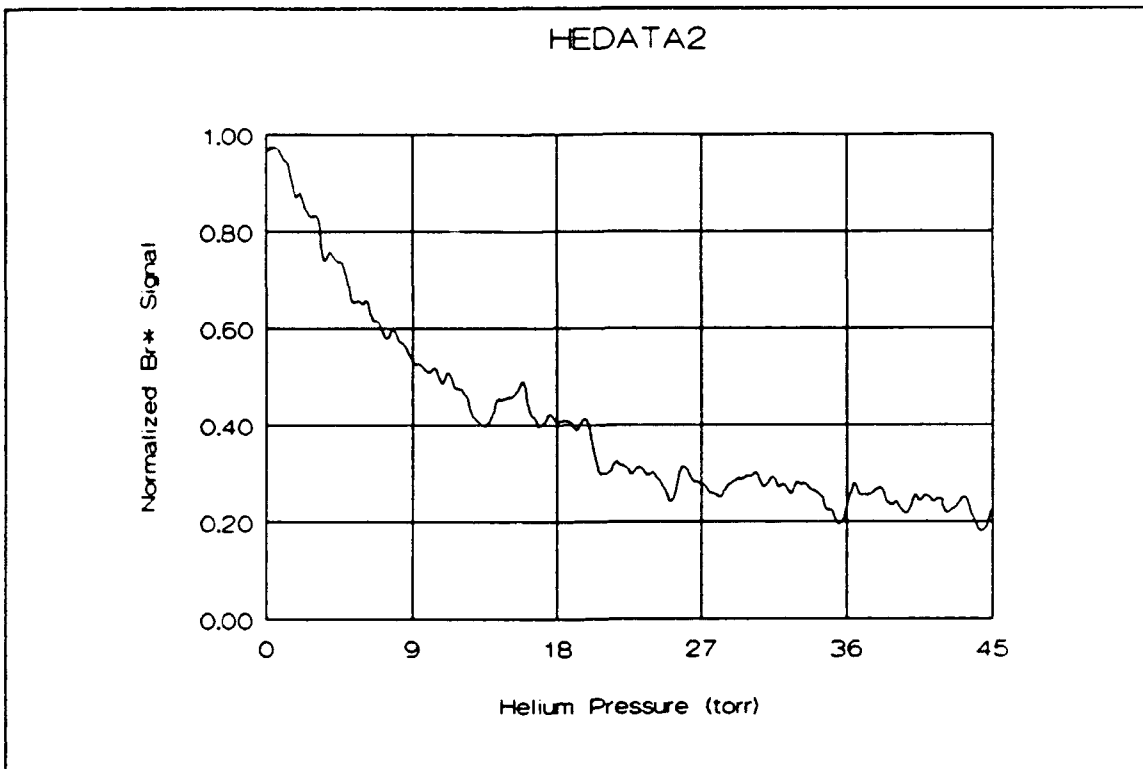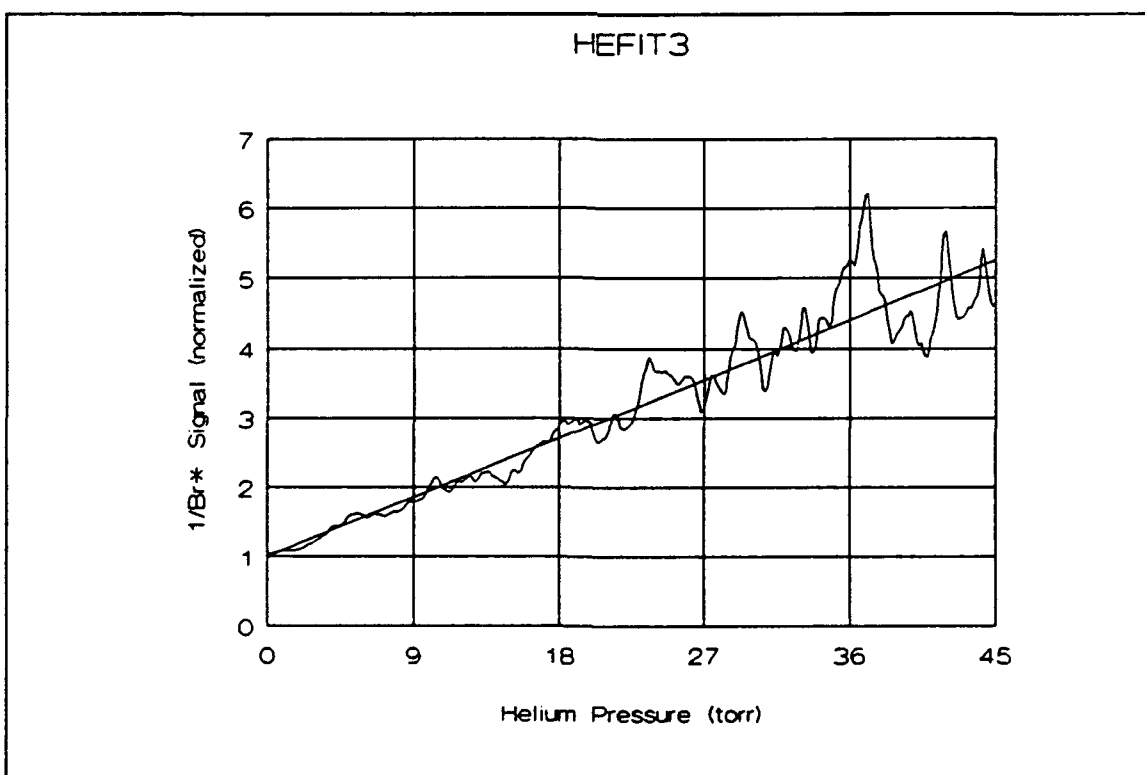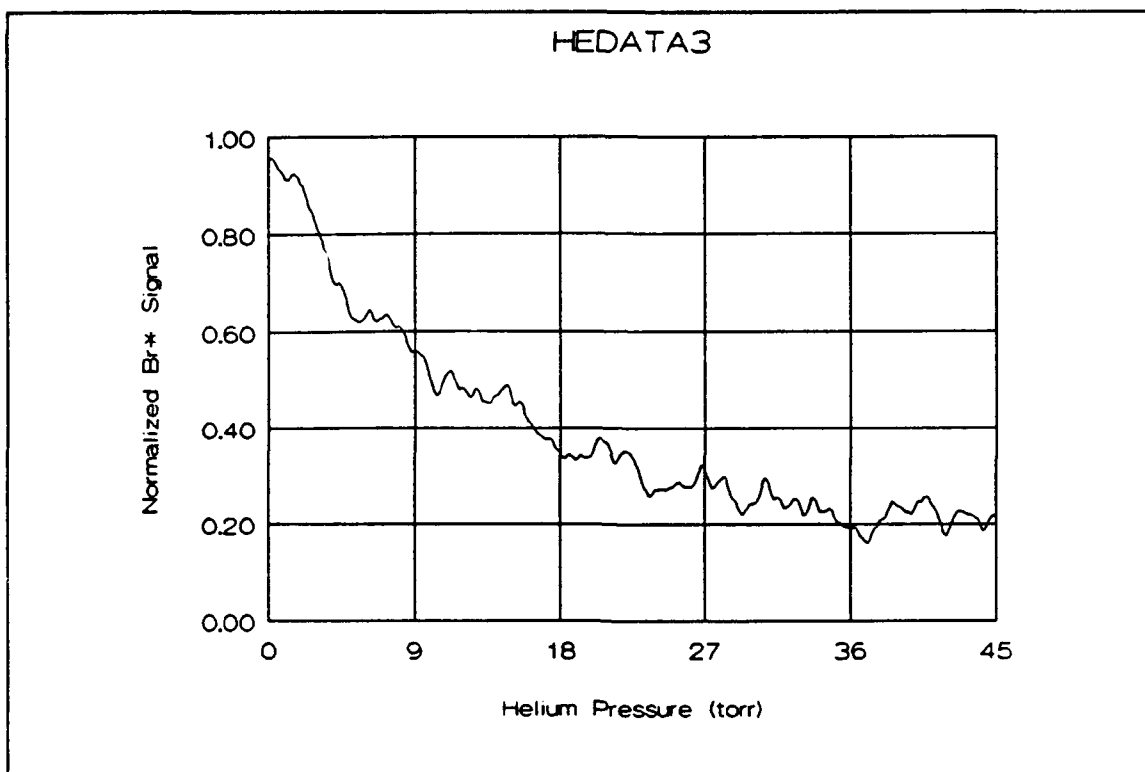
HEDATA 1

HEFIT 1

98

HEDATA2

HEFIT2

HEDATA3

HEFIT3

100
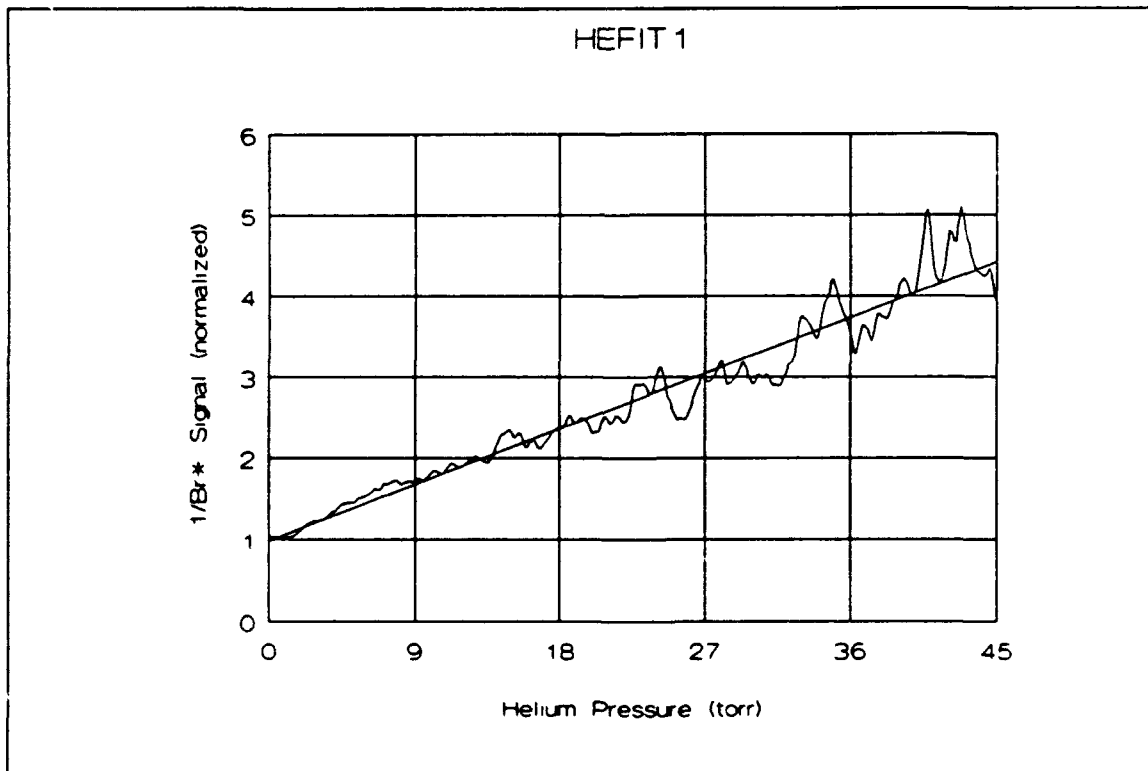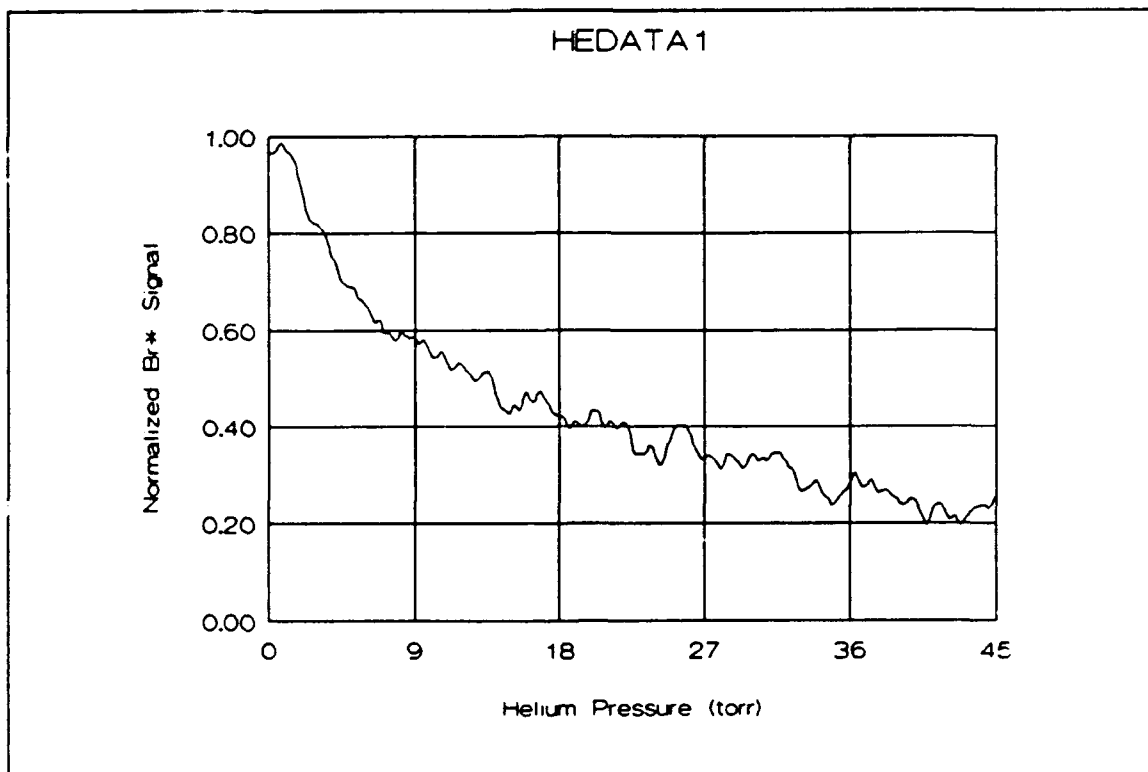
Weighted Linear Regression Routine
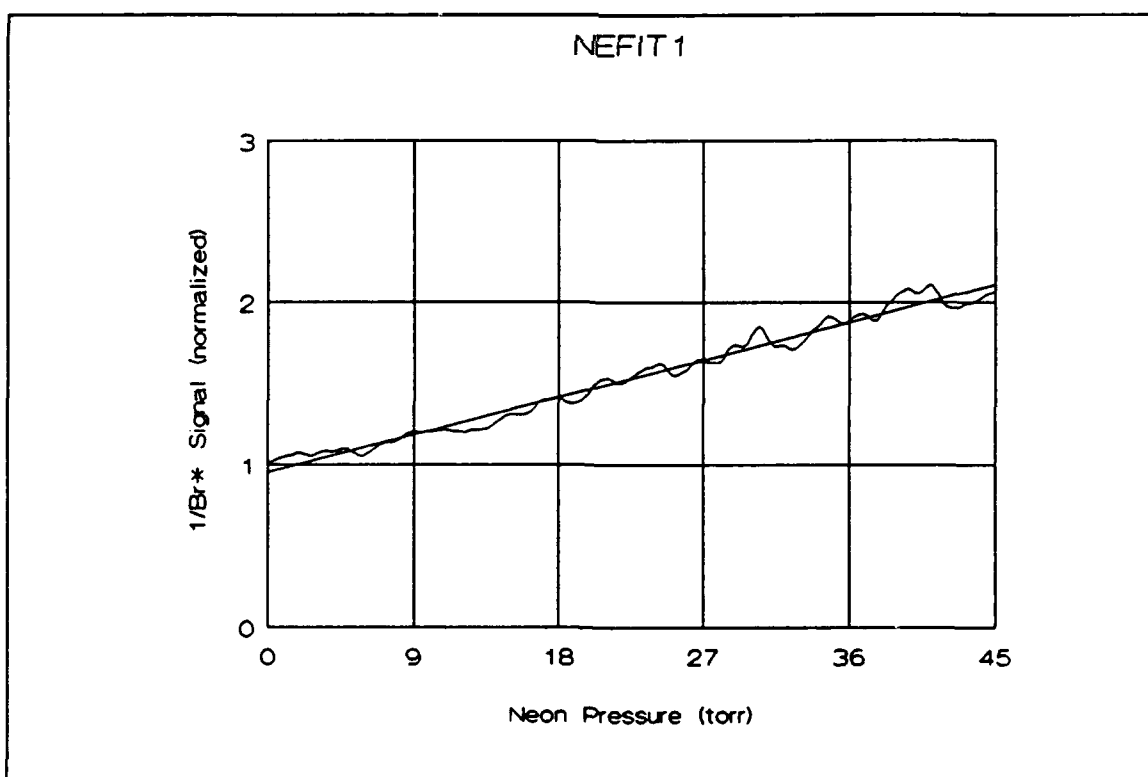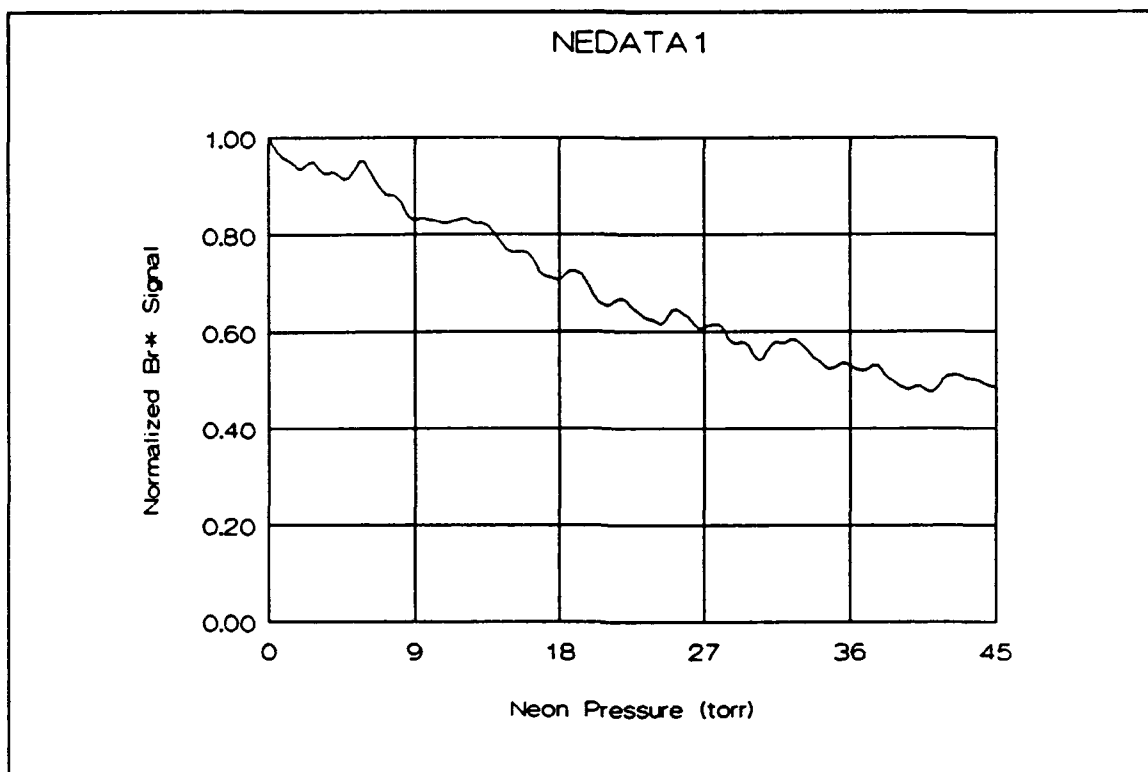
File: helium1.prn

intercept =   .9884714
uncert =   2.285353E-02

slope =   7.628008E-02
uncert =   8.762196E-04

variance =   5.336382E-02
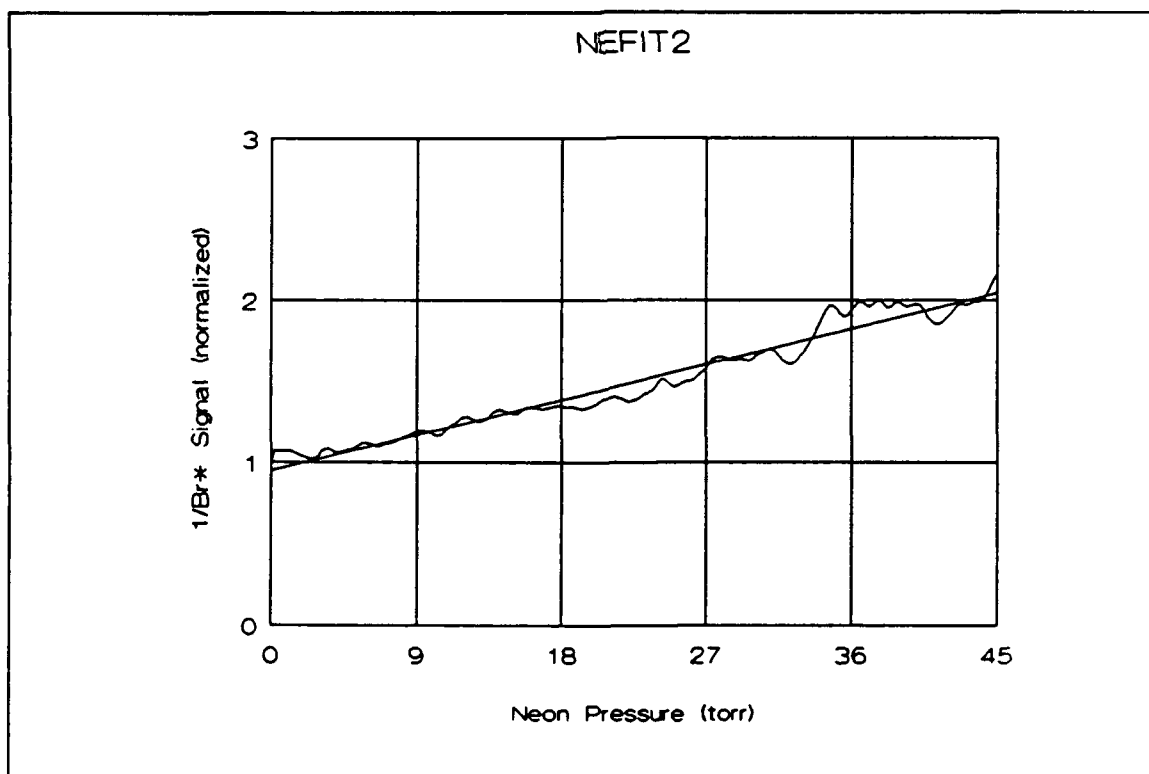correlation =   .9744881
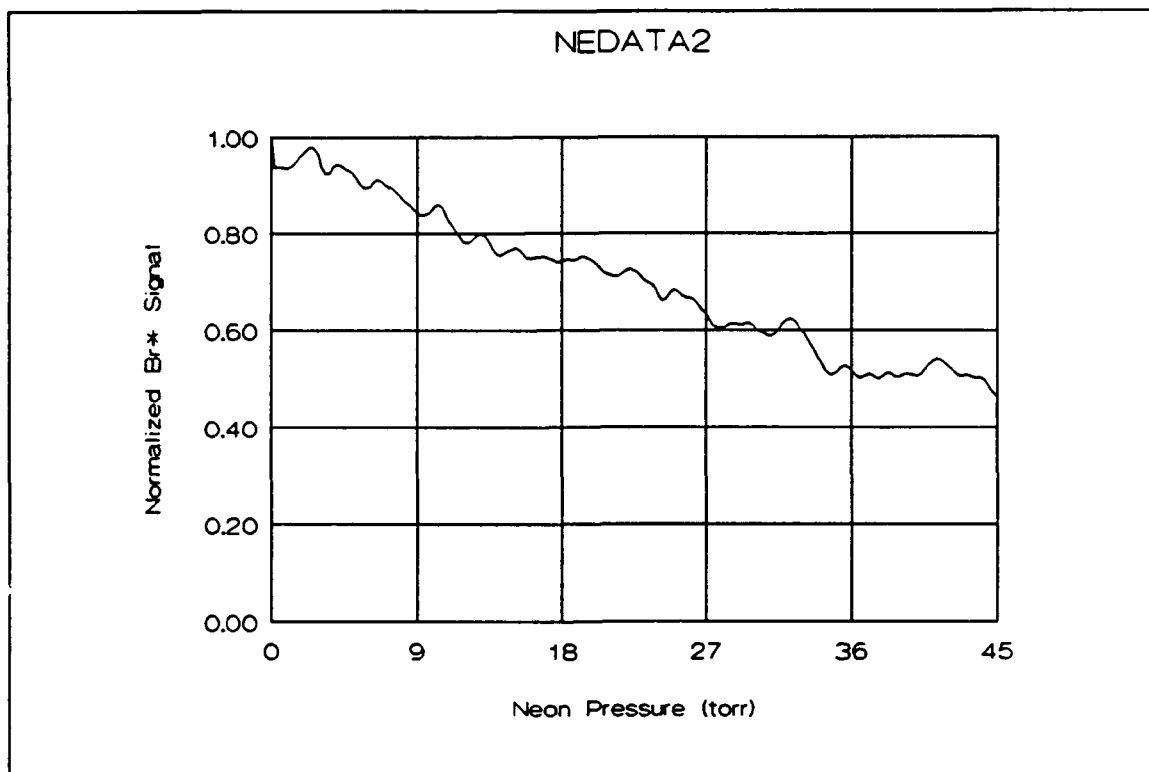

Weighted Linear Regression Routine

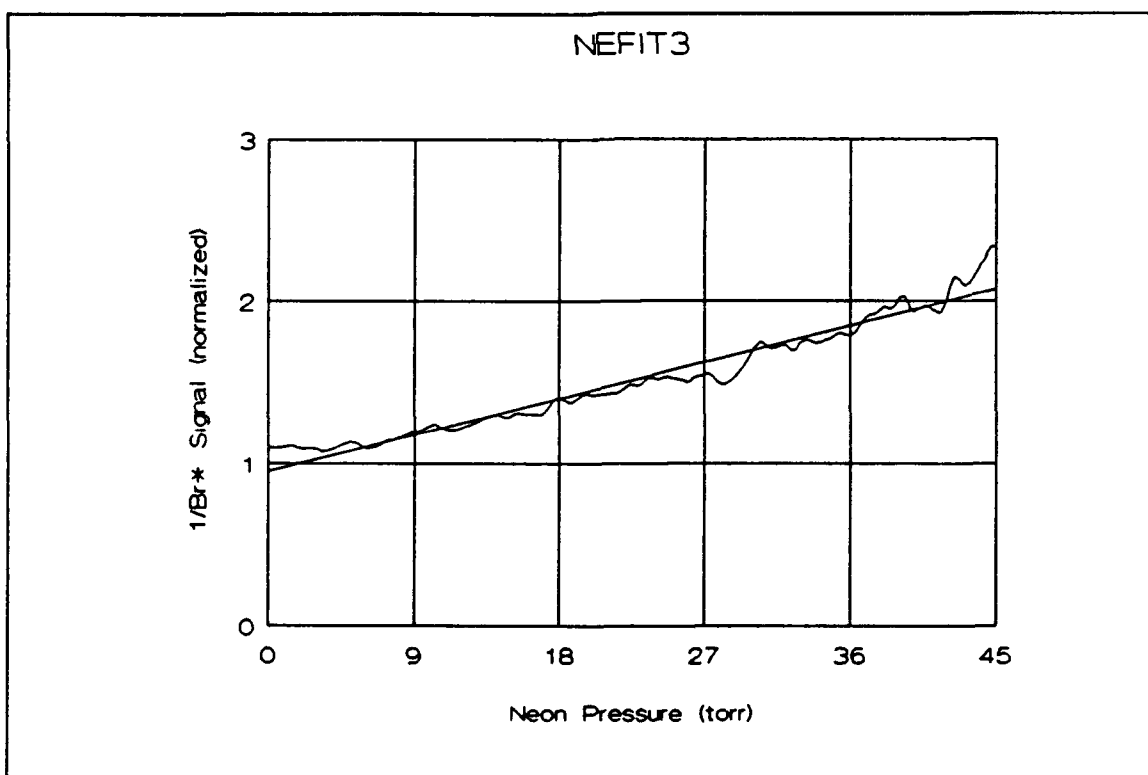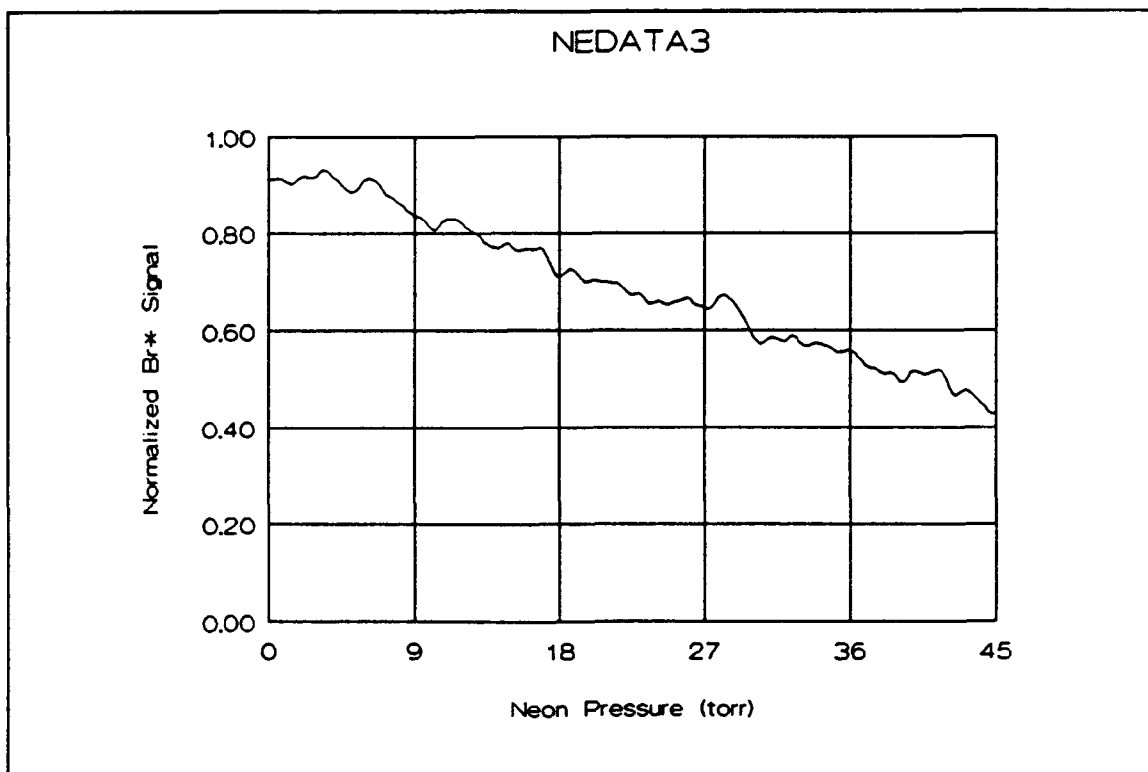File: helium2.prn

intercept =   1.110499
uncert =   2.946496E-02

slope =   8.222998E-02
uncert =   1.146164E-03

variance =   8.777279E-02
correlation =   .9645756

Weighted Linear Regression Routine

File: helium3.prn

intercept =   1.008644
uncert =   3.839567E-02

slope =   9.422892E-02
uncert =   1.462962E-03

variance =   .1380299
correlation =   .9582889

NEDATA 1

Normalized Br* Signal vs Neon Pressure (torr)

NEFIT 1

1/Br* Signal (normalized) vs Neon Pressure (torr)

NEDATA2

Normalized Br∗ Signal vs Neon Pressure (torr)

NEFIT2

1/Br∗ Signal (normalized) vs Neon Pressure (torr)

NEDATA3

Normalized Br* Signal vs Neon Pressure (torr)

NEFIT3

1/Br* Signal (normalized) vs Neon Pressure (torr)

104

Weighted Linear Regression Routine

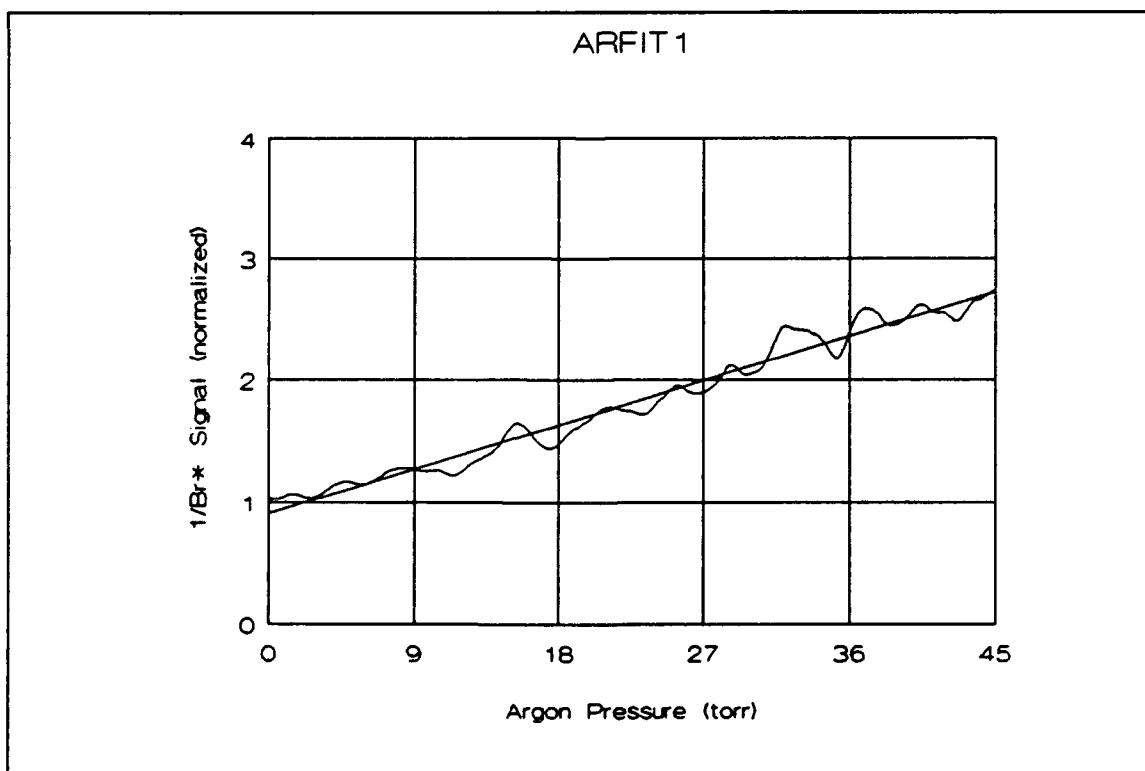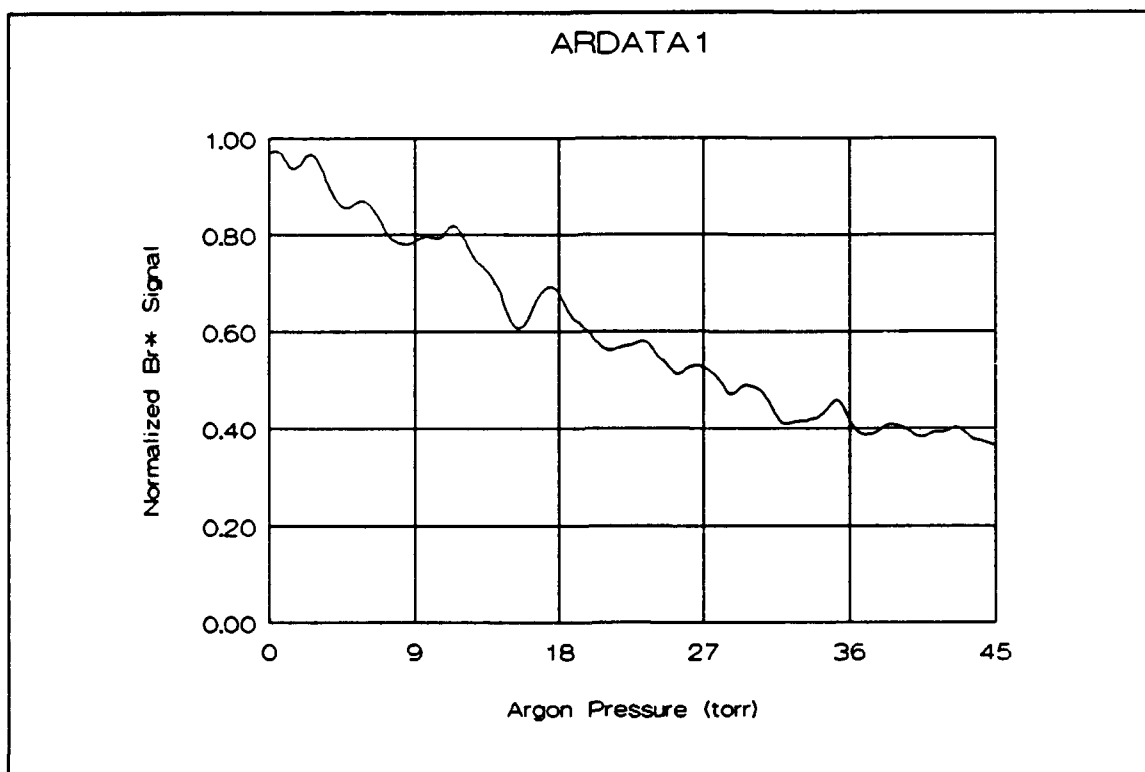File: neon1.prn

intercept =   .9523962
uncert =   6.936615E-03

slope =   2.570697E-02
uncert =   2.669958E-04

variance =   2.347278E-03
correlation =   .9898556
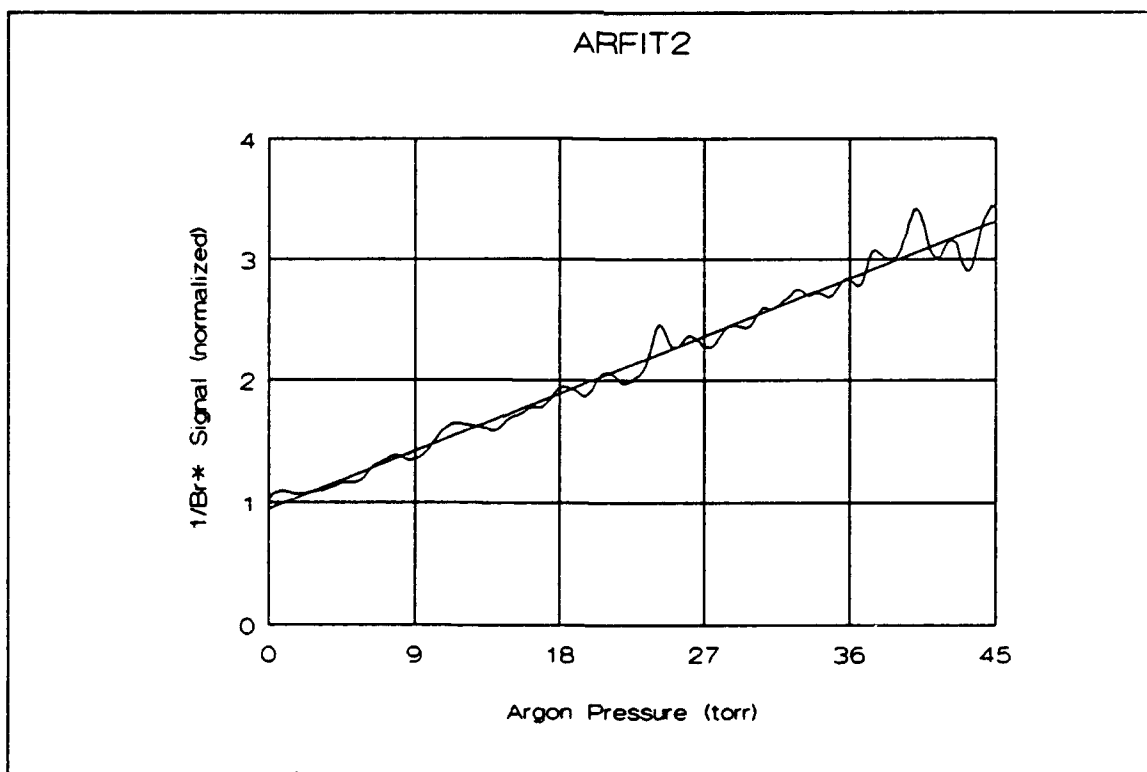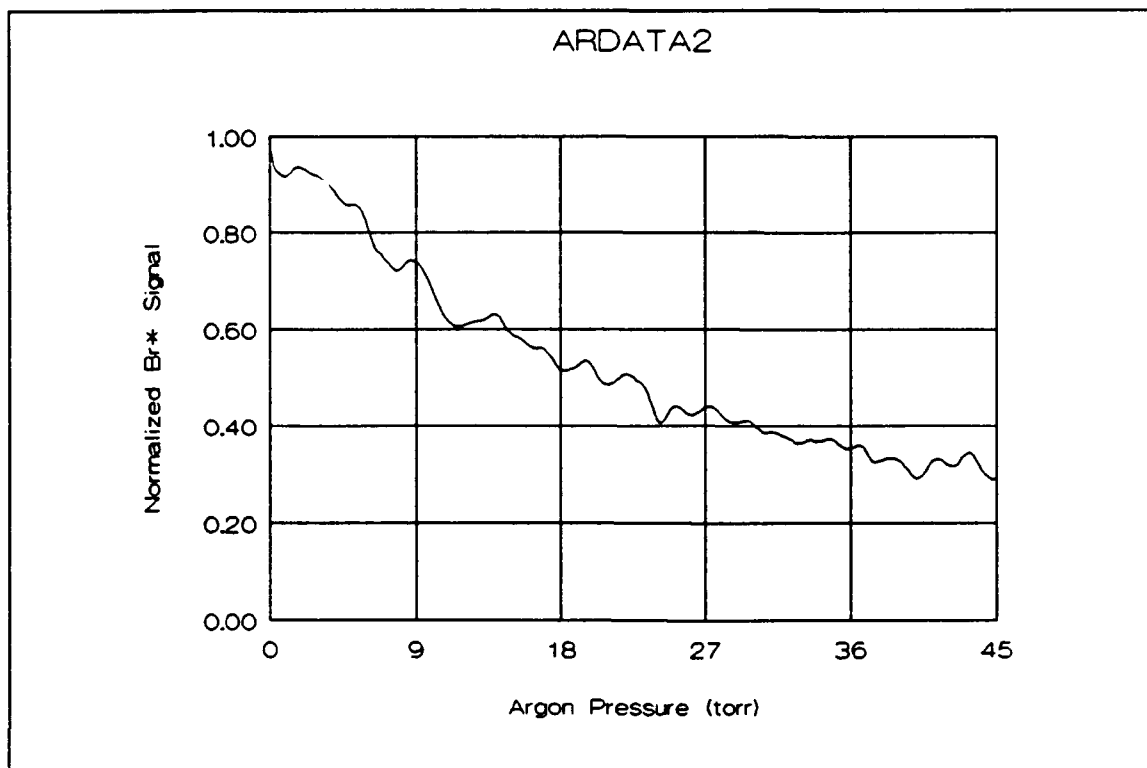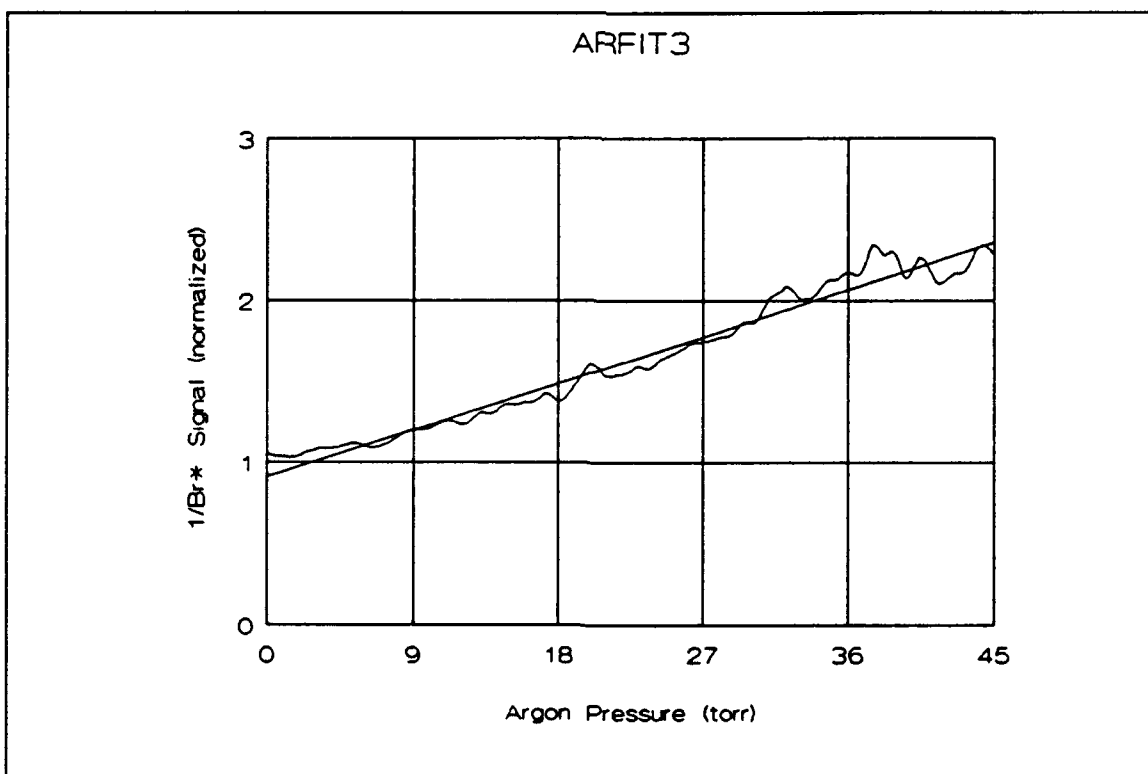

Weighted Linear Regression Routine

File: neon2.prn

intercept =   .9469901
uncert =   9.20663E-03

slope =   2.434685E-02
uncert =   3.540122E-04

variance = ,   4.301008E-03
correlation =   .9795954

Weighted Linear Regression Routine

File: neon3.prn

intercept =   .9535108
uncert =   9.797996E-03

slope =   2.485261E-02
uncert =   3.748077E-04

variance =   5.028464E-03
correlation =   .9772592

ARDATA1

Normalized Br* Signal vs. Argon Pressure (torr)

ARFIT1

1/Br* Signal (normalized) vs. Argon Pressure (torr)

ARDATA2

Normalized Br* Signal vs Argon Pressure (torr)

ARFIT2

1/Br* Signal (normalized) vs Argon Pressure (torr)

ARDATA3

Normalized Br* Signal vs Argon Pressure (torr)

ARFIT3

1/Br* Signal (normalized) vs Argon Pressure (torr)
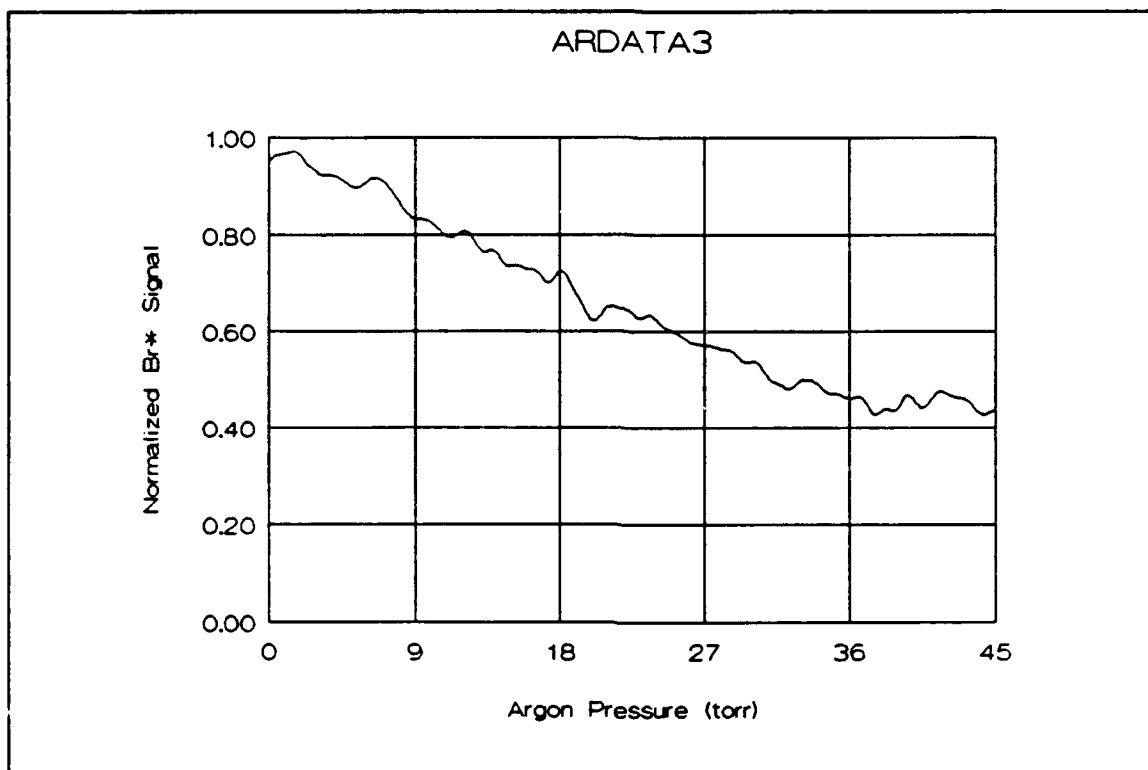
```
Weighted Linear Regression Routine

File:            argon1.prn

intercept =      .9066268
uncert =         1.091726E-02

slope =          4.033522E-02
uncert =         4.200766E-04

variance =       7.903499E-03
correlation =    .9860368




Weighted Linear Regression Routine

File:            argon2.prn

intercept =      .9431412
uncert =         1.123187E-02

slope =          5.270806E-02
uncert =         4.313045E-04

variance =       8.479259E-03
correlation =    .9911811




Weighted Linear Regression Routine

File:            argon3.prn

intercept =      .9101511
uncert =         8.531119E-03

slope =          3.215603E-02
uncert =         3.26488E-04

variance =       5.140481E-03
correlation =    .9856738
```
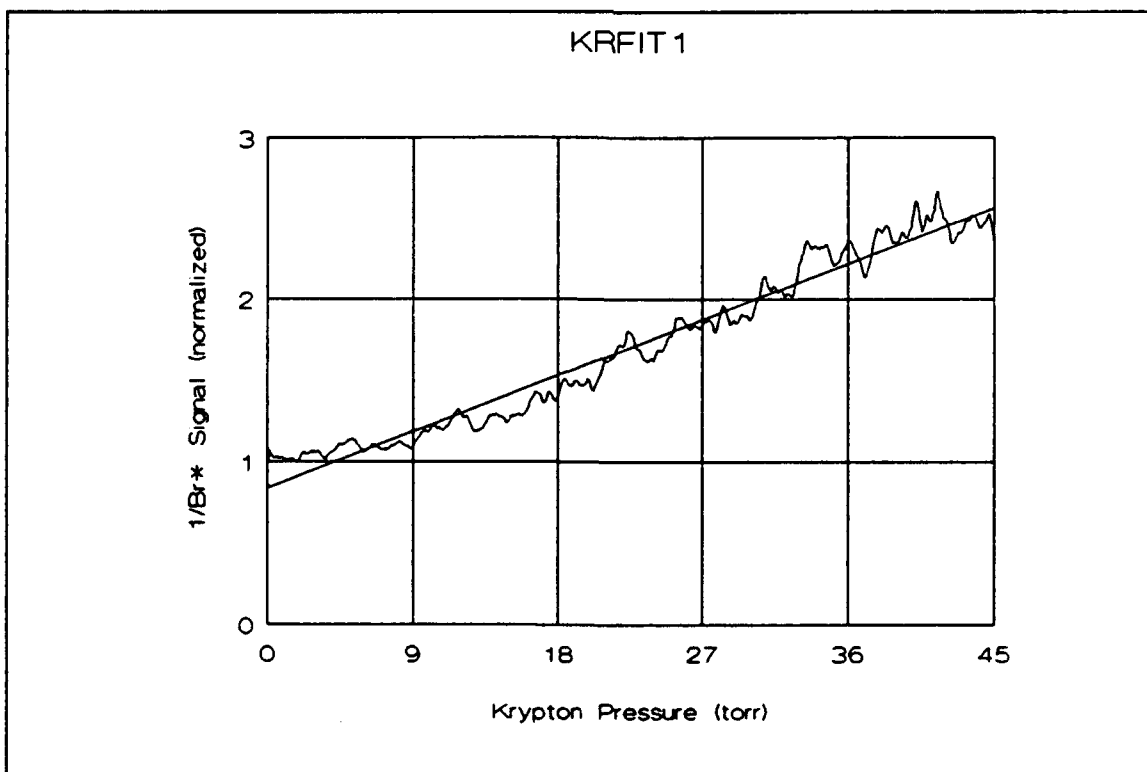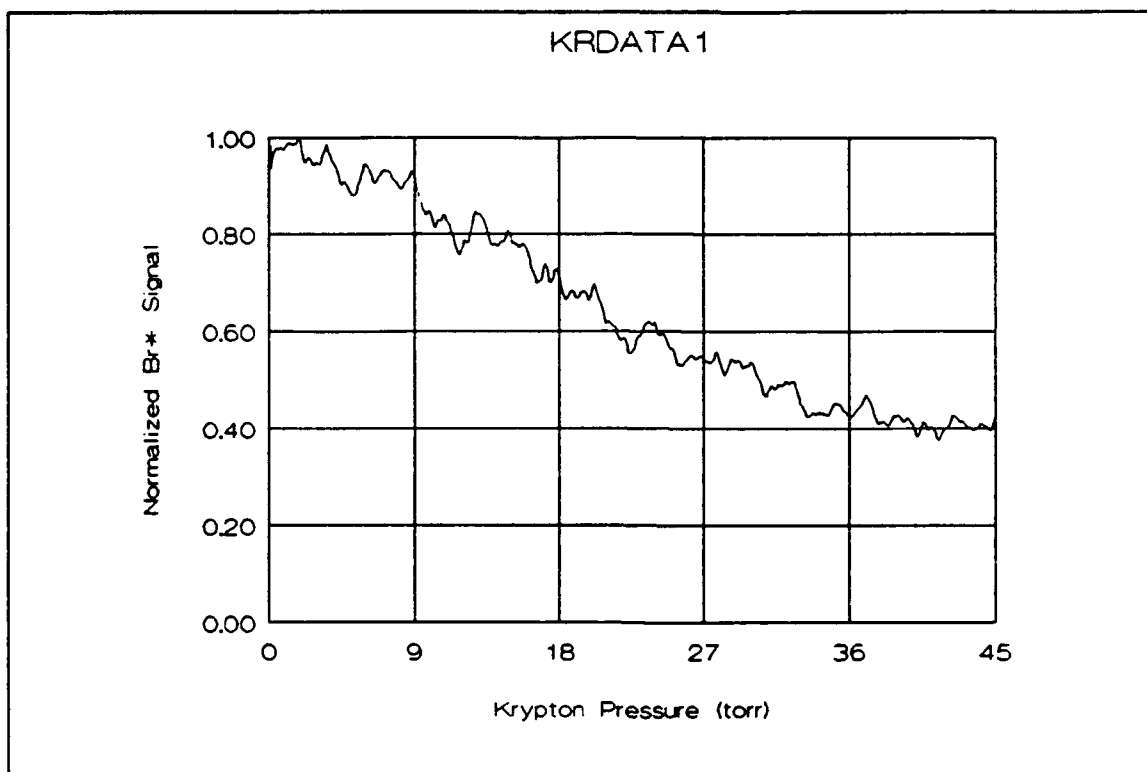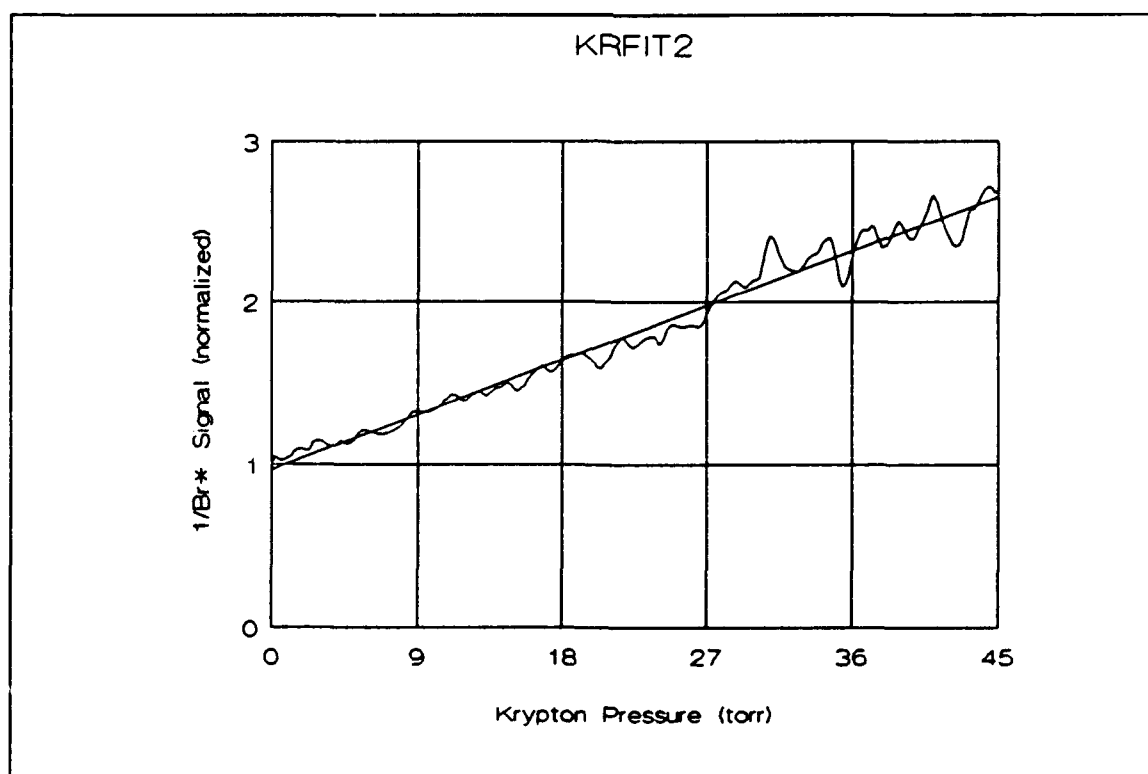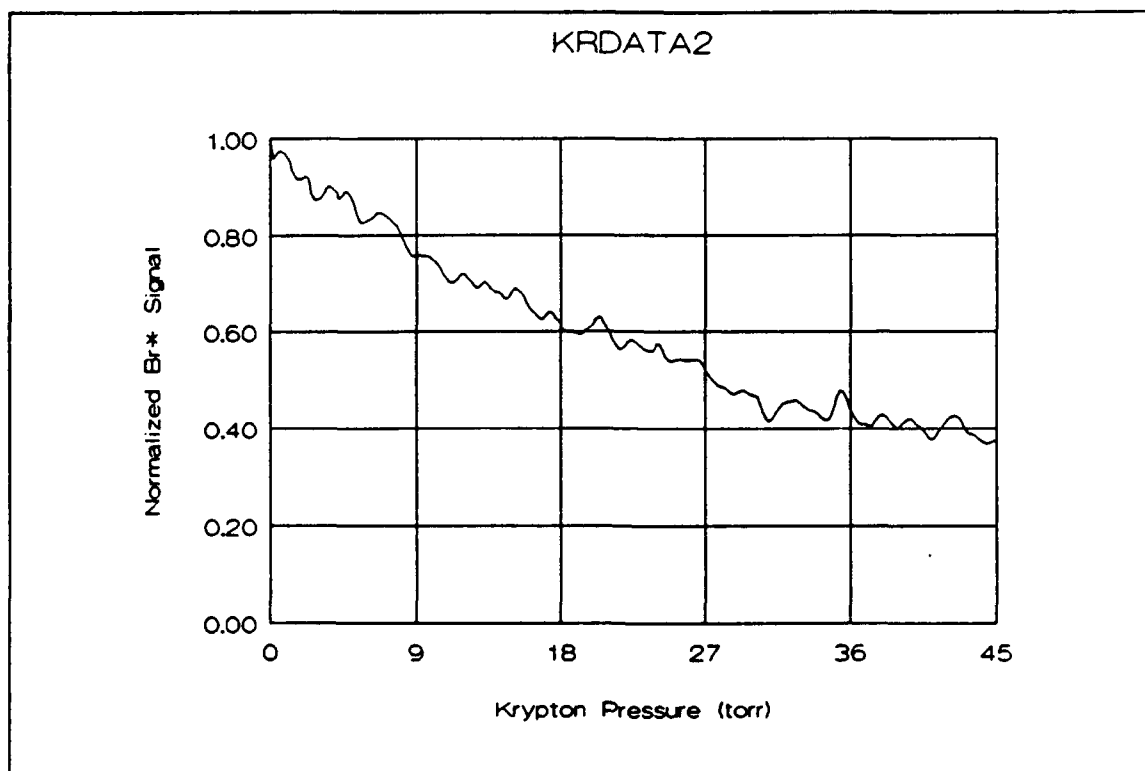
KRDATA1

Normalized Br* Signal vs Krypton Pressure (torr)

KRFIT1

1/Br* Signal (normalized) vs Krypton Pressure (torr)

110

KRDATA2

Normalized Br* Signal vs Krypton Pressure (torr)

KRFIT2

1/Br* Signal (normalized) vs Krypton Pressure (torr)

111

KRDATA3

Normalized Br* Signal vs. Krypton Pressure (torr)

KRFIT3

1/Br* Signal (normalized) vs. Krypton Pressure (torr)
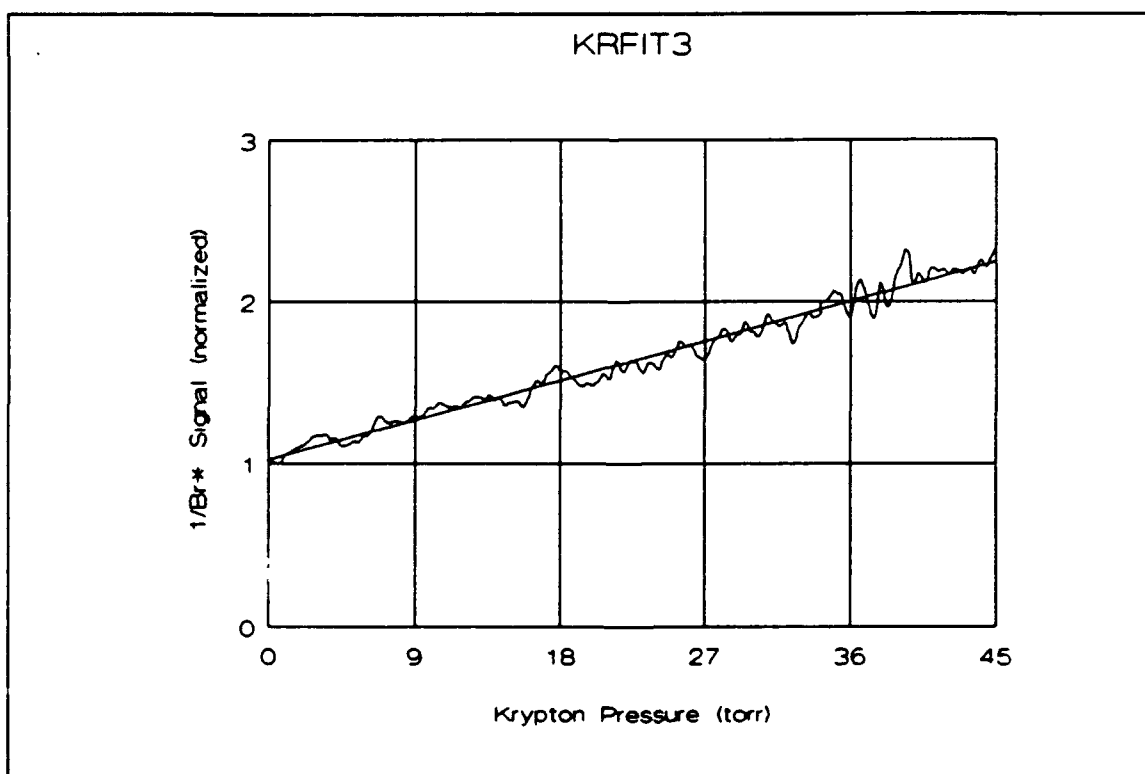
Weighted Linear Regression Routine

File: krypton1.prn

intercept =   .837058
uncert =   8.226315E-03

slope =   3.834118E-02
uncert =   3.202298E-04

variance =   9.555691E-03
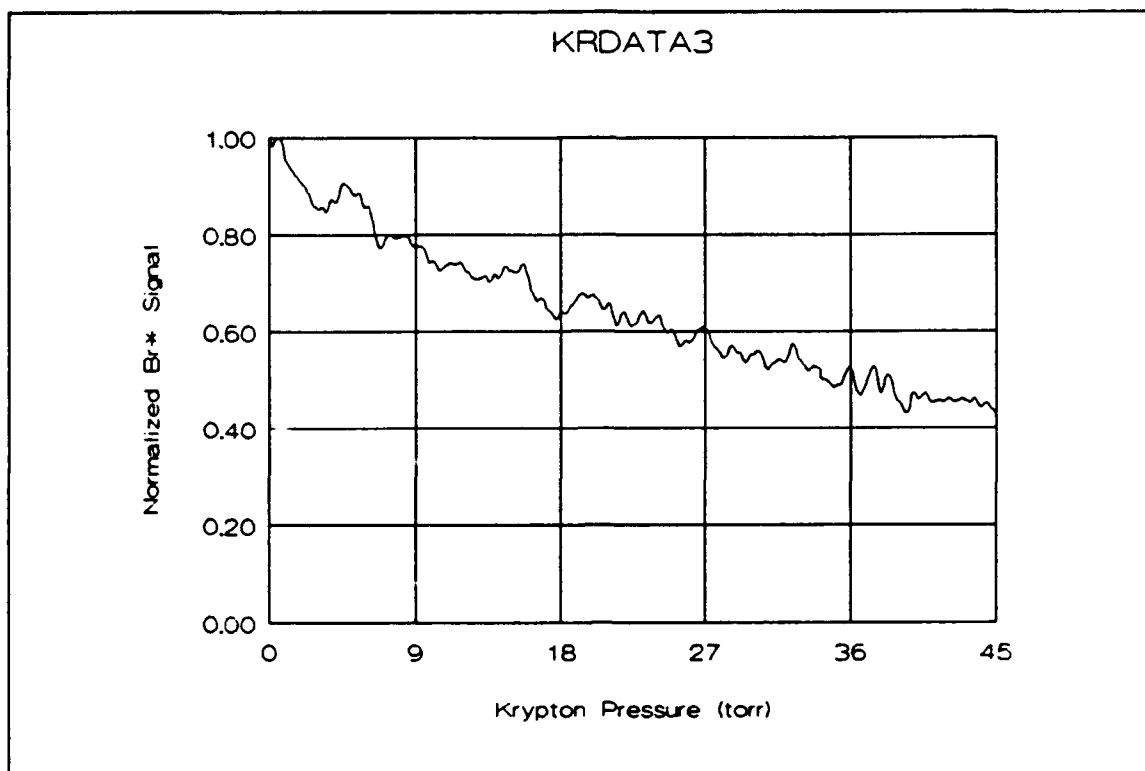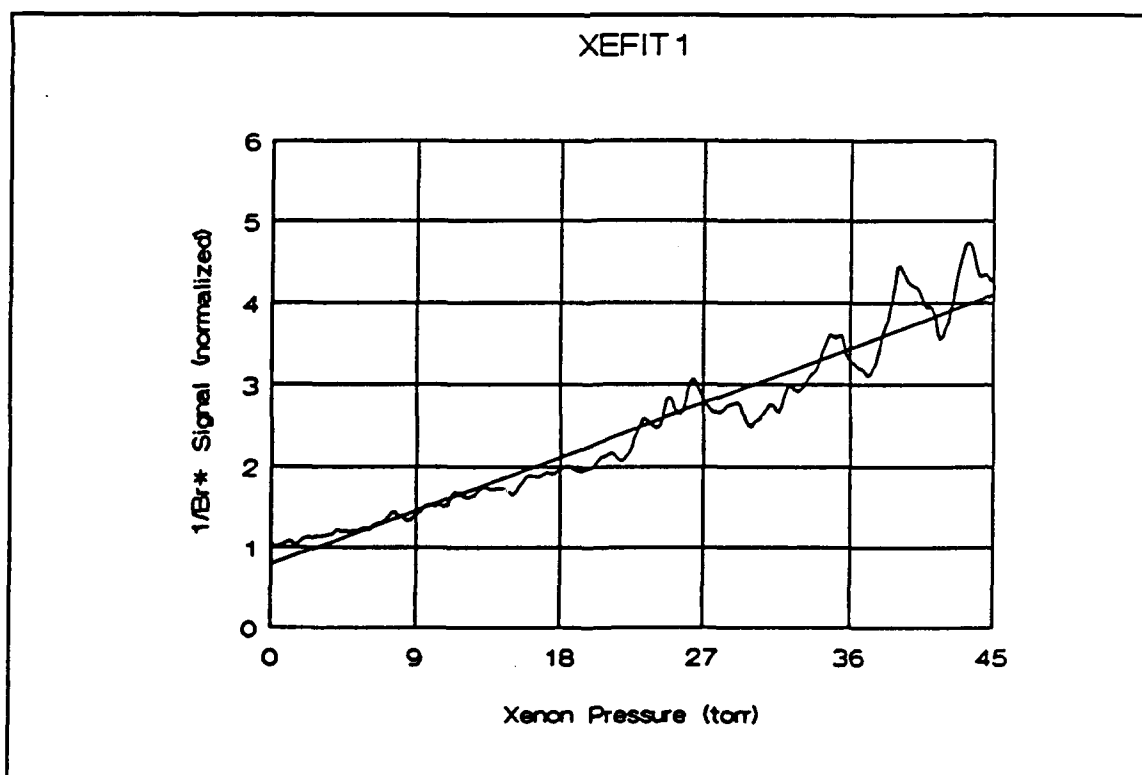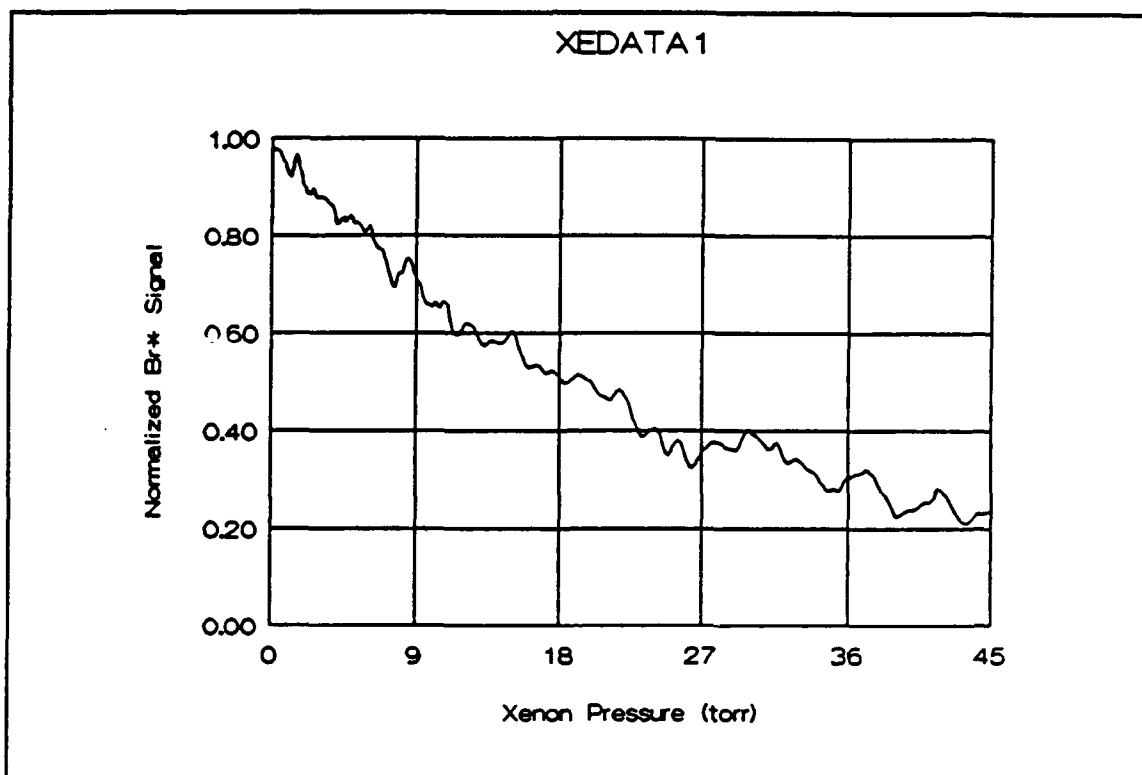correlation =   .9818821

Weighted Linear Regression Routine

File: krypton2.prn

intercept =   .9662156
uncert =   8.843552E-03

slope =   .0374262
uncert =   3.45776E-04

variance =   5.546351E-03
correlation =   .9890029

Weighted Linear Regression Routine

File: krypton3.prn

intercept =   1.024318
uncert =   5.352675E-03

slope =   2.713035E-02
uncert =   2.06454E-04

variance =   3.167846E-03
correlation =   .9875538

XEDATA1

(Y-axis) Normalized Br* Signal

1.00
0.80
0.60
0.40
0.20
0.00

(X-axis) Xenon Pressure (torr)

0 9 18 27 36 45

XEFIT1

(Y-axis) 1/Br* Signal (normalized)

6
5
4
3
2
1
0

(X-axis) Xenon Pressure (torr)

0 9 18 27 36 45

114

XEDATA2
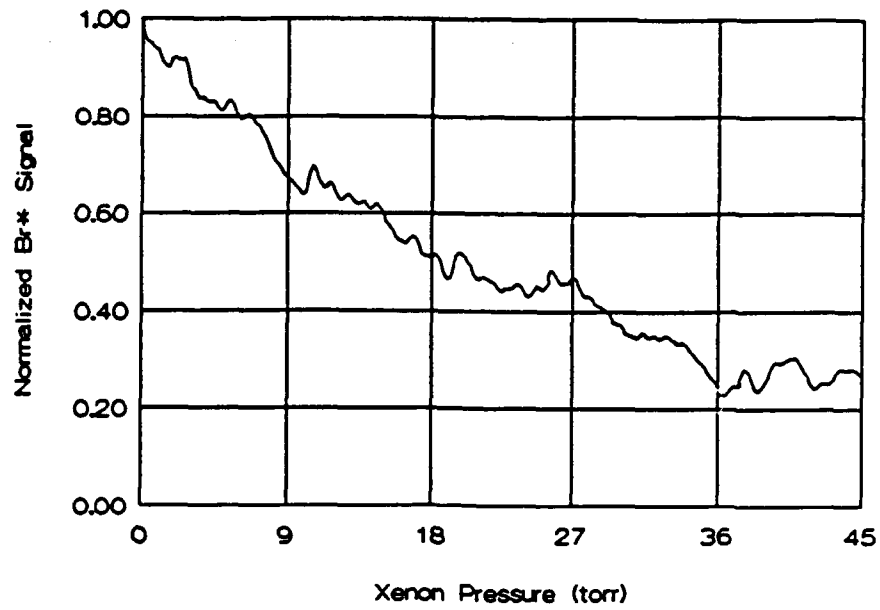
XEFIT2
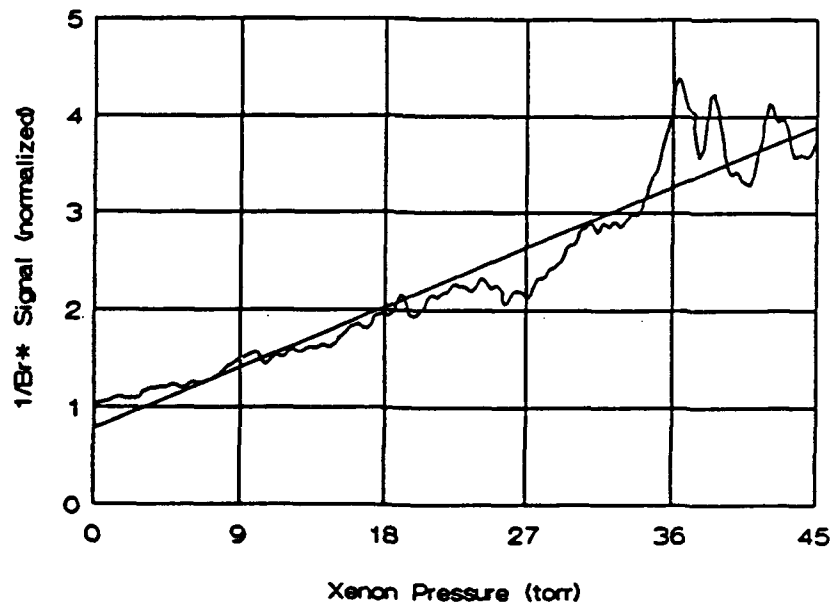
Weighted Linear Regression Routine

File: xenon1.prn

intercept =   .7944716
uncert =   2.135908E-02

slope =   7.340807E-02
uncert =   9.064206E-04

variance =   5.056316E-02
correlation =   .9755433

Weighted Linear Regression Routine

File: xenon2.prn

intercept =   .7846844
uncert =   2.992797E-02

slope =   6.888659E-02
uncert =   1.193827E-03

variance = ´   7.505545E-02
correlation =   .9568613

Bibliography

1. Boriev, I. A. and others. "Determination of the Emission Cross Section for the $^2P_{1/2} - {}^2P_{3/2}$ Transition of the Bromine Atom," Optical Spectroscopy (USSR), 54: 233-237 (March 1983).

2. Calvert, Jack G. and James N Pitts, Jr. Photochemistry. New York: John Wiley and Sons, 1966.

3. Cowan, Robert D. The Theory of Atomic Structure and Spectra. Berkeley CA: University of California Press, 1981.

4. Donovan, R. J. and D. Husain. "Chemistry of Electronically Excited Atoms," Chemical Reviews, 62: 509-516 (1970).

5. Finzi, Jack and C. P. Moore. "Relaxation of $CO_2(101)$, $CO_2(021)$, and $N_2O(101)$ Vibrational Levels by Near-resonant V→V Energy Transfer," Journal of Chemical Physics, 63: 2285-2288 (September 1975).

6. Grimley, A. J. and P. L. Houston. "Electronic to Vibrational Energy Transfer from $Br(4^2P_{1/2})$ to H_2, HD, and D_2," Journal of Chemical Physics, 70: 5184-5189 (June 1979).

7. Hariri, A., A. B. Petersen, and C. Wittig. "Electronic-Vibrational Energy Transfer from $Br(4^2P_{1/2})$ to HCN, and Deactivation of $HCN(001)^*$," Journal of Chemical Physics, 65: 1872-1875 (September 1976).

8. Hariri, A. and C. Wittig. "Electronic to Vibrational Energy Transfer from $Br(4^2P_{1/2})$ to CO_2, COS, and CS_2," Journal of Chemical Physics, 67: 4454-4462 (November 1977).

9. Herzberg, Gerhard. Molecular Spectra and Molecular Structure. New York: Van Nostrand Reinhold Company, 1950.

10. Herzberg, Gerhard. <u>Molecular Spectra and Molecular Structure II. Infrared and Raman Spectra of Polyatomic Molecules</u>. New York: Van Nostrand Reinhold Company, 1945.

11. Hofmann, Hubert and Stephen R. Leone. "Collisional Deactivation of Laser-Excited $Br^*(^2P_{1/2})$ Atoms With Halogen and Interhalogen Molecules," <u>Chemical Physics Letters</u>, 54: 314-319 (March 1978).

12. Houston, Paul L. "Electronic to Vibrational Energy Transfer from Excited Halogen Atoms," <u>Advances in Chemical Physics</u>, Vol. 47, edited by J. Jortner, R. D. Levine, and S. A. Rice. New York: Wiley and Sons, 1981.

13. Kasper, J. V. V. and others. "Observation of the $^2P_{1/2}$ ← $^2P_{3/2}$ Transition of the Br Atom by Color Laser Spectroscopy," <u>Chemical Physics Letters</u>, 77: 211-213 (January 1981).

14. Kelly, Michael A. <u>Zeeman Spectroscopy of Photolytically Pumped Atomic Iodine</u>. PhD dissertation. University of New Mexico, Albuquerque NM, 1989.

15. Leone, Stephen R. and Francis J. Wodarczyk. "Laser-Excited Electronic-to-Vibrational Energy Transfer from $Br(4^2P_{1/2})$ to HCl and HBr," <u>Journal of Chemical Physics</u>, 60: 314 (January 1974).

16. Okabe, Hideo. <u>Photochemistry of Small Molecules</u>. New York: John Wiley and Sons, 1978.

17. Perram, Glen P. Professor, School of Engineering Physics, Personal Interview. Air Force Institute of Technology, Wright-Patterson AFB OH, September 1991.

18. Petersen, Alan B., Curt Wittig, and Stephen R. Leone. "Infrared Molecular Lasers Pumped by Electronic-Vibrational Energy Transfer from $Br(4^2P_{1/2})$: CO_2, N_2O, HCN, and C_2H_2," <u>Applied Physics Letters</u>, 27: 305-306 (September 1975).

19. Petersen, Alan B., Curt Wittig, and Stephen R. Leone. "Electronic-to-Vibrational Pumped CO_2 Laser Operating at 4.3, 10.6, and 14.1 μm," Journal of Applied Physics, 47: 1051-1054 (March 1976).

20. Seery, Daniel J. and Doyle Britton. "The Continuous Absorption Spectra of Chlorine, Bromine, Bromine Chloride, Iodine Chloride, and Iodine Bromide," Journal of Physical Chemistry, 68: 2263-2266 (August 1964).

21. Taatjes, Craig A., Christopher M. Lovejoy, Brian J. Opansky, and Stephen R. Leone. "Laser Double Resonance Measurements of the Quenching Rates of $Br(4^2P_{1/2})$ with H_2O, D_2O, HDO, and O_2," Report to Phillips Laboratory, Advanced Concepts Branch, Kirtland AFB, NM, April 1991.

22. Verdeyen, Joseph T. Laser Electronics. Englewood Cliffs NJ: Prentice-Hall, 1981.

23. Weast, Robert C. Handbook of Chemistry and Physics (67th Edition). Boca Raton FL: CRC Press, 1986.

24. Wight, Charles A. "Infrared Fluorescence Studies of Near-Resonant Electronic-to-Vibrational Energy-Transfer Collisions: $Br(4^2P_{1/2})$ + NO," Journal of Physical Chemistry, 90: 2683-2687 (1986).

25. Wodarczyk, Francis J. and Phillip B. Sackett. "Electronic-to-Vibrational Energy Transfer from $Br(4^2P_{1/2})$ to HF," Chemical Physics, 12: 65-70 (1976).